CHARACTERIZATION OF THE MECHANICAL PROPERTIES OF TACTORS USED IN TACTILE DISPLAYS

by

David A. Held

B.S. Mechanical Engineering
Massachusetts Institute of Technology, 2005

SUBMITTED TO THE DEPARTMENT OF MECHANICAL ENGINEERING IN PARTIAL FULFILLMENT OF THE REQUIREMENTS FOR THE DEGREE OF

MASTER OF SCIENCE IN MECHANICAL ENGINEERING

AT THE

MASSACHUSETTS INSTITUTE OF TECHNOLOGY
[September 2007]
AUGUST 2007

Signature of Author _____
Department of Mechanical Engineering
August 19, 2007

Certified by _____
Lynette A. Jones
Principal Research Scientist in Mechanical Engineering
Thesis Supervisor

Accepted by _____
Lallit Anand
Chairman, Department Committee for Graduate Students

Characterization of the Mechanical Properties of Tactors Used in Tactile Displays

by

David A. Held

Submitted to the Department of Mechanical Engineering
on 19 August 2007 in partial fulfillment of the
requirements for the Degree of Master of Science in
Mechanical Engineering

Abstract

Pancake motors used in a tactile display were analyzed to understand the characteristics of their operation, as well as to suggest improvements in the design of the display. The frequencies and forces produced by unencased and encased pancake motors were measured, and a motor model was formulated to simulate the motion of the motors. It was found that there was considerate variability between pancake motors, and it was proposed that this may be due to a varying damping coefficient. A viscoelastic substrate, named Skinsim, was selected based on mechanical tests to have similar material properties to skin. It was found that when the motors were mounted on Skinsim their frequency of vibration was reduced by 62%. Measurements of the effects of damping in Skinsim led to the recommendation that inter-tactor spacing on a tactile vest should be at least 60 mm if the display is to be used for precise tactor localization. Finally, a GPS device was integrated into the tactile display. This allows appropriate navigational commands to be sent to the user through the tactile vest, based on information about the user's location.

Thesis supervisor: Lynette A. Jones
Title: Principal Research Scientist

Acknowledgements

I would like to give my thanks to various individuals, without the help of whom, this thesis would have never been completed. First, I would like to thank Dr. Lynette Jones for funding my Research Assistantship, and for helping me make the difficult transition into the unstructured environment of research. She has offered me invaluable advice regarding dealing with frustration and making the most of my circumstances. Additionally, she has spent countless hours reading and correcting many drafts of this thesis, for which I am extremely grateful. She has also been a wonderful person to work with and a great help in my research and in understanding the significance of research results.

Second, I would like to thank two people who have been a tremendous inspiration during my research. My neighboring lab-mate, James Tangorra, has offered me an abundance of advice on how to proceed when performing research. Additionally, he has truly been a role model in teaching me the value of taking the time to understand a problem instead of taking shortcuts. I would also like to thank Michal Ruchelsman, who was one of my teammates from a class project. She has inspired me with her amazing work ethic and her commitment to perfection.

I also give my thanks to thank Ian Hunter and the members of the Bio-Instrumentation Lab for offering advice and help in my research. I additionally give thanks to the Mechanical Engineering department for accepting me into their graduate program and for the large amount of administrative work required during my graduate studies. Last, I would like to thank my parents and my sister, for the loving support that I have always received.

This research was supported in part through the Advanced Decision Architectures Collaborative Technology Alliance sponsored by the U.S. Army Research Laboratory under Cooperative Agreement DAAD 19-01-2-0009.

Table of Contents

1. Introduction

We perceive the environment through our various sense organs, which receive stimuli from the outside world. The most common methods for communication involve the senses of sight and sound, through pictures, written words, or speech. However, the sense of touch can also be used as a means of conveying information. In situations where the user is stationary, this can be done using Braille or refreshable Braille displays. For situations in which the user is moving, a wearable tactile display is more appropriate. Although many different types of tactile displays have been designed, there are still many challenges to be overcome that would allow for more information to be conveyed through these displays.

This thesis analyzes the performance of pancake motors used in tactile displays to understand the characteristics of their operation, as well as to suggest improvements in the design of tactile displays. A viscoelastic substrate, named Skinsim, was selected after experimentation as a substrate that mimicked some of the material properties of skin. Acceleration measurements were made with the motors mounted on this material to characterize the properties of the motors on compliant materials and to measure the traveling waves produced in Skinsim by vibrotactile stimuli. Finally, a GPS device was integrated into the tactile display, thus improving the functionality of the tactile display as a communication system for navigation.

2. Background

2.1. Tactile Displays

The sense of touch is used to convey information in a static sense using Braille, which allows someone to read at a rate of 100 to 250 words per minute (Reed and Durlach, 1998). Information can also be presented to a user dynamically through a refreshable Braille display. Such a display normally makes use of a screen reader to capture information on a computer screen. The information is sent to a piece of hardware which actuates up to eight dots to present the screen contents to the user in the form of Braille. Because only six dots are needed to represent a Braille character in English, the remaining two dots can be used to signify capitalization, highlighting, or some other piece of information. Most Braille displays present the information as a line of Braille characters, generally ranging from 18 to 84 characters per line (Stageberg, 2004).

An improvement to this design was created by the National Institute of Standards and Technology (NIST) in 2000, which built a prototype of a rotating-wheel refreshable Braille display. Screen capture information is presented to the user on a rotating wheel, in which the Braille patterns are changed outside of the active reading area. This gives the user the impression of reading one infinitely long line of text, rather than forcing the reader to return his/her finger to the beginning of a tactile display after reaching the limit of a linear Braille display. This is not only more convenient, but also reduces the risk of repetitive stress injuries. Additionally, by presenting the display on a rotating wheel rather than a long array of characters, only two characters need to be displayed at once, rather than a line of 80 characters. Thus the design is simplified, reducing the cost as well as the need for repairs (Roberts et al, 2000).

Tactile displays have also been used to assist hearing-impaired individuals as a supplement to lip-reading, to aid the user in perceiving speech. The Spens MINIVIB3, developed in Sweden, works by using amplitude modulation to create a vibration level that corresponds to the envelope of a speech signal (Cholewiak and Sherrik, 1986). The Tactaid-7, manufactured by Audiological Engineering Corp, encodes certain properties of speech as a tactile signal on an array of seven vibrators placed on the forearm, as well as the sternum, neck, and abdomen. This device has been shown to improve the user's ability to read lips by as much as 40% (Cholewiak and Collins, 2003).

Tactile displays can also be used to allow users to gain a physical awareness of their surroundings. For instance, electronic travel aids have been used to alert blind users to the presence of obstacles using tactile feedback. A non-mobile Tactile-visual Substitution System, designed by Bach-y-Rita and his colleagues in the 1960s, converted an image detected by a camera into a tactual image presented through 400 individual vibrators on the back of the user. By manipulating the orientation and zoom-factor of the camera, users were able to engage in active exploration of their surroundings, even while remaining stationary (Sherrick, 1991).

There are also circumstances in which tactile devices can be beneficial as a supplemental channel of information, even for sighted individuals. Using his prenav model of information processing for human navigation, Van Erp (2007) predicts that tactile displays can be beneficial when the user is subjected to sensory overload. In such a situation, "the visual and auditory channels are not available or are overloaded" (Van Erp, 2007). For example, the cockpit of an airplane often presents pilots with a great deal of visual information, which may cause sensory overload of the visual system to occur.

If the aircraft attitude information is presented in the form of tactual feedback, sensory overload on the visual system is reduced (Rupert, 2000). Using tactual feedback in this form "has been shown to be of use to novice pilots as well as to experienced ones in stressful conditions" (Sherrick, 1991).

A related reason for tactual feedback, known as reduced information availability, occurs when some of the normal channels for receiving information are in some way hindered or obstructed. For example, a tactile display may be useful for divers in dark waters, for whom auditory and visual transmission of information may be almost completely blocked. Similarly, firefighters often have to work in conditions of dense smoke in which visual signals are obstructed. In these types of situations, tactual displays may prove to be extremely useful as one of the only remaining channels available for communication (Van Erp, 2007).

2.2. Physiological Basis for the Sense of Touch

In order to understand how tactile displays convey information to their user, the sense of touch must be understood. Touch is conveyed through the skin, which is the body's largest organ, covering 1.8 m^2 over the human body (Cholewiak and Collins, 1991). Skin can be classified as either glabrous or hairy. Glabrous, or smooth, skin is found on the hands, feet, and face, whereas hairy skin is found on the rest of the body. Both glabrous and hairy skin are multilayered structures, and can be divided into the epidermis, dermis, and subcutaneous tissue. The epidermis provides a waterproof covering for skin. This layer is not vascularized, and varies in thickness and texture. Beneath the epidermis lies the dermis, which is "tough, flexible, and highly elastic"

(Gray, 1974, p. 1138). In hairy skin, the dermis contains sweat glands, hair follicles, nerve findings, and blood vessels. Beneath the dermis is subcutaneous connective tissue and fat (Cholewiak and Collins, 1991).

The sense of touch is actually a multi-step process. When pressure is applied to the human skin, various end organs beneath the skin change shape. Activation of these receptors causes nerve impulses to travel along the nerve fibers that innervate the receptor. The nerve impulses eventually reach the dorsal root ganglion, where the signal is sent along the spinal cord to the brain stem, and eventually to the somatic sensory cortex, where the sensation of touch is realized (Kandel et al., 2000).

The various afferent units that are believed to create these nerve impulses can be categorized as FA I, FA II, SA I, and SA II. The SA I and SA II afferent units are slowly-adapting, meaning that they will discharge at a rate proportional to the pressure on the skin; more action potentials will be fired when the pressure on the skin is increased, and fewer when the pressure is decreased. In contrast, the FA I and FA II afferent units are rapidly adapting, and respond only to *changes* in pressure. Thus when pressure is increased or decreased, the neurons associated with rapidly-adapting receptors will fire, but they will not respond to a constant pressure (Cholewiak and Collins, 1991).

The afferent units are associated with receptive fields on the surface of the skin. In general terms, if sufficient pressure is applied to an area within a receptive field of an afferent unit, then the unit will create a nerve impulse; outside of this receptive field, no nerve impulse is created. Unfortunately, the picture is not actually this simple, and the receptive field is often not so precisely defined. Regardless, FA I and SA I afferent units

are characterized by having smaller receptive fields, and FA II and SA II afferent units are characterized by having larger receptive fields (Cholewiak and Collins, 1991).

Bolanowski et al. (1988) proposed that the various mechanoreceptors in the skin and the nerve fibers that innervate them combine to form distinct "channels" that differ in terms of their sensitivity to vibrotactile frequency and the associated sensation. Each channel is believed to respond differently to frequency, pressure, skin-surface temperature, stimulus size and duration. However, the ranges of frequencies to which these channels are responsive partially overlap, so vibrotactile sensation is thought to result from activity in all of the channels (Bolanowski et al., 1994).

Bolanowski et al. (1988) proposed that four channels create the sensations of touch in glabrous skin. These channels can be classified as P_g, NP I, NP II, and NP III. The first, P_g channel, is believed to be associated with Pacinian corpuscles, and the nerve impulses are transmitted via PC fibers. They respond best to frequencies in the range of 40 to 800 Hz, with a peak response to frequencies near 300 Hz. P channels are associated with a sensation of "vibration" as reported by subjects (Bolanowski et al., 1988, 1994). Sensations in the NP I channel are believed to be caused by Meissner's corpuscles and transmitted via RA fibers. The NP I channel is associated with frequencies in the range of 10 to 100 Hz, and activating this channel generally produces the sensation of "flutter". The NP II channel may be associated with the SA II fibers and Ruffini end organs. This channel has a range of 15 to at least 500 Hz, and is associated with a "buzzing" sensation. The last channel is NP III, which is believed to be associated with SA I fibers and Merkel cell-neurite complexes. This channel responds to frequencies in the range of 0.4 to 3 Hz, and produces a sensation of "pressure" (Bolanowski et al., 1988, 1994).

In contrast to glabrous skin, Bolanowski et al. (1994) have proposed that hairy skin is only associated with three channels, known as P_h (Pacinian, hairy skin), $NP_{h\ low}$ (non-Pacinian, hairy skin, low frequencies), and $NP_{h\ mid}$ (non-Pacinian, hairy skin, mid frequencies). The P_h channel is similar to the P_g channel found in glabrous skin. This channel is associated with PC nerve fibers and Pacinian corpuscles, although probably those that are located deep within subcutaneous tissue. The P_h channel responds to frequencies in the range of 40 to at least 500 Hz. The $NP_{h\ low}$ channel is thought to be associated with SA II fibers and Ruffini endings, and responds to frequencies in the range of 0.4 – 4 Hz, producing a sensation of "pressure". This is in contrast to glabrous skin, in which the SA II fibers are associated with a range of 15 to 500 Hz. The $NP_{h\ mid}$ channel responds to frequencies ranging from 4 to 150 Hz, producing a sensation of "flutter", and is thought to be associated with RA fibers. Unlike in glabrous skin, the SA I fiber does not appear to be associated with any vibrotactile channel in hairy skin (Bolanowski et al., 1994).

2.3. Measuring the Sense of Touch

2.3.1. Sensitivity

As with all sensory phenomena, there is a threshold below which a tactile stimulus cannot be perceived. This limen, also called the sensory threshold, is a function of several variables, including the frequency of vibration, temperature, contact area, and duration of the stimulus. The different channels differ in their sensory thresholds, which change as a function of their response to conditioning stimuli, as well as variations in stimulus dimensions and skin temperature (Bolanowski et al., 1988).

In glabrous skin, the most sensitive channel is the proposed P_g channel, which is believed to transmit sensations of touch through vibrations affecting Pacinian corpuscles (PCs). At 250 Hz, Pacinian corpuscles can detect vibrations as small as 1 μm (Kandel et al., 2000). The sensitivities of the four channels combine to produce an overall sensitivity level at each frequency. At room temperature, the overall maximum sensitivity occurs between 200 and 300 Hz. In the range of 40 to 100 Hz, the displacement threshold decreases maximally as a function of frequency.

Similar data were found by Bolanowski et al. (1994) when thresholds were measured on the hairy skin of the human forearm. There are many differences in both the types of mechanoreceptors and the numbers of channels found in hairy skin compared to glabrous skin. Still, the sensitivity curve for the forearm, which is composed of hairy skin, has the same overall shape as that for glabrous skin, but with a much lower sensitivity. As before, the peak sensitivity occurs between 200 and 300 Hz, corresponding to the proposed P_h channel. In hairy skin, the location of the maximum slope of sensitivity as a function of frequency occurs in the range of 100 to 200 Hz. The main differences in the shape of the sensitivity curves occur in the lower and middle frequency ranges of 0.4 to 40 Hz.

2.3.2. Discrimination Tests

Other experiments have been performed to determine the ability to distinguish between two tactile stimuli that differ in some respect. Weinstein (1968) performed tests of pressure sensitivity, two-point discrimination, and point-localization, comparing different areas of the body as well as gender differences. The results for point-

localization and two-point discrimination were highly correlated, but both were found to be uncorrelated with pressure sensitivity. For the back, which is of greatest interest in this thesis, a threshold of 40 mm was found for two-point discrimination, and a threshold of about 11 mm was found for point localization. Based on these tests, body parts could be grouped based on similar sensitivity values. For all three tests, the back had similar sensitivity values to the forearm, shoulder, and upper arm. Other general observations include observing greater sensitivity at points farther from the centerline of the body (a proximal-distal sensitivity gradient), as well as greater sensitivity in motile body parts, compared to non-motile parts.

Although new, more accurate methods have since been created for testing static spatial acuity (Johnson and Phillips, 1981), more relevant to the design of tactile displays is vibrotactile acuity. Eskildsen et al. (1969) found a simultaneous and successive two-point vibrotactile threshold to be near 11 mm on the back. Under stroboscopic illumination, it was found that the vibrating motors, or tactors, used in their experiment were in contact with the skin for only about one-third of their period. The tactors depressed the skin 1 mm, and then rose about 3 mm above the skin surface.

2.3.3. Localization

In order to maximize the amount of information that can be transmitted through a tactile display, the display might be designed to allow the user to localize points of stimulation in the display. Localization seems to be only minimally affected by the frequency of the stimulus. In a study by Cholewiak and Collins (2003), seven tactors were placed in a linear array on the arm, and subjects were asked to identify the location

of a tactor, actuated at 100 or 250 Hz. In most cases, performance in this task did not seem to be affected by the frequency of vibration. They found that for young subjects, there was a small increase in localization performance for tactors near the wrist and elbow, when the tactors were driven at 250 Hz instead of 100 Hz. When the tactors were driven at 100 Hz, localization accuracy near the wrist and elbow was around 70%, whereas when they were driven at 250 Hz, localization accuracy at the wrist and elbow increased to 75 to 80%. For tactors in the middle of the array, and for older subjects at all tactor locations, frequency had no effect on localization.

Localization may also not be dependent on the underlying tissue type (Cholewiak et al., 2004). In a set of localization experiments, twelve tactors were attached to a belt worn by the subjects. The localization tests were performed with the belt in two locations: around the waist, and 10 cm higher, on the bottom of the rib cage. The location of the belt had no effect on localization performance. Those tactors that were positioned over the abdomen were perceived as accurately when the belt was moved up, placing the tactors on top of the ribs. Additionally, the localization results showed front-to-back symmetry. Tactors that were placed over the ribs or abdomen had very similar localization values to the corresponding tactors that were on the back's muscular tissue. This study will be discussed in further detail below.

Although frequency and tissue type do not seem to affect localization, the specific locations of the tactors in an array do seem to have a strong effect on localization. Cholewiak and Collins (2003) found that tactors near the wrist and elbow were more easily identified than tactors in the middle of the forearm. Tactors near the wrist and elbow were localized with accuracies greater than 65%, whereas tactors in the middle of

the array were localized with accuracies ranging from 30 to 40%. This effect persisted even when the elbow was placed in the middle of the array, thus demonstrating that this is not simply a boundary effect. Location similarly affected localization when tested around the torso. Using the belt display described above, Cholewiak et al. (2004) showed that localization was greatest at the spine or naval, with accuracies of 98% and 96%, respectively. Localization performance decreased with increasing distance away from the spine and naval. Thus the worst localization occurred at the sides of the body, with accuracies of 67% and 71%.

This increased localization performance near the wrist, elbow, spine, and navel may be caused by a phenomenon called "anchor points", in which certain parts of the body act as reference locations for localization. One category of proposed anchor points are points of mobility, such as those located at the joints of the wrist or elbow. The spine and naval are not points of mobility, so other reasons are proposed for their behavior as anchor points. One proposed explanation is that stimuli on the spine or naval may be transmitted to both cerebral hemispheres, thus making these locations distinguishable from nearby locations that are only transmitted to one hemisphere (Van Erp and Werkhoven, 1999). Another possible explanation is simply that the spine and naval are along the midline of the body, and thus provide a "stable frame of reference . . . [for] spatial awareness" (Cholewiak et al., 2004).

In order to improve spatial localization, artificial anchor points may be created in a number of ways. In one experiment, Cholewiak et al. (2004) placed a belt of tactors in a semicircle in the front of the body, and in another experiment, the belt was placed in a semicircle in the back. Localization in this setup was compared to localization when

tactors were placed around the entire waist. When tactors were positioned in a semicircle in the front or back of the body, the endpoints of the array became unique, identifiable locations. Localization accuracies at the sides were previously 67% and 71%, but using only a semicircle, the localization accuracies at the sides increased to values ranging from 75% to 90%. In contrast, when the belt was placed in a semicircle on the right or left of the body, in which the sides did not act as anchor points, localization performance at the sides remained below 75%. These experiments demonstrate that the endpoints of the array can act as reference points and improve localization performance.

Localization can also be improved by creating artificial anchor points by introducing tactors with distinct characteristics. In an experiment by Cholewiak and Collins (2003), seven tactors were placed along the forearm, as described above. Localization was first tested with the tactors either all actuated at 100 Hz or all actuated at 250 Hz. Due to the anchor point phenomenon described above, localization accuracy was found to be highest at the ends of the array near the wrist or elbow (greater than 65%), and lowest in the middle of the array (30 to 40%). Next, the middle tactor was actuated at a different frequency from the other six tactors, and a localization test was again performed. In other words, if the other six tactors were actuated at 250 Hz, the middle tactor was actuated at 100 Hz, and vice-versa. Although subjects were not informed of the presence of a unique tactor, actuating this tactor at a unique frequency significantly improved localization. This effect was even more significant in younger subjects, in which localization at the unique tactor increased from less than 40% to greater than 60%.

2.3.4. Frequency Discrimination

In the aforementioned test, localization improved when one tactor was actuated at a different frequency from the other six tactors. One might wonder how different the frequency of activation needs to be in order for localization to improve. A reasonable value for this might be the just-noticeable-difference (jnd) determined from frequency discrimination tests. In an experiment by Mahns et al. (2006), a probe would vibrate against the forearm at some frequency, and after a pause, the probe would vibrate again. The task would be to report whether the frequency of the second stimulus was the same or higher than that of the first stimulus. The jnd was calculated by averaging the frequencies at which the subject correctly said "higher" 75% and 25% of the time. At frequencies of 20, 50, 100, and 200 Hz, the jnd was found to be 7.6, 18.0, 27.2, and 33.9 Hz, respectively. Presumably, tactors would have to differ by at least this amount in order to be used as artificial anchors.

2.3.5. Learning

It is possible that, through repeated trials and feedback, subjects can learn to localize with increasing accuracy. One experiment in which this was tested was performed by Cholewiak et al. (2004), using the belt tactor array described above. Subjects were tested for 10 consecutive days, with 300 trials each day, and with feedback after each trial. Mean improvement of localization accuracy over all trials and people was less than 2% per day. However, while some subjects stopped improving within the first 3000 trials, other subjects were still improving even after all 3000 trials, so the mean is not indicative of individual learning rates.

2.4. Tactor Design

Many different types of tactors have been tested for tactile displays, and sometimes the type of tactor can affect performance in identifying spatial patterns of vibration. In a set of experiments on the forearm and torso, Piateski (2005) tested pancake tactors with rigid and flexible mountings, as well as cylindrical tactors. There was no significant difference between the subjects' ability to identify vibration patterns when using the pancake tactors with flexible mountings compared to rigid mountings. However, the ability to identify patterns presented using the cylindrical tactors was better than when using either of the pancake tactor mountings. In another experiment comparing just the cylindrical tactors to the pancake tactors with rigid mountings, the cylindrical tactors resulted in an accuracy of 93.5% in identifying vibration patterns, whereas the pancake tactors resulted in an accuracy of only 85% (Piateski & Jones, 2005).

Tests performed by Redden et al. (2006) compared performance using three different tactile displays in static localization tests. Tests were performed with the user either stationary or moving through a woodland individual movement techniques (IMT) course. All three tactile display systems used a belt of eight tactors, worn around the waist. The first system, named TACTICS 1, used the C-2 vibrotactile transducer (Engineering Acoustics), which consisted of an inner mass that moved perpendicular to the surface of the skin, and a stationary outer ring. The second system, TACTICS 2, consisted of the same tactors used in TACTICS 1, but the intensity of vibration was reduced to create the same perceived intensity of vibration as the third system, WTCU.

The tactors in WTCU were inertial shaker motors, and are the same tactors that were used by Piateski and Jones (2005).

Although there was no statistically significant difference in localization during static tests, a significant difference in performance between tactor types appeared in the IMT course experiment. The TACTICS 1 system yielded the greatest response accuracy (78.7%), followed by TACTICS 2 (70.7%), with the WTCU system performing worst (48.8%). Subjects also gave highest subjective assessment scores to TACTICS 1, with second highest scores received by TACTICS 2 and worst scores received by WTCU. The greater localization accuracy of TACTICS 2 over WTCU suggests that a vibrotactile transducer which creates perpendicular motion leads to better localization performance than an inertial shaker motor. Additionally, the greater localization accuracy of TACTICS 1 over TACTICS 2 suggests that stimuli of greater intensity are easier to localize.

Mortimer et al. (2007) proposed various requirements for tactors used in tactile displays. One suggested requirement is that the displacement produced should be independent of loading. In a test using eccentric mass motors, the displacement of these tactors was found to drastically decrease with a loading of less than 3 g. In contrast, when using a linear actuator, the displacement was found to increase as a function of loading. Mortimer et al. thus suggested that linear actuators might be better suited for tactile displays than eccentric mass motors.

2.5. Skin

2.5.1. Surface Waves in Skin

Vibrations imposed on the skin surface, such as those from a tactile display, create traveling waves. Franke (1951) used stroboscopic illumination to view these waves, which enabled measurement of the group velocity of the waves. He found that the group velocity ranged from 2 to 40 m/s. However, the velocity of these waves depends on a number of factors, including frequency, skin temperature, and the constituency of the underlying tissue (Cholewiak et al., 2001).

Traveling waves are produced because skin is a viscoelastic material. When energy is imposed on a piece of skin, some of it will be transmitted, and some of it will be absorbed and used to restore the skin to its original state. The transmitted energy travels in a wave, and the shearing forces produced diminish at a rate proportional to the inverse square of the distance from the source (Cholewiak and Collins, 1991)

Although the intensity of these waves diminishes with distance, vibrations on the finger can be seen traveling up the arm, many centimeters from the source (Cholewiak and Collins, 1991, 2003). Thus traveling waves may excite afferent units that are located far from the source of the waves, possibly contributing to errors in localization. Attempts to reduce this effect have been made by placing a static ring, known as a surround, on the skin around the source of the vibration, to dampen the traveling waves. While this may reduce the degree to which remote mechanoreceptors located in the dermis are affected by the vibration, receptors located deeper within tissue may still be affected (Cholewiak and Collins, 1991). Because this may lead to errors in localization, characterizing this traveling wave is important in the design of tactile displays.

2.5.2. Material Properties of Skin

In order to characterize the traveling wave produced from the vibration of a tactile display, the material properties of skin must be modeled. Many different experiments have been performed to measure the material properties of skin. Agache et al. (1980) applied torques to the forearms of 138 subjects with ages ranging from 3 to 89 in order to measure the stiffness of the skin. Torques were applied by rotating a disc fixed to the skin, and the resulting angle of the disc was measured. Young's modulus was found to increase with age, ranging from 420 kPa for the youngest subjects to 850 kPa for the oldest subjects.

Animal and artificial substitutes are often used to simulate the material properties of human skin. Studies have shown that pig skin and human skin have similar material properties (Shergold et al., 2006), and that the thickness of human and pig dermis is similar. On the back, human dermis averages about 4 mm, and for the pig it ranges from 1 mm to 6 mm. In contrast, rat or mouse dermis is generally only about 0.6 mm thick.

Silicone rubbers that simulate the material properties of human skin are also often used instead of animal skin (Leskovsky et al., 2006, Shergold et al., 2006). Silicone rubbers have a longer lifetime than isolated animal skin, and thus are better suited for repeated testing. Additionally, they are generally more isotropic and homogenous, and respond less to changes in temperature, making them easier to model. Experiments have shown that "the constitutive response and strain rate sensitivity of silicone rubber is close to that of [human] skin" (Shergold et al., 2006). Thus, silicone rubbers are often used for experiments as a substitute for human skin when longevity, consistency, and ease of modeling are important factors.

3. Tactors for a Tactile Display

A wirelessly controlled, wearable tactile display has been designed by Jones et al. (2006) for use in navigation. The display is controlled by a Wireless Tactile Control Unit (WTCU), which receives navigational commands through a Bluetooth connection from a computer. The WTCU converts these navigational commands into vibration patterns which are presented to the user. This display, shown in Figure 1, uses 4x4 grid of vibrating motors, or tactors, on the user's back to present the vibrotactile patterns.

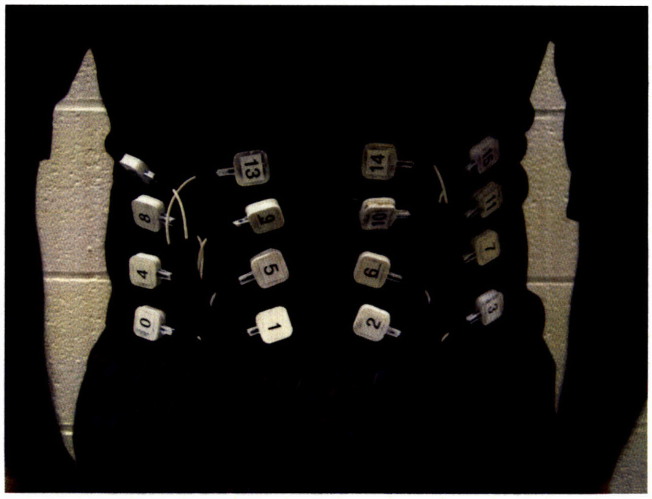

Figure 1: Tactile display, similar to that used by Piateski and Jones (2005), being worn on the back

This thesis explores the mechanics of the vibrotactile display developed by Lockyer (2004). Measurements were made of the frequencies and forces produced by the tactors used in this tactile display. A model of the tactors was designed, and the tactor motion was simulated. The results from these simulations were compared to actual tactor measurements, in order to understand how various parameters affect the motion of the tactors. To determine how these tactors behave when placed on skin, a silicone substrate was formed that had similar mechanical properties to skin. The tactors were attached to

this substrate, and the accelerations of these tactors were measured. Acceleration was also measured at various points on the silicone platform, in order to describe the traveling wave that is created from the vibration of the tactors.

3.1. Tactor Characterization Experiments

3.1.1. Tactor Description

The tactors used in the tactile display are pancake motors with a diameter of 14 mm and a thickness of 3.5 mm (Sanko Electric, Model 1E120), shown in Figure 2a. At 3 V, they are rated to oscillate at a rate of at least 4500 rpm (75 Hz), with a current of 45 mA. The recommended operating range is 2.5 – 3.8 V, and in the WTCU they are driven at 3.3 V. Each motor weighs 2.08 g. When a DC voltage is applied to the motor, an eccentric mass, shown in Figure 2b, rotates around the center of the motor. The oscillation of the eccentric causes the entire tactor to vibrate. The direction of the force produced by the vibrating tactor varies as the eccentric rotates. The motor has two solder pads that connect to two wires, which are used to power the motor (Figure 2c).

Before the motors are attached to the vest, they are encased in 1.5 mL of liquid plastic (Smooth-On, Smooth-Cast 300) as shown in Figure 2d. This is done to "make the tactors more robust and increase the contact area between the tactor and the skin" (Piateski, 2005). The encased tactor has dimensions of 19 mm x 19 mm x 6 mm. An encased tactor weighs 3.31 g, so the encasing adds 1.23 g to the weight of the motor, increasing the weight by 59%.

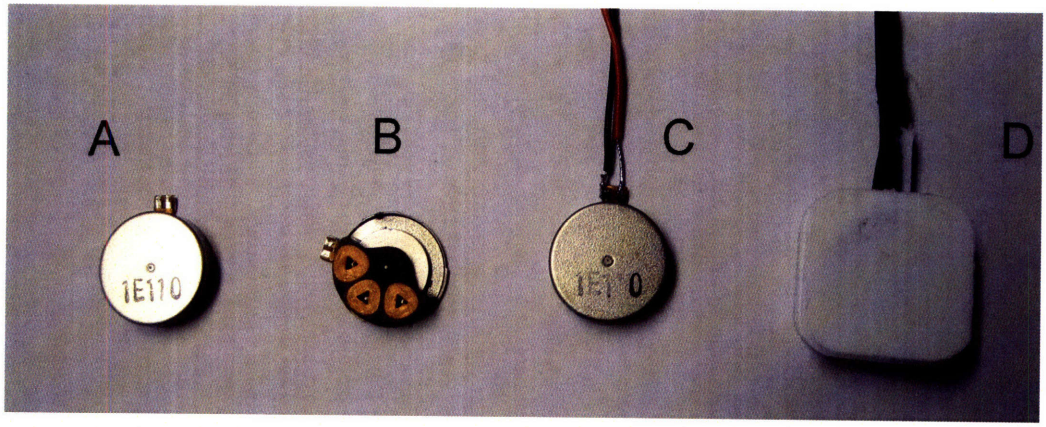

Figure 2: (a) the outside of an unencased motor; (b) the inside of a motor, showing the eccentric mass; (c) unencased motor with wires attached; (d) encased tactor

3.1.2. Equipment for Tactor Characterization

In order to characterize the forces that are imposed on skin during vibration, the forces produced by the tactors were measured. An experimental setup was designed to automate these measurements. To reproduce the voltages used by the WTCU (Lockyer, 2004), a voltage regulator (National Semiconductor, LP2592AIN-3.3) was used to regulate the voltage applied to the tactors at 3.3 V. The regulator used consistently output a voltage of 3.291 V.

The tactors were controlled using an analog breakout board (National Instruments, BNC-2080) and a MOSFET transistor (International Rectifier IRLZ44), as shown in Figure 3. The breakout board drove the transistor, which acted as a switch. When the computer output 4 V, current flowed through the transistor, driving the tactor at 3.3 V. When the computer output 0 V, the tactor voltage was floating, and the tactor did not vibrate.

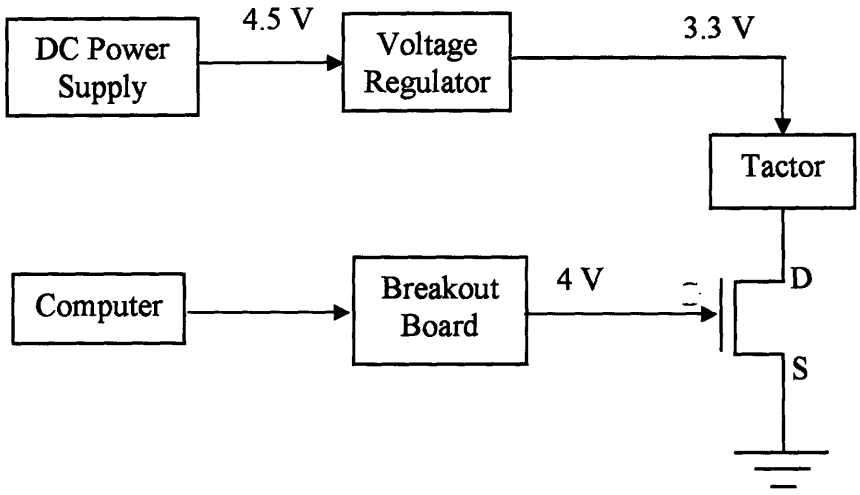

Figure 3: Schematic of the experimental setup for driving the tactor

Epoxy was used to attach each tactor to a screw, which was then attached to an impedance head (Bruel and Kjaer, Type 8001) as shown in Figure 4. The impedance head measured the force produced by the tactor when vibrating, and output a voltage proportional to the force. This voltage was sent to a charge amplifier (Bruel and Kjaer, Type 2635), which filtered and amplified the measurement. The data were then sent to a breakout board (National Instruments, BNC-2080), which sent the data to a computer, where they were recorded in a text file at a sampling rate of 10 kHz.

To keep the impedance head stationary, a jig was machined to bolt the impedance head to an optical board (Technical Manufacturing Corporation, 77-107-12R), as shown in Figure 5. The mass and stiffness of the optical board kept the impedance head relatively stationary. The tactors were tested in three different configurations. In the first configuration, shown in Figure 4, the forces produced by unencased tactors were measured. Screws were attached to the side of the tactors, to measure the forces produced in the plane of rotation of the eccentric. The next configuration, shown in

Figure 5, measured the forces produced by encased tactors, again in the plane of rotation of the eccentric. Finally, screws were attached to the faces of the tactors, as shown in Figure 6, to measure the forces produced by the tactor in the direction normal to the surface of the skin (as seen in Figure 1).

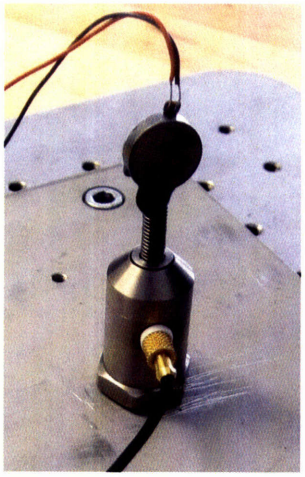

Figure 4: Tactor attached to the impedance head, to measure the force produced during vibration

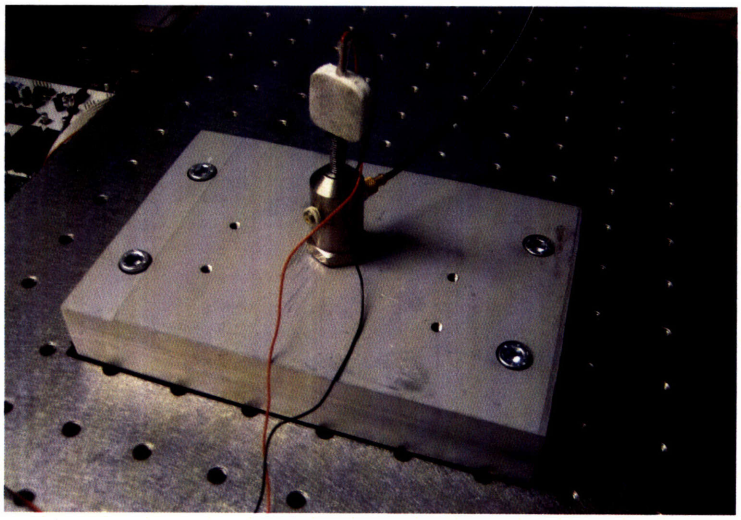

Figure 5: Impedance head bolted to a jig, which was bolted to an optical board. This setup helped to keep the impedance head in place during tests.

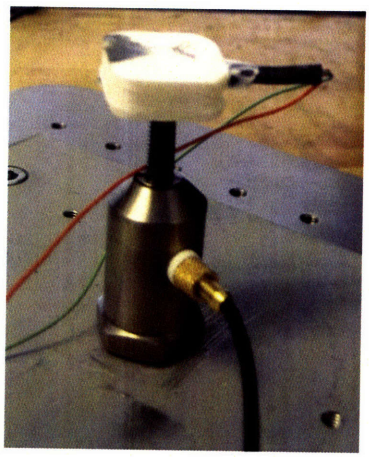

Figure 6: Screw attached to face of tactor, to measure forces produced by the tactor in the direction normal to the surface of the skin

3.1.3. Procedure

The experimental setup described in section 3.1.2 was used to characterize the behavior of the tactors under controlled conditions. A set of nine unencased tactors and 14 encased tactors were analyzed to characterize the ranges of frequencies and forces that are created by the tactors. During normal operation of the WTCU, tactors are turned on for only 500 ms. Thus these experiments focus on the initial tactor behavior. Each tactor was turned on for 10 seconds and then off for 10 seconds. This was repeated 10 times for each tactor. However, because of possible transient effects due to warm-up during the first tactor trial, only trials 2 through 10 were analyzed. In addition, only data from t = 5 to t = 10 seconds were analyzed for each trial.

3.1.4. Results

Figure 7 shows a plot of the oscillating force produced by an unencased tactor during the first 2 seconds of operation, measured in the plane of rotation of the eccentric. The amplitude of the oscillating force started at 0 N and increased to a value of 1.13 N.

There was an overshoot at a time of 0.8 seconds, which can be seen more clearly in Figure 8. The 2% settling time occurred after this overshoot, at 1.226 seconds. The force is oscillating at a rate of 136.3 Hz, which can be seen more clearly in Figure 9 below.

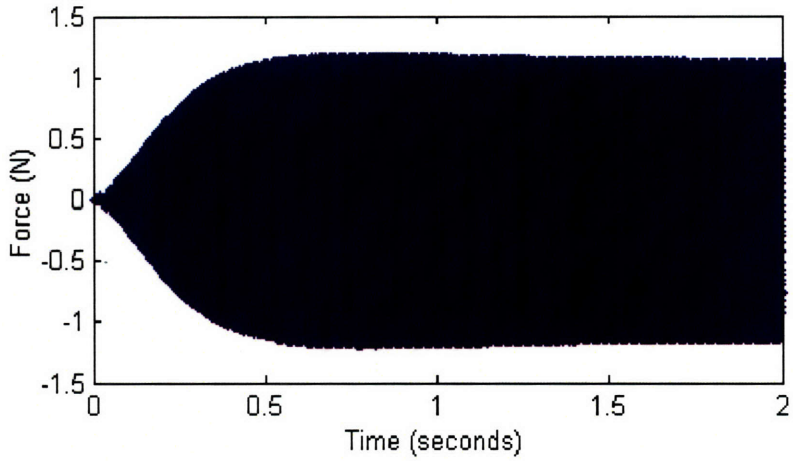

Figure 7: Force data for a tactor, as recorded by the impedance head, during the first 2 seconds after being turned on.

Figure 8 shows the amplitude of the oscillating force produced by this tactor. The overshoot can be clearly seen in this figure, at 0.8 seconds. In this example, the overshoot has an amplitude of 104% of the final value, which is 1.13 N.

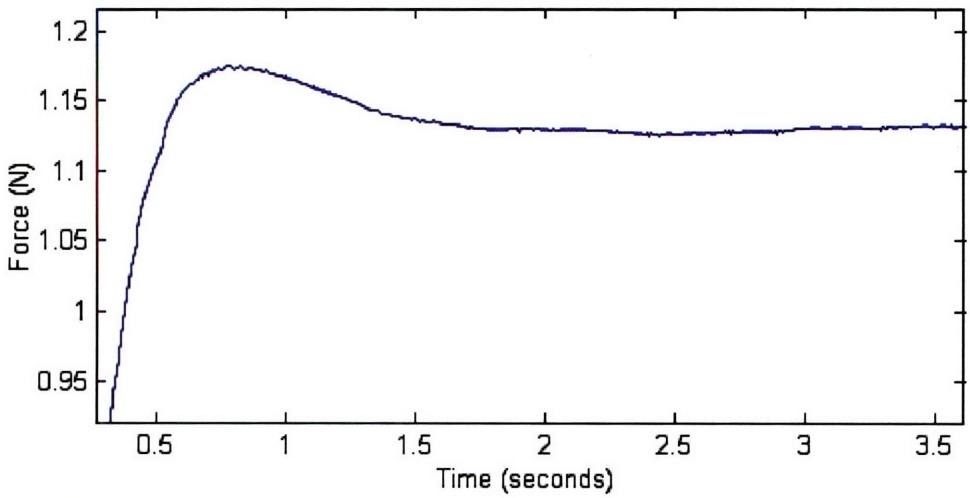

Figure 8: Amplitude of the oscillating force produced by a tactor.

Figure 9 shows the steady-state operation of this tactor. As the eccentric rotates, the force oscillates between 1.13 N and -1.13 N. A Fourier transform of these data, shown in Figure 9, reveals the peak frequency of oscillation of 136.3 Hz.

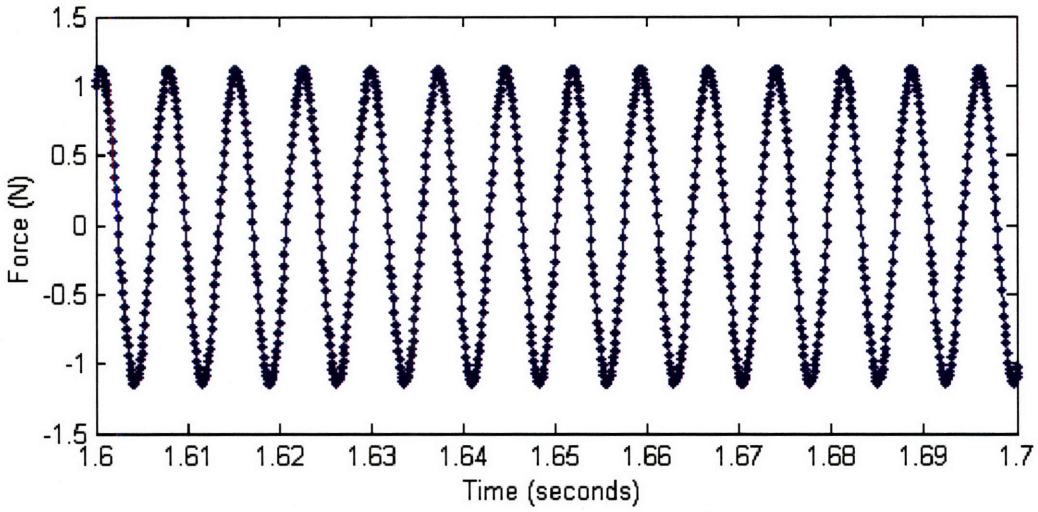

Figure 9: Steady-state oscillation of a tactor

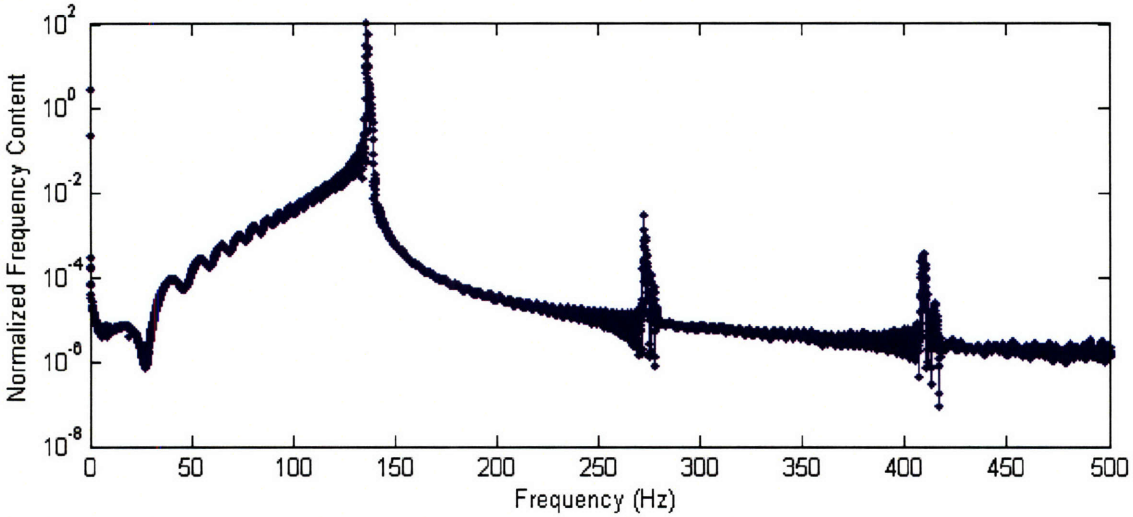

Figure 10: Frequency content of a tactor, plotted on a semi-log scale, revealing the peak frequency of oscillation

3.1.5. Characterization of Encased and Unencased Tactors

Figures 11 through 13 summarize the frequency data collected for nine unencased tactors and 14 encased tactors. For each tactor, data from nine trials were analyzed. Figure 11 illustrates the data obtained with the setup shown in Figure 4, in which the

measurements are from unencased tactors in the plane of rotation of the eccentric. Figure 12 shows the data obtained using the setup shown in Figure 5, measuring the force output of encased tactors in the plane of rotation of the eccentric. Figure 13 illustrates the data obtained with the setup shown in Figure 6, measuring the force produced by encased tactors in the direction normal to the plane of rotation. Each number on the x-axis represents a different tactor, and each point on the y-axis shows the peak frequency of the tactor's oscillation for a single trial. The data in Figures 11 and 12 are rank ordered by mean peak frequency. The tactor numbers in Figure 13 are the same as those in Figure 12.

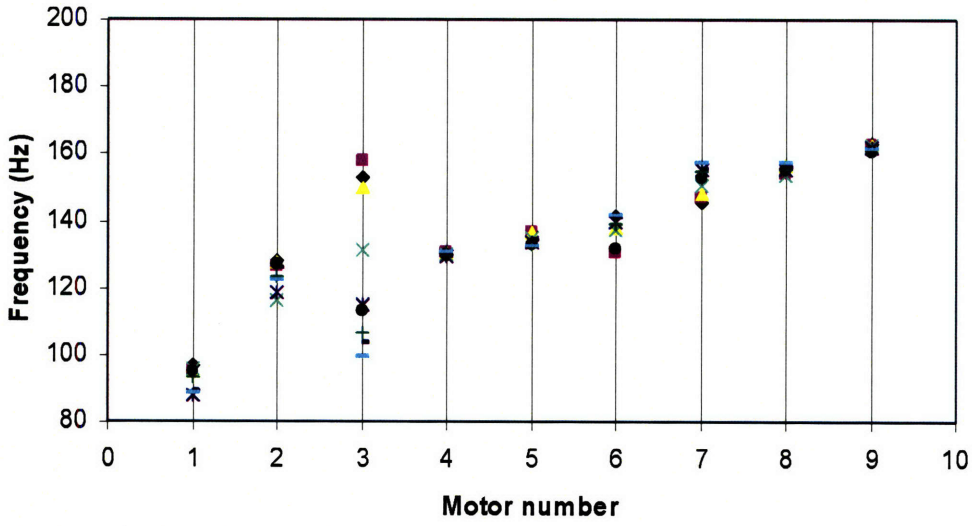

Figure 11: Peak frequencies on each of nine trials for nine unencased tactors, with the measurement performed in the plane of rotation of the eccentric

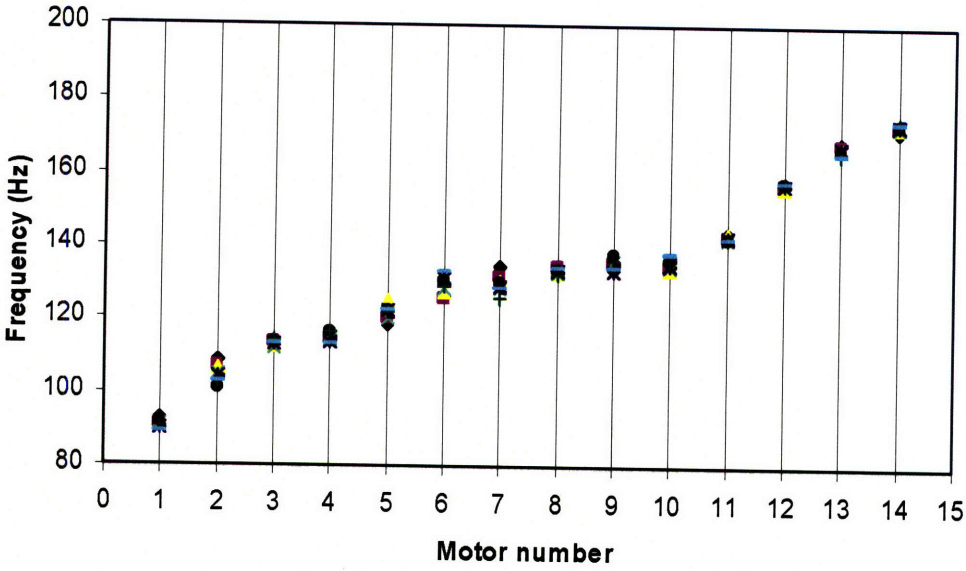

Figure 12: Peak frequencies on each of nine trials for 14 encased tactors, with the measurement performed in the plane of rotation of the eccentric

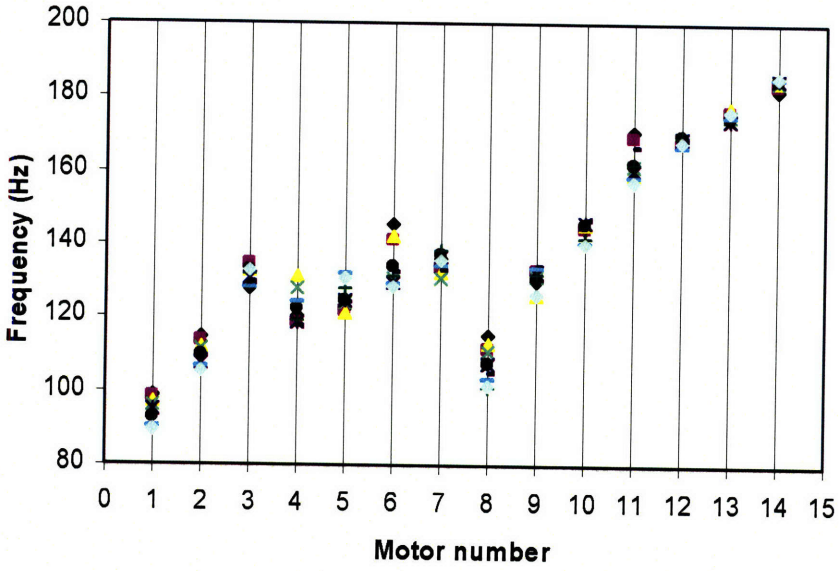

Figure 13: Peak frequencies on each of nine trials for 14 encased tactors, with the measurement normal to the plane of rotation of the eccentric

The Fourier transform for each tactor trial revealed the peak frequency of vibration. For the nine unencased tactors tested, the mean peak frequencies ranged from 92.9 to 162.0 Hz, with an overall mean of 134.9 Hz (SD: 20.8 Hz). For the 14 encased tactors tested, when tested in the plane of rotation, the mean peak frequencies ranged

from 90.5 to 173.5 Hz, with an overall mean of 131.9 Hz (SD: 23.2 Hz). When tested normal to the plane of rotation, the mean peak frequencies ranged from 93.7 to 184.7 Hz, with an overall mean of 137.5 Hz (SD: 26.9 Hz).

In general, an individual tactor did not oscillate at exactly the same frequency each time it was turned on. For each tactor, the difference between the maximum and minimum frequencies was calculated to give a frequency range. The frequency range for unencased tactors varied from 1.2 to 58.6 Hz, with an overall mean of 12.6 Hz (SD: 17.8 Hz). However, there was one tactor (tactor 3) with a range of 58.6 Hz, which is 2.6 standard deviations away from the mean. If this tactor is removed from the analysis, then the range of the remaining eight tactors varied from 1.2 to 12 Hz, with an overall mean of 6.8 Hz (SD: 4.5 Hz). The frequency range for the 14 individual encased tactors, tested in the plane of rotation, varied from 1.2 to 8.8 Hz, with an overall mean of 4.3 Hz (SD: 2.5 Hz). The frequency range for the 14 encased tactors, when tested normal to the plane of rotation, varied from 3 to 17.2 Hz, with an overall mean of 9.0 Hz (SD: 4.6 Hz).

For each tactor, the forces produced were recorded on each trial. Figures 14 through 16 show the mean force data for all nine unencased tactors and 14 encased tactors. Each number on the x-axis represents a different tactor, and each point on the y-axis shows the mean amplitude of the oscillating force produced in a single trial. Figure 14 shows the forces produced by the unencased tactors in the plane of rotation of the eccentric. Figure 15 shows the forces produced by the encased tactors in the plane of rotation of the eccentric. Figure 16 shows the forces produced by the encased tactors normal to the plane of rotation of the eccentric. The numbering used in each of these figures is the same as that used in figures 11 through 13.

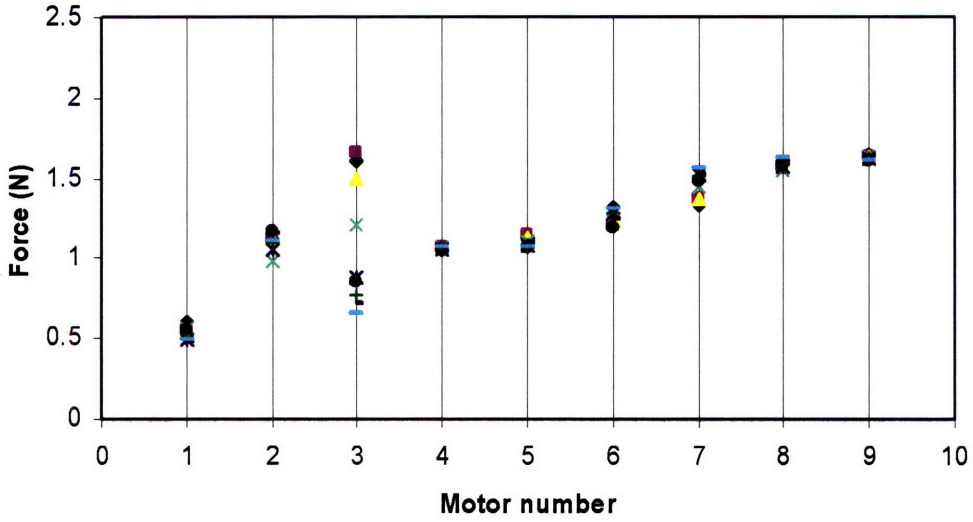

Figure 14: Forces produced on each of nine trials for nine unencased tactors, with the measurement performed in the plane of rotation of the eccentric.

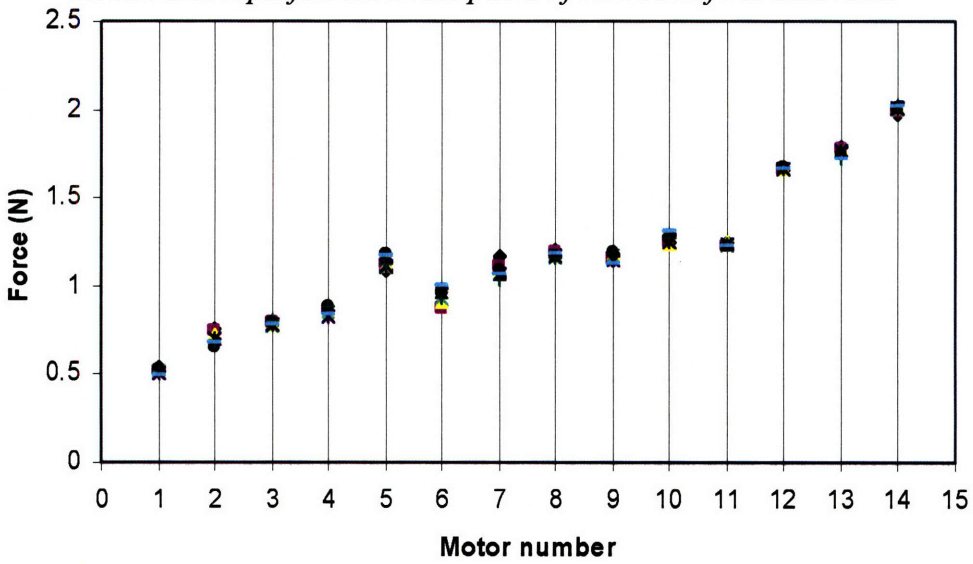

Figure 15: Forces produced on each of nine trials for 14 encased tactors, with the measurement performed in the plane of rotation of the eccentric.

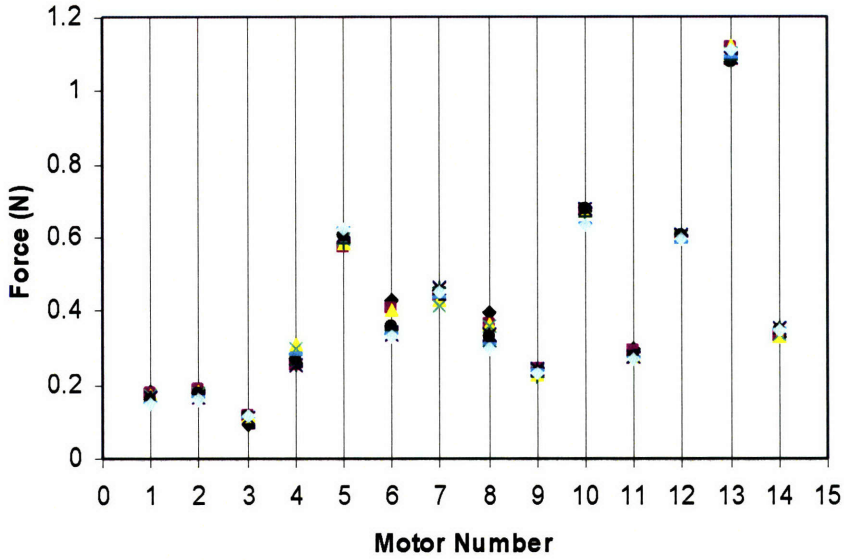

Figure 16: Forces produced on each of nine trials for 14 encased tactors, with the measurement normal to the plane of rotation of the eccentric.

For the nine unencased tactors tested in the plane of rotation of the eccentric the mean amplitude of the forces ranged from 0.54 N to 1.63 N, with an overall mean of 1.20 N (SD: 0.33 N). For the 14 encased tactors tested in the plane of rotation the forces ranged from 0.52 N to 2.01 N, with a mean of 1.16 N (SD: 0.42 N). In the direction normal to the plane of rotation, the mean forces produced by encased tactors ranged from 0.11 to 1.10 N, with a mean of 0.41 N (SD: 0.26 N).

An individual tactor does not produce exactly the same force each time it is activated. For each tactor, the difference between the maximum and minimum forces was calculated to give a force range. The force range for an individual unencased tactor varied from 0.02 N to 1.00 N, with a mean of 0.21 N (SD: 0.30 N). Again, tactor 3 is aberrant, with a force range of 1.00 N, which is again 2.6 standard deviations away from the mean. If this tactor is removed from the analysis, then the force range of the remaining eight tactors varied from 0.02 to 0.23 N, with an overall mean of 0.11 N (SD: 0.07 N). The force range for the nine individual encased tactors, in the plane of rotation,

varied from 0.01 N to 0.13 N, with a mean of 0.07 N (SD: 0.04 N). For the encased tactors, in the direction normal to the plane of rotation, the force range varied from 0.02 N to 0.10 N, with a mean of 0.04 N (SD: 0.03 N).

3.1.6. Comparison of Encased and Unencased Tactors

The overall mean peak frequency for the encased tactors was 3 Hz lower than that of the unencased tactors. Also, the overall force produced for the encased tactors was 40 mN lower than that of the unencased tactors. The differences between the encased and unencased tactors are within the range of variation within each type. In order to determine if the differences between the encased and unencased tactors tested were due to random variation, a two-sample *t*-test was performed. A two-tailed t-test performed on the mean peak frequencies recorded for each tactor showed no statistically significant difference between the encased and unencased tactors ($t(21) = 0.3107$, $p > 0.05$). A similar test comparing the forces produced by the tactors indicated that there was no statistically significant difference in the forces produced by encased and unencased tactors ($t(21) = 0.2410$, $p > 0.05$). These results indicate that encasing a tactor did not have a significant effect on the mean force or frequency produced by the tactor.

Even stronger evidence that encasing a tactor did not change its mean force or frequency can be seen by plotting the relationship between force and frequency for all encased and unencased tactors. Figure 17 shows a plot of the measured peak frequencies and forces, for all 207 trials, consisting of 81 trails from the unencased tactors and 126 trials from the encased tactors. Using the method of least-squares, the relation between force and frequency was fitted to the equation

$$f = 124.7 * n^{0.4839},$$

where f is the frequency in Hz, and n is the force produced by the tactor, in Newtons. The coefficient of determination for this model is 0.97.

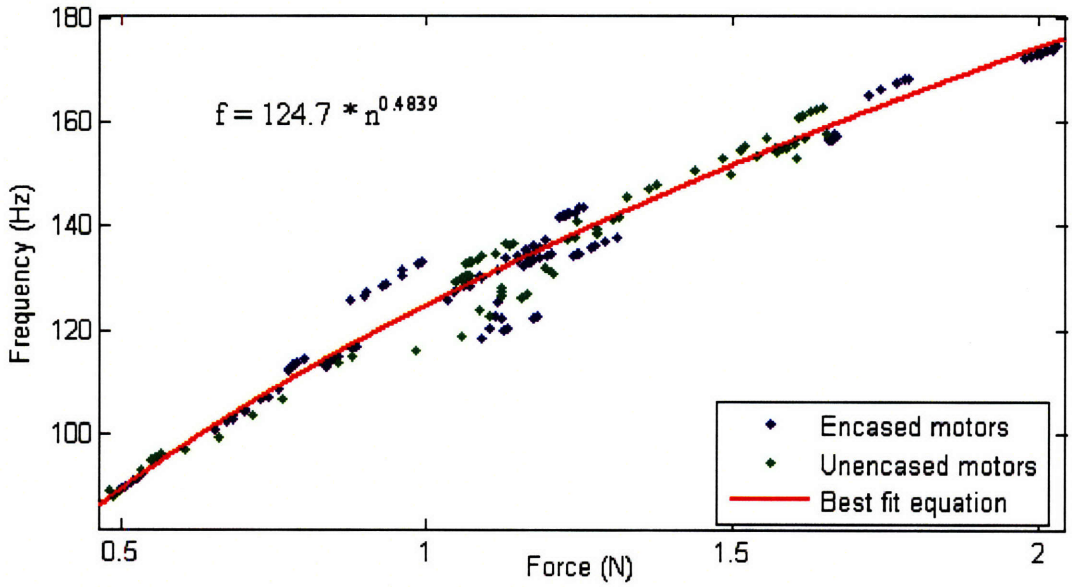

Figure 17: Peak frequency, as a function of the mean force produced by a tactor, for all tactor trials. Unencased tactor trials are shown in green; encased tactor trials are shown in blue; the red line is a power function fit to these data

It is noteworthy that 97% of the variance of the combined encased and unencased tactor data can be accounted for by this equation. This indicates that the differences between all 23 tactors tested can probably be attributed to differences in the friction and coils inside each tactor, rather than differences caused by the encasing process. Additionally, differences between trials for an individual tactor are probably also a result of a changing coefficient of friction inside the motor. This variation in friction might be caused by temperature changes or small amounts of dirt within the motor casing. The effect of changing the damping coefficient will be explored in more detail in the tactor model, below.

It is also apparent that the encased tactors are more consistent than the unencased tactors (compare figures 14 and 15). There was one unencased tactor that had a force and frequency range that was 2.6 standard deviations away from the respective ranges of the rest of the unencased tactors. Without this aberrant tactor, the mean range of peak frequencies for the unencased tactors was 6.8 Hz (SD: 4.5 Hz), whereas the mean range of peak frequencies for the encased tactors was 4.3 Hz (SD: 2.5 Hz). Similarly, the mean range of forces produced by unencased tactors, without the aberrant tactor, was 0.11 N (SD: 0.07 N), whereas the mean range of forces produced by encased tactors was 0.07 N (SD: 0.04 N). Although these differences are small, they do provide support for encasing the motors.

There are several possible explanations for why the encased tactors were more consistent than the unencased tactors. Variations in the forces and frequencies of unencased tactors may be caused by temperature changes, which change the coefficient of friction inside the tactor. Perhaps the encasing helps to keep the temperature of the encased tactors at a constant level, keeping the coefficient of friction at a constant level, and causing the encased tactors to be more consistent. It is possible that the encasing acts as a conductor and draws heat away from the tactor as it is heating up during operation. It is also possible that the encasing acts as an insulator, thus keeping the tactor at a constant temperature despite fluctuations in the room temperature.

3.1.7. Comparison of Planar and Normal Directions for Encased Tactors

Figure 18 compares the mean peak frequencies normal to the plane of rotation with those in the plane of rotation, for all 14 encased tactors. For 12 of the 14 tactors

tested, a higher peak frequency was measured normal to the plane of rotation than in the plane of rotation. The peak frequency measured normal to the plane of rotation was on average 5.6 Hz higher than that measured in the plane of rotation. The cause of this offset is unknown, and may be due to the complex nature of the force in the normal direction, as will be discussed below.

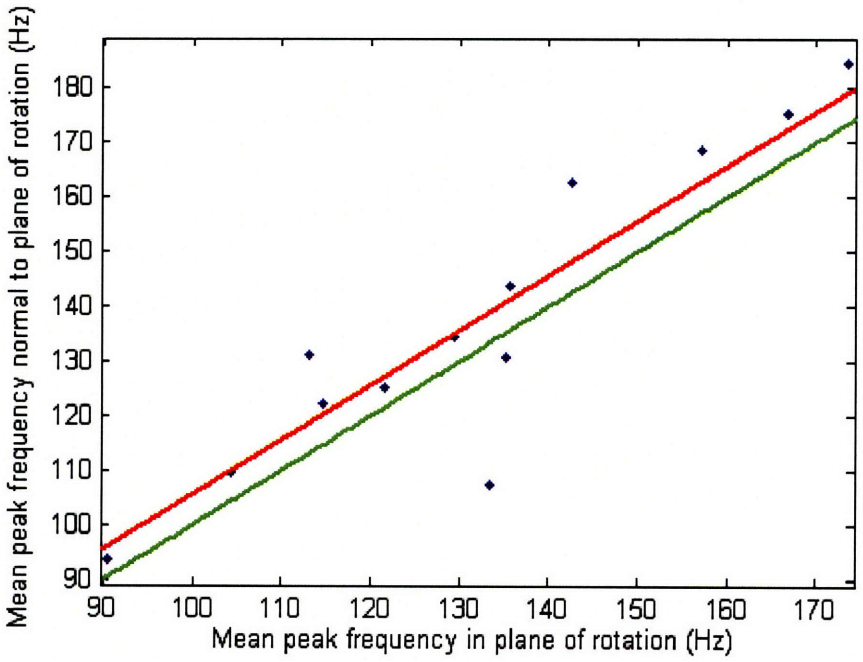

Figure 18: Peak frequency normal to plane of rotation versus peak frequency in the plane of rotation. The red line shows the best fit for a line of slope 1 with a constant offset. The green line has a slope 1, with no offset.

For the direction normal to the plane of rotation, a frequency-force curve is shown in Figure 19, for all 126 trials from the 14 encased tactors. The data do not fall on a single curve, as was the case for the direction within the plane of rotation. Thus the forces produced normal to the plane of rotation are caused by something more complex than simply a varying coefficient of friction.

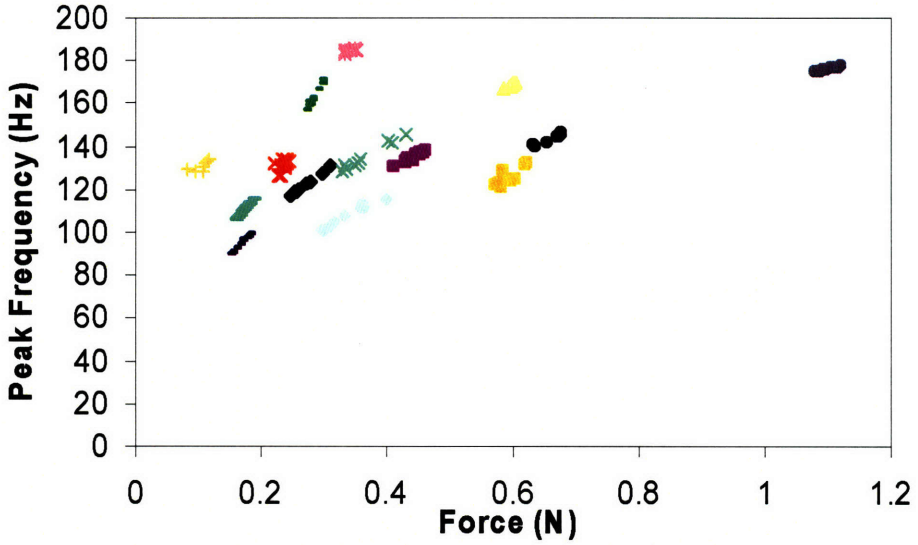

Figure 19: Peak frequency, as a function of the mean force produced by a tactor, for all 14 encased tactors, in the direction normal to the plane of rotation

It is important to note that meaningful data were still obtained when looking at the forces produced by individual tactors in the direction normal to the plane of rotation. Figure 20 shows that for individual tactors the force produced still increased as the voltage increased. Thus in the direction normal to the plane of rotation, a force-frequency curve can be obtained for an individual tactor by varying the voltage, as shown in Figure 21. As the voltage is increased, a greater torque is produced, which increases the rotational velocity of the eccentric. This has the effect of increasing the force produced by the tactor, even when measured normal to the plane of rotation, as well as increasing the peak frequency. Thus although there are significant and complex variations between tactors when considering the forces in the direction normal to the plane of rotation, these data are still meaningful when viewed in the context of a single tactor.

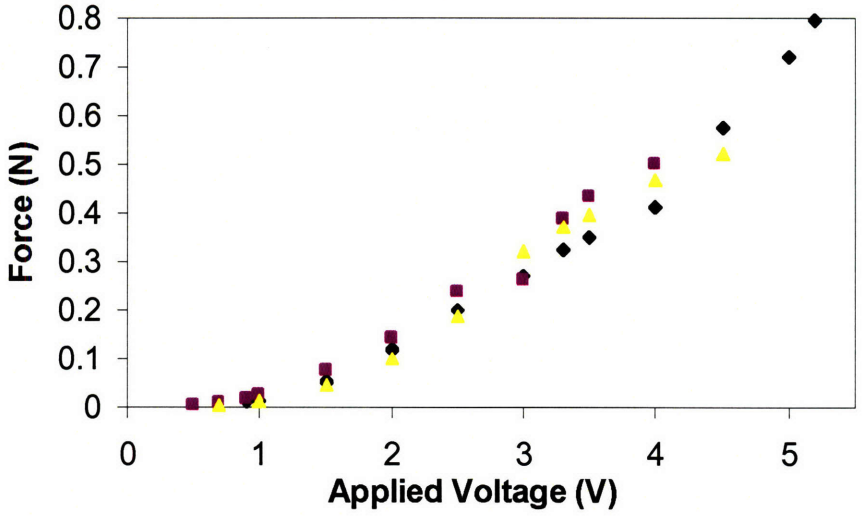

Figure 20: Force as a function of voltage for three tactors measured in the direction normal to the plane of rotation of the eccentric

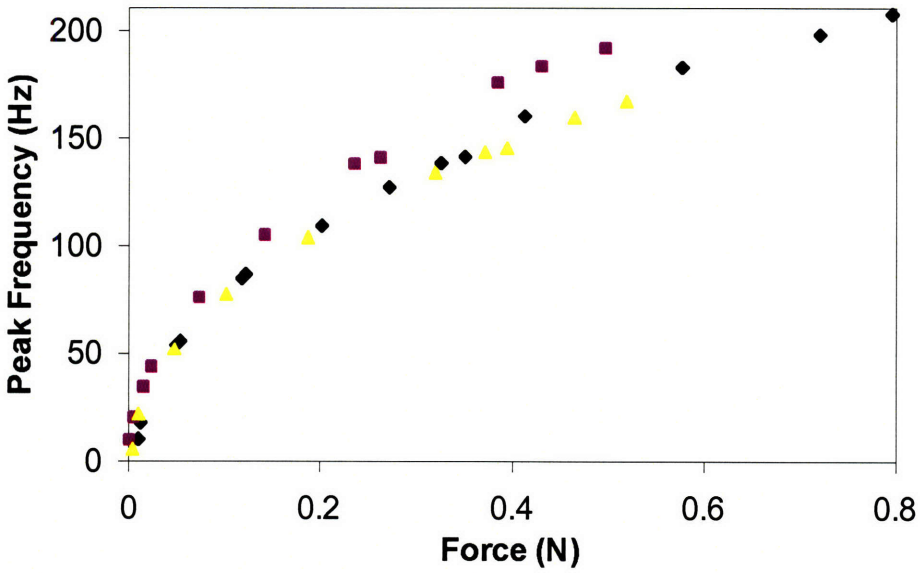

Figure 21: Force as a function of peak frequency for three tactors measured in the direction normal to the plane of rotation of the eccentric

The force produced normal to the plane of rotation has multiple possible causes. This force may be caused by slight asymmetries in the rotation of the eccentric, causing motion in the normal direction. In the case of the encased tactor, this force may also be

caused by a slight angle between the plane of rotation of the tactor and the face of the encasement. This angle can be seen in the model shown in Figure 22.

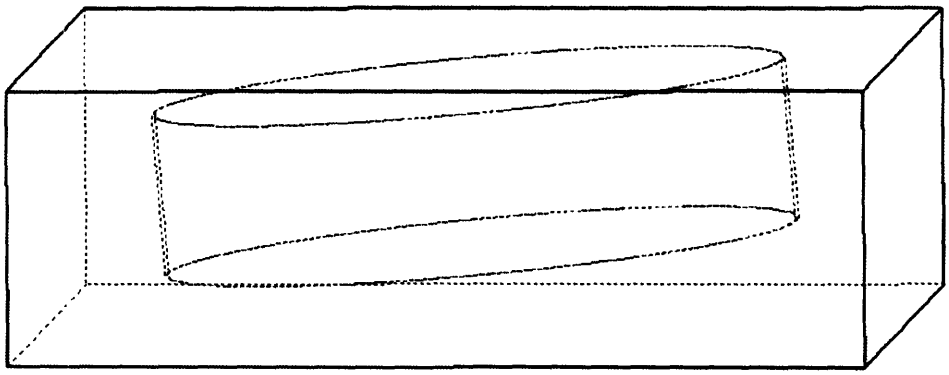

Figure 22: Schematic demonstrating an angle between the tactor and its encasement

The force produced in the plane of rotation can also be compared to the force produced normal to the plane of rotation. The force produced in the normal direction is always less than the force produced in the planar direction. Thus, the force in the normal direction can be viewed as a fraction of the force produced in the planar direction. The ratio of the force produced in the normal direction to the force in the planar direction ranged from 0.14 to 0.63 N, with a mean of 0.34 N. If the forces in the normal direction were caused by the offset angle in the encasement, then the ratio of these forces would equal the tangent of the angle, as shown in Figure 23. If this were the case, then these ratios would correspond to angles ranging from 7.9 degrees to 32 degrees, with a mean angle of 18 degrees.

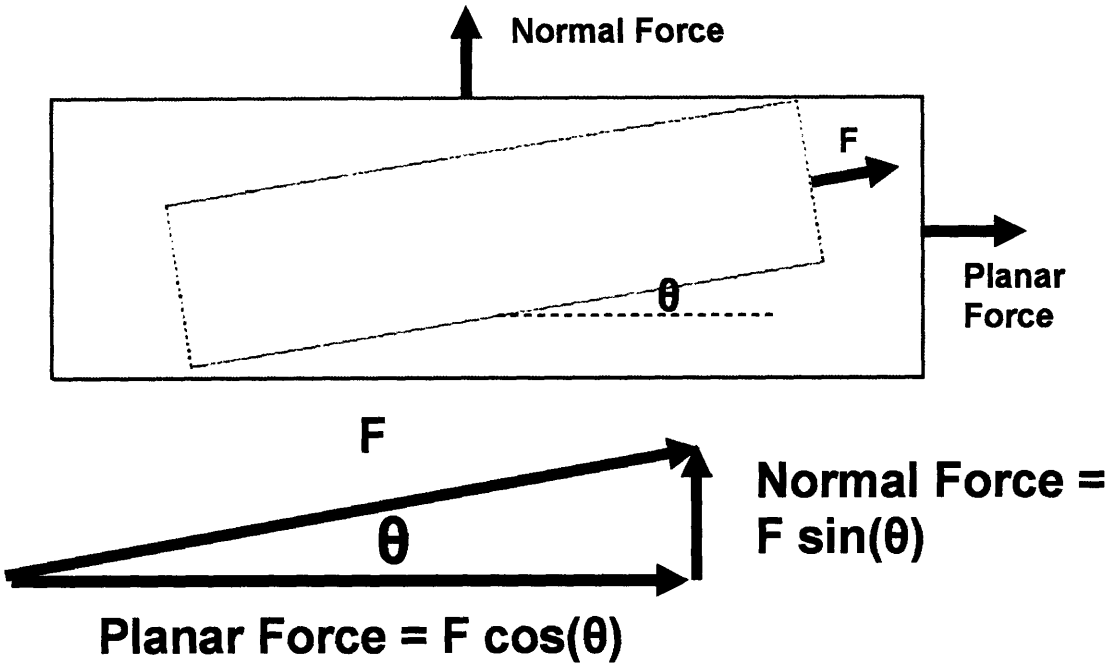

Figure 23: Diagram of a possible relationship between the forces in the planar and the normal directions for an encased tactor, as a function of the angle of the tactor to the surface of the encasement

3.2. Tactor Model

In order to understand the interaction between the tactors and the skin in tactile displays, the motion of the tactors themselves must be understood. A model of the tactor dynamics can be compared to measured tactor data in order to determine how closely the model captures the dynamics of the tactor. The model can then be used to understand the measurements recorded from each tactor, and to interpret the variations in these measurements. An accurate model of tactor dynamics might also be used in a realistic computer simulation of a tactile display.

A model of the interior motor dynamics of the type of motor used in the tactile display is shown in Figure 24. An applied voltage, u, creates a current in the motor. This current creates a torque, given by $T_m = i*K_t$, where T_m is the torque in N*m, i is the

current in Amperes, and K_t is the torque constant in N*m/A. This torque causes the eccentric to rotate at some speed w_m, and this rotation creates a back-emf of $E = K_t * w_m$. Thus the torque can be related to the applied voltage by:

$$T_m = \left(\frac{K_t}{R}\right)u - L/R\frac{dT_m}{dt} - \left(\frac{K_t^2}{R}\right)w_m,$$

where R is the resistance and L is the inductance in the motor windings.

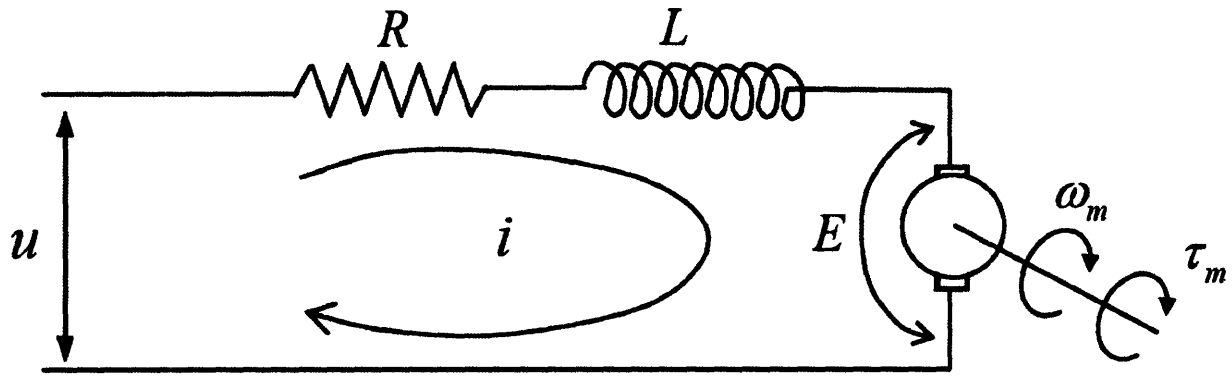

Figure 24: Model of motor dynamics (reproduced with permission of Asada, 2007).

A model of the entire tactor is shown in Figure 25. The tactor is modeled by a mass, M, which is attached to an eccentric, modeled as a pendulum of mass m. The pendulum is modeled as a point mass, located at the center of mass of the eccentric. The pendulum is driven by a torque, T_m, causing it to rotate around the mass. The pendulum is also subject to a linear rotational friction that is proportional to its velocity, given by $b\dot{\theta}$. When the tactor is attached to the impedance head, it is constrained to move in one direction; likewise, in this model, the mass is constrained to move in one direction labeled "x" in the figure. The number of degrees that the eccentric has rotated is given by θ, as marked in the figure.

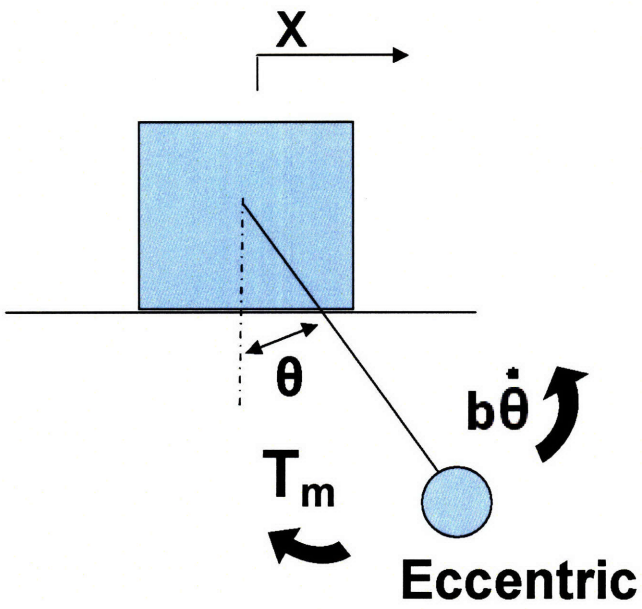

Figure 25: Tactor model. An eccentric rotates around a mass, which is constrained to move in one direction. The eccentric is subject to a tactor torque and rotational friction.

The motion of the tactor can then be modeled using Lagrangian mechanics. The Lagrangian is given by:

$$L = T - V = \tfrac{1}{2}(M+m)\dot{x}^2 + ml\dot{x}\dot{\theta}\cos\theta + \tfrac{1}{2}ml^2\dot{\theta}^2 - mgl\cos\theta$$

and the equations of motion are given by:

$$\frac{d}{dt}\frac{\partial L}{\partial \dot{x}} - \frac{\partial L}{\partial x} = 0$$

$$\frac{d}{dt}\frac{\partial L}{\partial \dot{\theta}} - \frac{\partial L}{\partial \theta} = T_m - b\cdot\dot{\theta}$$

3.2.1. Tactor Model Parameters

The eccentric, shown in Figure 1b, has a mass of 0.55 g. A model of the eccentric is shown in Figure 26. This model has a volume of 120.4 cubic millimeters, and the center of mass is located at (X = -2.57, Y = 0.89, Z = 0.00), at the green dot shown in

Figures 26 and 27. Thus the center of mass is located a distance of 2.57 mm from the axis of rotation, as shown in Figure 27.

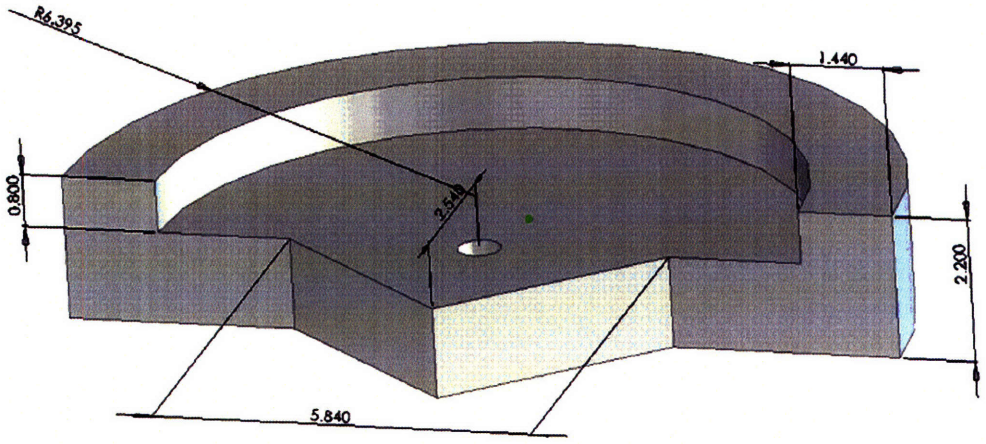

Figure 26: Motor eccentric, dimensions in mm. Center of mass is located at the green dot.

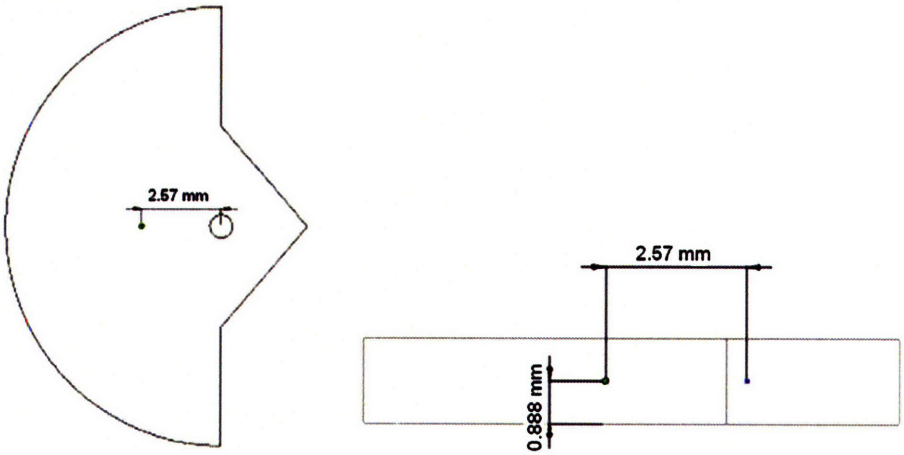

Figure 27: The center of mass of the eccentric is located at the green dot, with distances as shown from the axis of rotation

The resistance and inductance of a motor were measured using an impedance gain-phase analyzer (Hewlett-Packard, 4194A). The resistance was found to be 67 Ω,

and the inductance was found to be 1.1 mH. The torque constant is found by using the relationship

$$K_t = \frac{E}{w_m} = \left(u - R \cdot i - L\frac{di}{dt}\right) \Big/ w_m ,$$

with parameters defined as above. The current of one of the motors, when driven at 3.3 V, was measured using a multimeter (Agilent, 34401A), and was found have a steady-state value of 26.6 mA when attached to the impedance head. The frequency of the force produced by the motor, measured with the impedance head described above, had a mean of 128 Hz. The speed can then be calculated to be $w_m = 2\pi f = 804.2$ rad/sec. Thus the motor torque constant for that motor can be calculated to be 0.0019 N*m/A. All motors are assumed to have the same torque constant.

The mass parameters were measured using a digital scale (Mettler-Toledo, BD202). As shown in Figures 4 through 6, screws were used to attach the motors to the impedance head. The mass of an unencased motor with a screw attached is 3.7 g. The mass of an encased motor with a screw attached is 4.95 g.

3.2.2. Tactor Model Simulation

The tactor model was run in simulation using MATLAB (Mathworks, Inc.), for the encased and unencased tactors. The only parameter that had not been measured was the damping coefficient. For the following figures, a damping coefficient of 6.3*10^-8 N*sec was used. The simulated tactor data can be seen in Figures 28 through 31. The rotation of the pendulum is shown in Figure 28. The angle, θ, continually increases as the eccentric rotates. The rotational velocity, w, ramps up to $w_f = 834.2$ rad/sec, which corresponds to a frequency of oscillation of the tactor of $f \approx w_f / 2*\pi = 132.8$ Hz. This

value differs by 3.7% from the tactor that was measured above to determine the torque constant. The angular acceleration of the eccentric continued to oscillate as the eccentric rotated. This occurred because during part of the rotation, gravity helped the eccentric rotate slightly faster, while during the other part of the rotation, gravity slowed down the eccentric. Although this asymmetry caused the rotational acceleration to oscillate, the rotational speed only oscillated slightly around its steady-state value of 834.2 rad/sec.

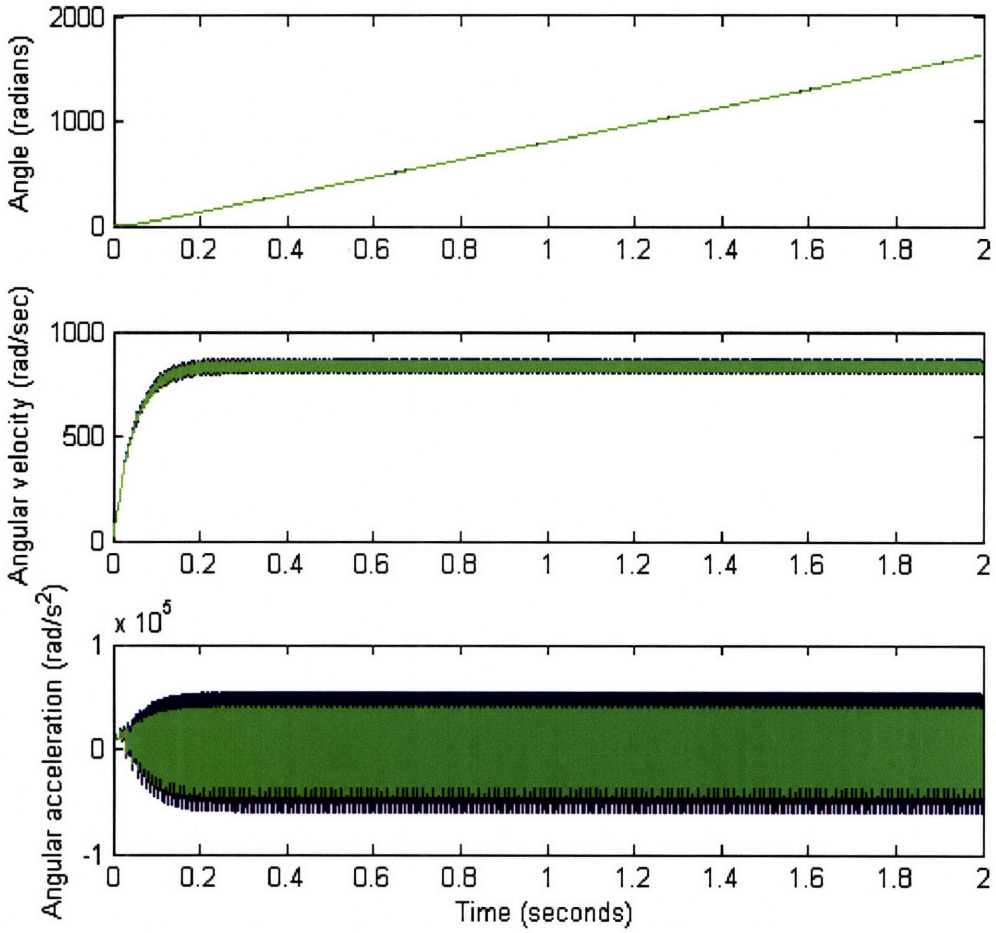

Figure 28: Simulated tactor data, showing the rotation of the pendulum as a function of time. Unencased data are shown in blue; encased data are shown in green.

Figure 29 shows the position of the tactor as a function of time. In the simulation, the tactor is not attached to an impedance head or a vest, so the tactor is free to move.

Because gravity creates a slight asymmetry in the motion of the eccentric as described above, the tactor drifts slightly leftward in the simulation. However, the position, velocity, and acceleration all oscillate as the eccentric rotates, representing the vibration of the tactor.

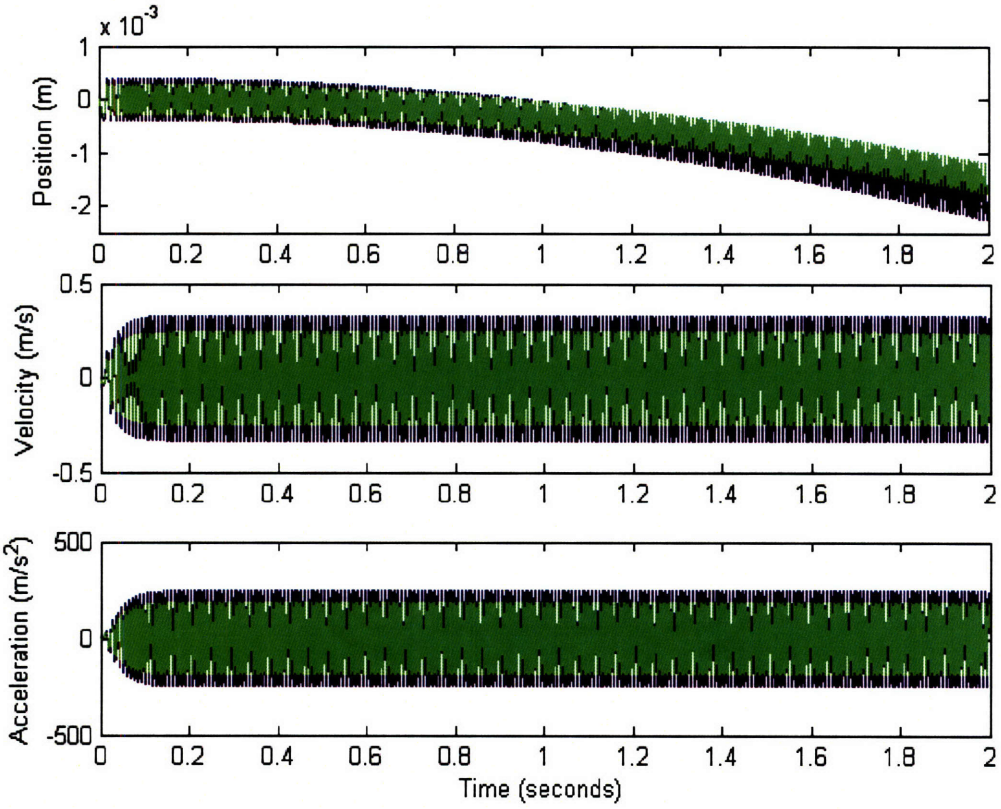

Figure 29: Simulated tactor data, showing the position of the tactor as a function of time. The unencased tactor trajectory is shown in blue, and the encased tactor trajectory is shown in green.

The differences in the accelerations between the encased and unencased tactors can be seen more easily in Figure 30, which illustrates the amplitude of the oscillating acceleration. In this simulation, the acceleration of the unencased tactor has an amplitude of 246.4 m/s², and the acceleration of the encased tactor has an amplitude of 187.8 m/s². The simulated acceleration of the unencased tactor differs by 3% from the recorded value in Jones et al. (2006).

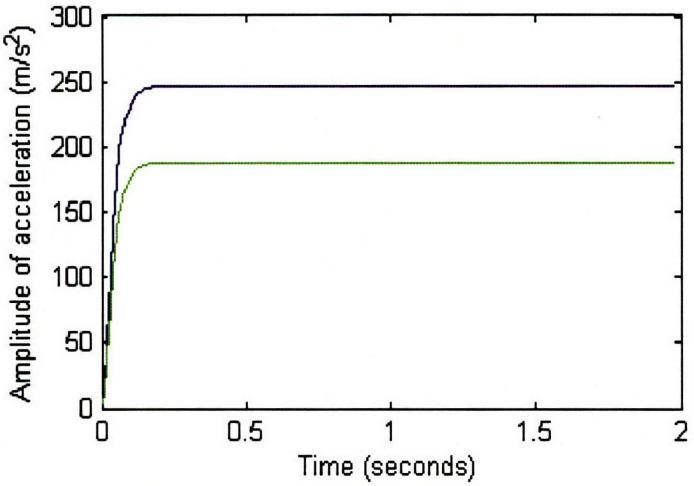

Figure 30: Simulated tactor data showing the amplitude of the oscillating acceleration of vibration of the tactor. The unencased tactor is shown in blue, and the encased tactor is shown in green.

Despite having different accelerations, these tactors produce very similar forces. Figure 31 shows the forces produced by each tactor, calculated by multiplying its acceleration by its mass. The unencased tactor produces a force of 0.91 N, and the encased tactor produces a force of 0.93 N. This is a difference of only 2%, and can possibly be attributed to an accumulation of rounding errors in the approximation, or is caused by the discrete nature of the simulation. Intuitively, it makes sense that a tactor will produce the same force during vibration regardless of whether it is encased.

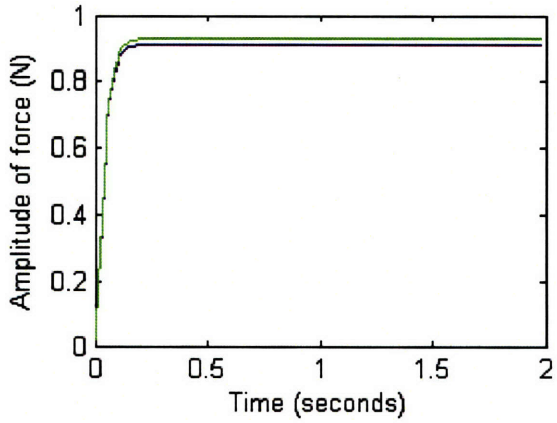

Figure 31: Simulated tactor data showing the amplitude of the oscillating forces. The unencased tactor is shown in blue, and the encased tactor is shown in green.

Figure 32 shows the torque produced by the tactor in simulation. The torque starts at 101 μN*m, and reaches a steady-state at 52.5 μN*m.

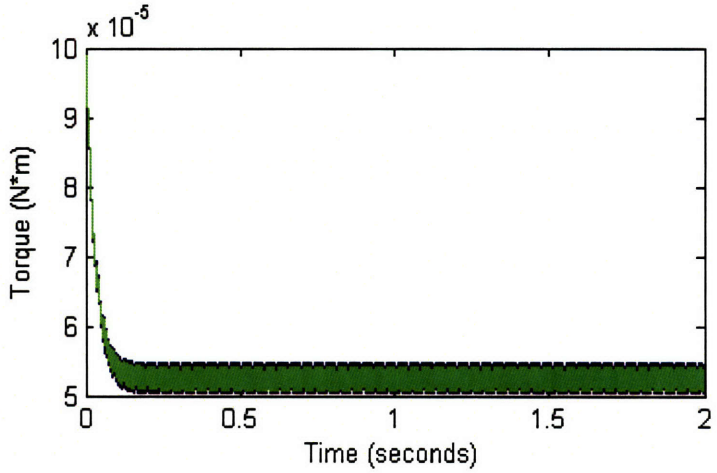

Figure 32: Torque produced by the tactor in simulation. The unencased tactor is shown in blue, and the encased tactor is shown in green.

Figure 33 shows the motor current for the simulation. The current starts at a value of 53.2 mA, and reaches a steady-state value of 27.6 mA. For the motor that was used to determine the torque constant above, this value differs from the measured current by 3.8%.

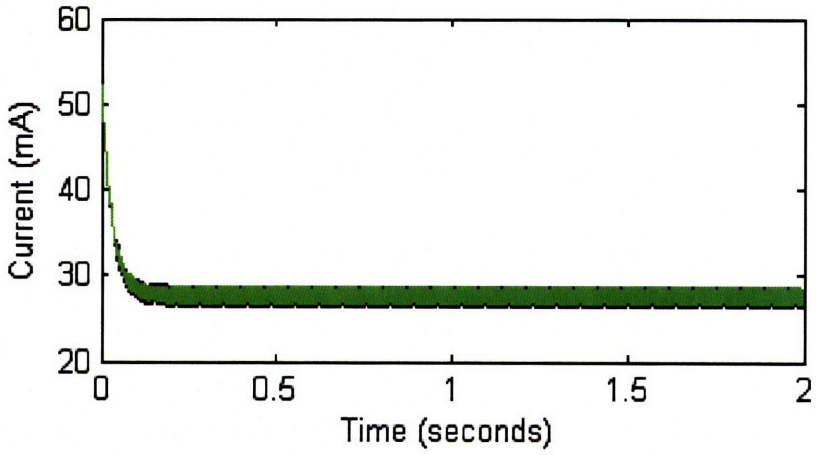

Figure 33: Current through the motor in simulation. The unencased motor is shown in blue, and the encased motor is shown in green.

Figure 34 shows the frequency spectrum of the tactor acceleration, calculated using a Fourier transform. The peak frequency is approximately given by

$$f \approx \frac{T_m}{2\pi b},$$

which is 132.6 Hz for the chosen parameters. The measured peak frequency, from the Fourier transform, is 133.0 Hz. This frequency spectrum is very similar for the encased and unencased tactor simulations.

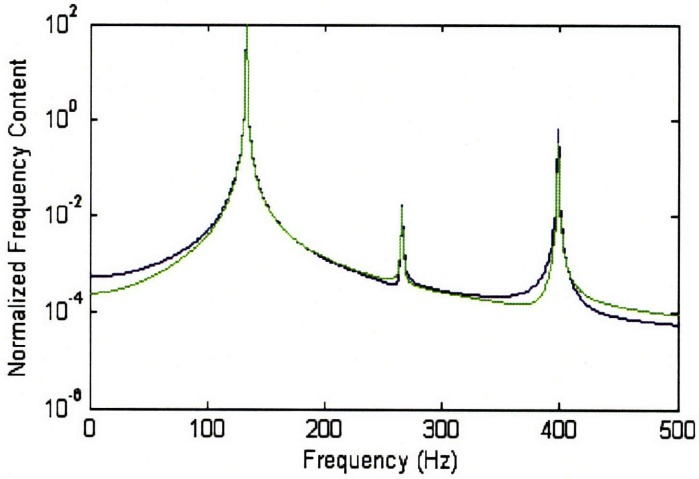

Figure 34: Frequency content of the simulated tactor acceleration, plotted on a semi-log scale. The unencased tactor is shown in blue, and the encased tactor is shown in green.

The force and frequency of the tactor can be changed by varying the damping coefficient. The relationship between the force and frequency of the tactor, for a varying damping coefficient, can be seen in Figure 35. From the simulated tactor data of the encased tactor, the frequency can be seen as a function of force given by

$$f = 137.5 \cdot n^{0.5025},$$

where f is the frequency of the tactor in Hz, and n is the force in Newtons.

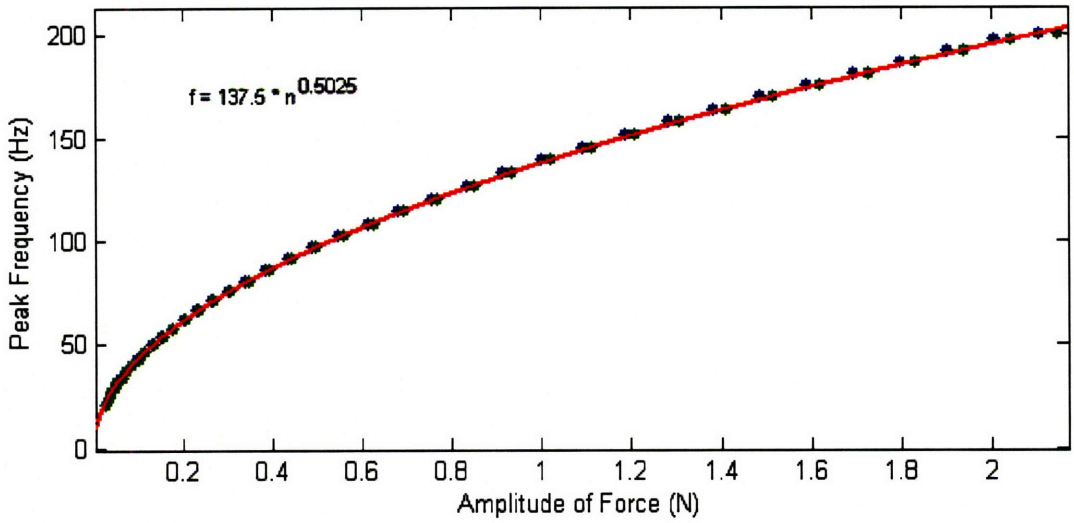

Figure 35: Frequency as a function of force for the simulated tactor, for a varying damping coefficient. The unencased tactor is shown in blue, and the encased tactor is shown in green. The red line indicates a power function fit to the encased tactor data.

3.2.3. Testing the Tactor Model

The frequency-force curve for the tactors can be compared to the frequency-force curve for the tactor model, as shown in Figure 36. The simulated data were produced by varying the damping coefficient in the tactor model. When the damping coefficient is reduced, the net torque on the eccentric is increased, thus resulting in a greater force produced by the tactor. Additionally, a reduced damping coefficient allows the eccentric to vibrate with a faster rotational velocity, which increases the peak frequency for the tactor.

The measured tactor data are also shown in Figure 36, for all 207 trials from 14 encased and nine unencased tactors. The measured data have a slight offset from the predicted data from the tactor model. The model can be made to fit the data better if a radius of 3.2 mm is used for the pendulum instead of 2.57 mm. This change increases the radius by 25%. Although the value of 2.57 mm was calculated using a model of the shape of the eccentric, different parts of the eccentric might be made of different

materials, and thus the center of mass would differ from the center of geometry. Additionally, there might be differences between the model and the eccentric that were not taken into account.

With a radius of 3.2 mm, the model predictions coincide with the measured data, as shown in Figure 36. However, the model predictions were produced by varying the damping coefficient of a single tactor model, whereas the measured data came from vibrating 23 different tactors 9 times each. Thus it is suggested that the main difference between the different tactors are their damping coefficients. It is further suggested that the variability within an individual tactor is also caused by a varying damping coefficient of that tactor.

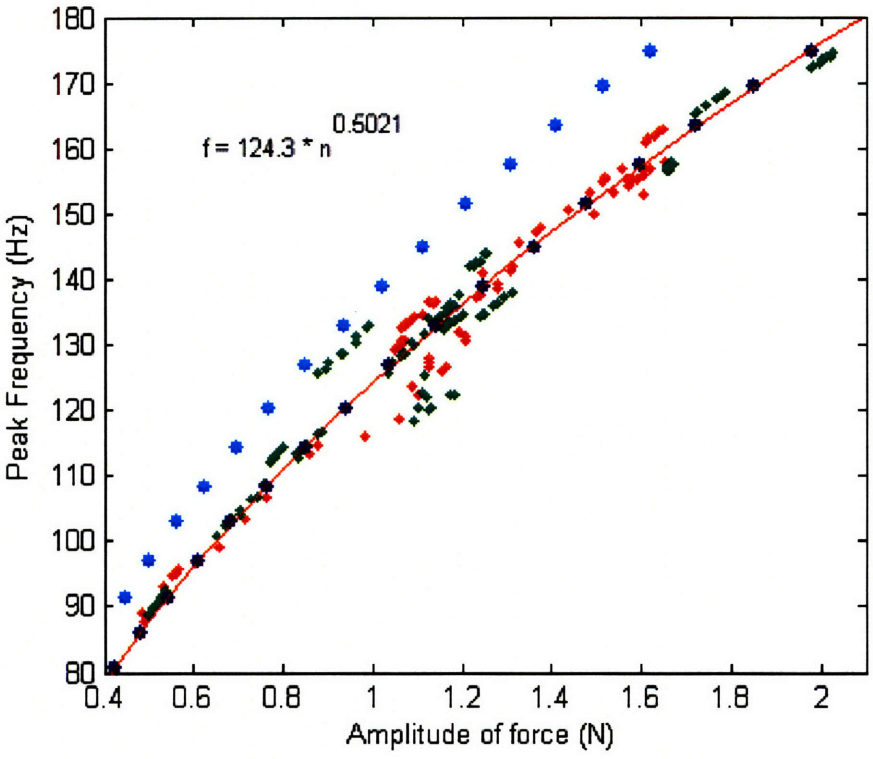

Figure 36: Cyan points are from the predicted tactor model. Blue points are from the tactor model using a radius of 3.2 mm. Green points are from the encased tactors and red points are from the unencased tactors. The red line is fit to the tactor data using a least-squares regression.

The mean peak frequency also varies with the mean steady-state current. A simulation of this can be seen in Figure 37, for a varying damping coefficient. This relationship can be derived from the motor equations, by

$$i_{ss} = \frac{T_m}{K_t} = \frac{u}{R} - \left(\frac{2\pi \cdot K_t^2}{R} \right) \cdot f$$

where i_{ss} is the steady-state current in Amperes, f is the peak frequency, and the other parameters are as defined above. Using the parameters from above, this equation predicts the relationship

$$f = -5.61 \cdot 10^3 \cdot i_{ss} + 276.4$$

This can be compared to the measured motor data, shown in green in Figure 37. As before, the different data points from the simulation are produced by varying the damping coefficient for a single tactor model, whereas the measured data are taken from different tactors. This further supports the idea that the main differences between tactors are their damping coefficients.

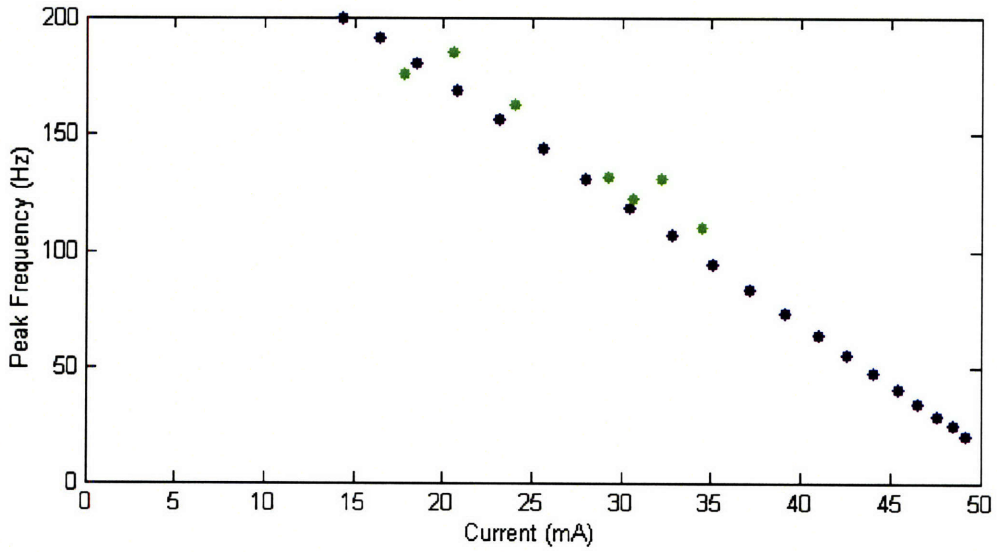

Figure 37: Relationship between motor frequency and current. The simulated data from motor model are shown in blue, and the measured data are shown in green.

The tactor model assumes that a changing damping coefficient is the general cause of the changes in the force and frequency of each tactor trial. The damping coefficient of motors may vary due to variations in the friction and coils inside the tactors, caused by manufacturing differences. Additionally, the forces and frequencies for a single motor vary as a result of a changing damping coefficient, possibly due to changes in the motor temperature.

Thus for any given tactor trial, the mean force and frequency can be used to determine the appropriate damping coefficient to be used to fit the tactor data. A graph that can aid with this selection is shown in Figure 38. Once the peak frequency for a given tactor is determined, the appropriate damping coefficient can be found by

$$b = 1.712 \cdot 10^{-5} (f + 1.061)^{-1.009} - 5.969 \cdot 10^{-8}$$

Using this equation, a damping coefficient can be chosen so that the data from the tactor model simulation can be compared to real tactor data. The first tactor tested had a peak frequency of 133.2 Hz, which corresponds to a damping coefficient of $6.232*10^{-8}$ N*sec. A better match is actually achieved using b = $6.265*10^{-8}$. Using this parameter, the simulated tactor data can be seen in Figures 39 through 41.

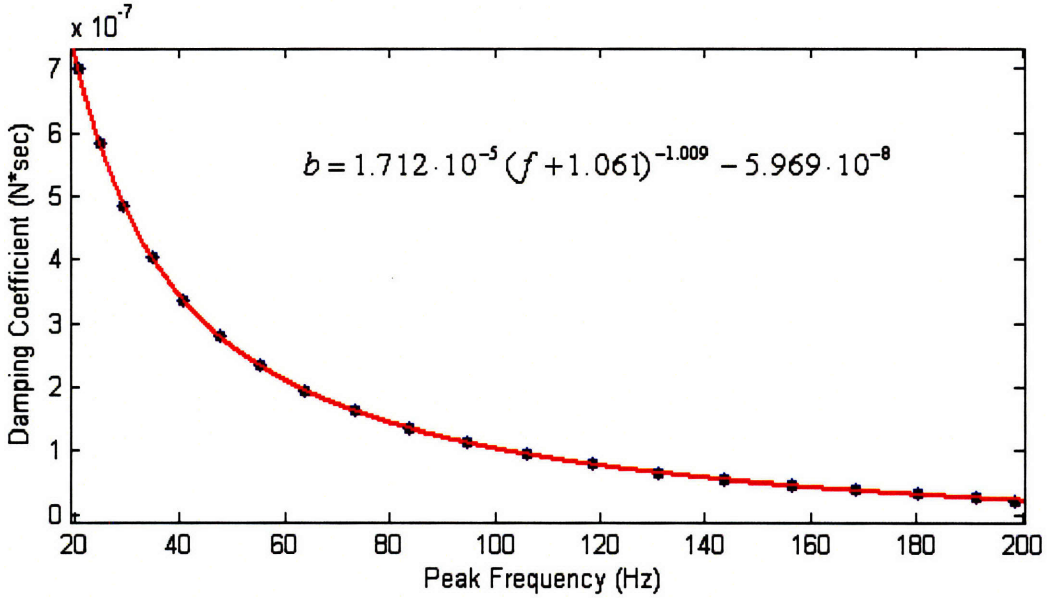

Figure 38: Damping coefficient as a function of the peak frequency of the tactor

Figure 39 shows the amplitude of the oscillating forces produced by a real and simulated tactor, over 10 seconds. One difference is that the real tactor exhibits an overshoot in force, whereas the simulated tactor has no overshoot. Additionally, the forces produced by the real tactor increase at a faster rate than those by the simulated tactor, as can be seen more clearly in Figure 40. However, the force and frequency of this tactor have been matched, as can be seen in Figure 41.

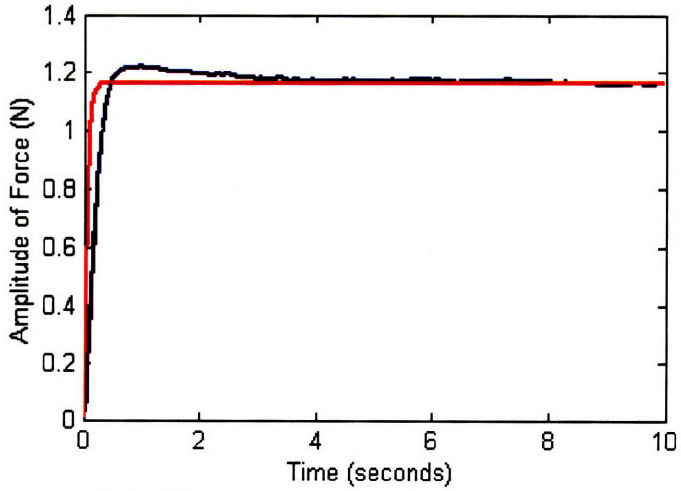

Figure 39: Forces produced by a tactor over 10 seconds. Blue shows the real tactor data; red shows the simulated tactor data

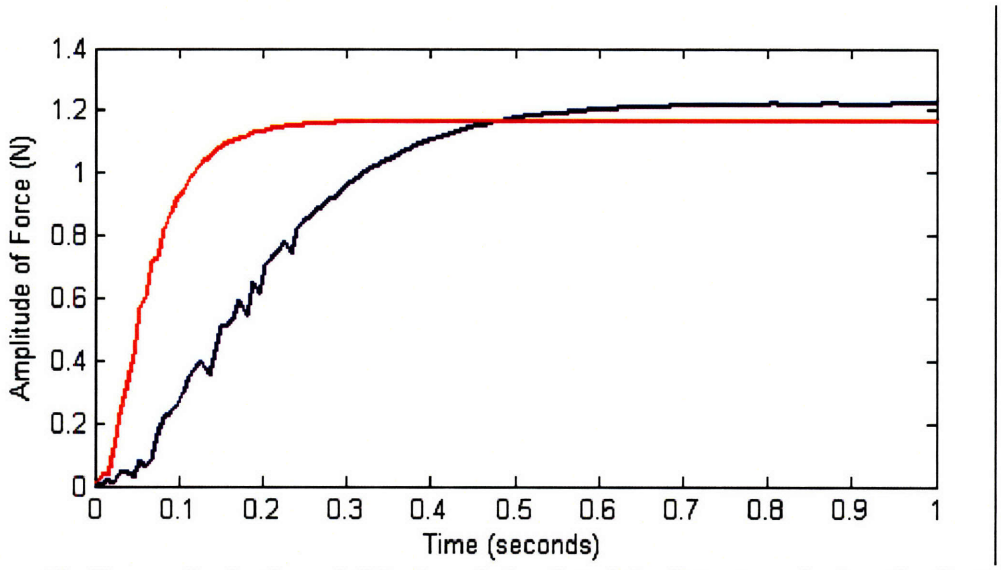

Figure 40: Forces for both real (blue) and simulated (red) tactors during the first 1 s.

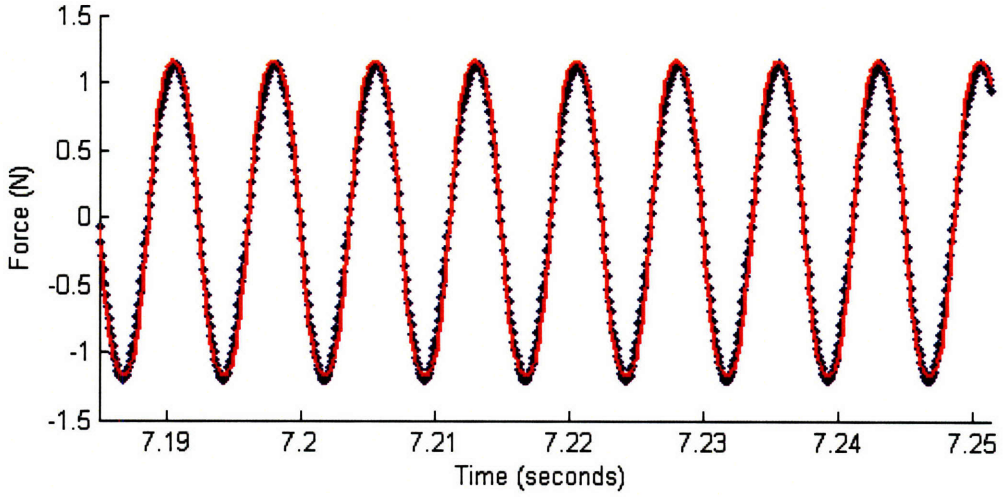

Figure 41: Steady-state forces produced by the real (blue) and simulated (red) tactors

4. Simulating Skin

4.1. Simulation of the Tactor-skin Interaction

The vest used by Piateski and Jones (2005) conveys signals to the user through various vibration patterns. In one study, 15 patterns were tested, resulting in a mean identification accuracy of 96% (Jones et al., 2007). Still, further modifications to the vest, such as varying the number of tactors or the inter-tactor spacing, may yield an even greater number of patterns that can be recognized. In order to test the effect of modifying the spatial configuration of the vest, a material that was similar to skin was sought so that measurements could be made with motors attached to the material in different spatial configurations. A number of different silicone rubber compounds were evaluated, and one was selected which exhibited material properties similar to skin. Tactors were attached to the simulated skin with varying distances between tactors, and the vibration of the silicone rubber was measured at various locations relative to the tactors. The results from these experiments should provide a better understanding of how the dimensions of the array, such as the number of tactors or the inter-tactor spacing, affect the perception of vibrotactile patterns, leading to suggestions for improving the design of a tactile display.

4.1.1 Experimental Setup and Methods

A silicone rubber platform, named Skinsim, was designed to have similar material properties to that of skin. In order to determine the desired material properties of Skinsim, a Dynamic Mechanical Analyzer (Perkin-Elmer, DMA7E) was used to analyze samples of skin taken from the back of a pig. As mentioned in the Introduction, pig skin has been found to have similar material properties to human skin (Shergold, et al., 2006).

A stress-strain curve was measured for each of five samples of pig skin. The stresses under consideration were within the range of those produced by the tactors in the direction normal to the skin. As discussed below, normal to the plane of rotation of the eccentric, the mean forces produced by the encased tactors ranged from 0.11 to 1.10 N, with a mean of 0.41 N. The area of an encased tactor was 360 mm^2, so the stresses produced by the encased tactors ranged from 305.6 to 3056 Pa.

For the five samples of pig skin, strains at 305.6 Pa ranged from 0.86% to 1.9%, and strains at 3056 Pa ranged from 8.4% to 13.9%. For each sample, a modulus of elasticity was determined at stresses of 305.6 and 3056 Pa, by finding the slope of the tangent line, as shown in Figure 42. At 305.6 Pa, the modulus of elasticity ranged from 17.0 to 28.3 kPa, and at 3056 Pa, the modulus ranged from 36.5 to 54.1 kPa.

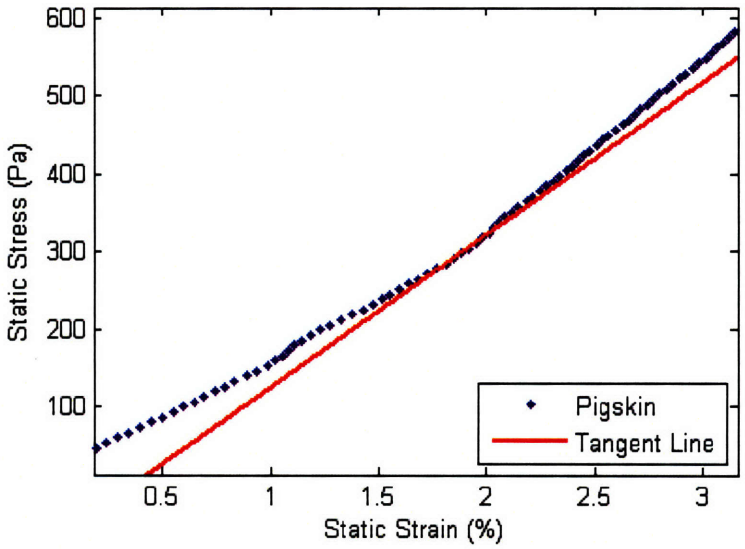

Figure 42: Stress vs. strain relationship for a sample of pig skin. Young's modulus at 305.6 Pa is calculated by finding the slope of the tangent line at this point.

The silicone rubber compound selected to simulate skin is a combination of a two-part mixture (Smooth-On, Ecoflex 00-30) with a silicone fluid (Smooth-On, Silicone Thinner). The ratio used for the mixture was 2.2:3:1 for Ecoflex 00-30 part B: Silicone

Thinner: Ecoflex 00-30 part A. The stress-strain curve for Skinsim, along with the stress-strain curves for the 5 samples of pig skin, can be seen in Figure 43. A stress of 305.6 Pa produced a strain in Skinsim of 1.78%, and a stress of 3056 Pa produced a strain of 11.7%. At 305.6 Pa, Skinsim had a modulus of 18.4 kPa, and at 3056 a modulus of 32.9 kPa.

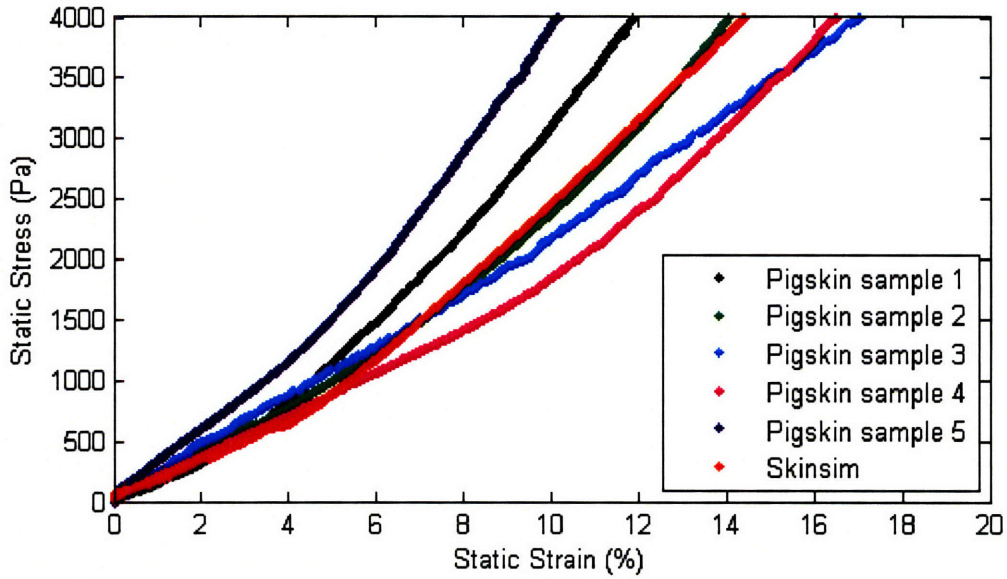

Figure 43: Stress-strain curves for five samples of pig skin, and a sample of Skinsim (shown in red), a silicone rubber designed to have similar material properties to skin

In order to simulate the interaction between the tactors and skin, encased tactors were glued to Skinsim in various configurations, and one-axis accelerometers (Measurement Specialties, ACH-01-03) were used to measure the vibrations of the Skinsim at various locations relative to the tactors. These accelerometers have a sensitivity range of 7 – 11 mV/g (mean: 9 mV/g), and have a noise level of about 0.2 m/s^2. They can record changes in acceleration ranging from 2 Hz to 20 kHz, and can measure acceleration levels up to 1470 m/s^2. The accelerometers have a mass of 3.03 g, and thus they applied a small amount of loading to the tactors. Additionally, the

accelerometers have a long wire attached, which has a mass of about 5 g, although only some portion of the mass of the wire actually provides loading on the tactor.

Figure 44 shows the setup that was used for the Skinsim experiments. Epoxy was used to attach each tactor to Skinsim, and also to attach accelerometers to the tactors. As before, data were sent to a breakout board (National Instruments, BNC-2080), and then to a computer, where they were recorded at a sampling rate of 10 kHz. As in the tactor characterization experiments, each tactor was activated for 10 seconds, and then off for 10 seconds, and only the last 5 seconds of data were analyzed. Also, accelerations that were recorded from accelerometers that were placed on tactors were filtered. The filter used was a 5^{th} order Butterworth filter, with a cutoff frequency located 20 Hz above the peak frequency of the tactor.

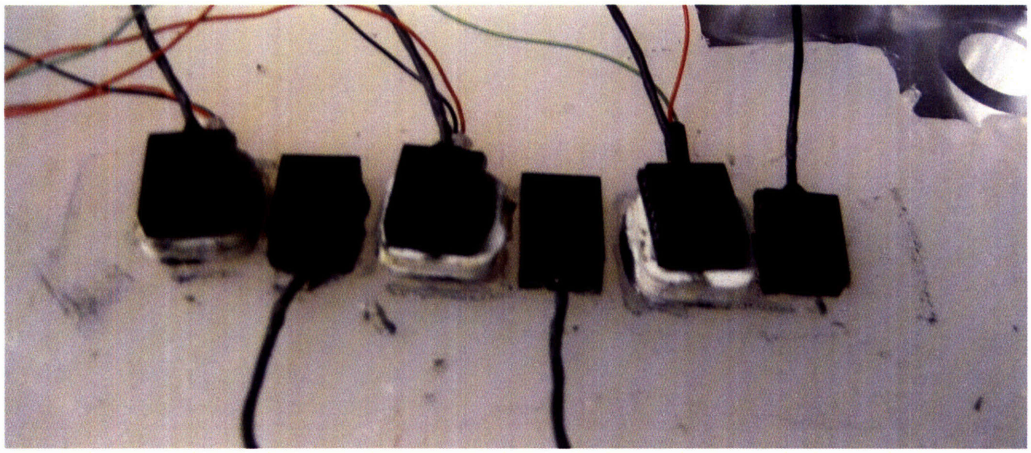

Figure 44: Tactors (in white) placed on top of a viscoelastic substrate named Skinsim. Accelerometers, in black, measure the movement of Skinsim when tactors are actuated.

To determine the effect of Skinsim on the frequency and acceleration of the tactor, eight tactors that were tested in the tactor characterization experiments were attached to Skinsim. Each tactor was activated for 10 seconds, and then turned off for 10 seconds. This was repeated 11 times, although the first trial was ignored to remove transient warm-up effects. The frequency and acceleration data that were recorded were

compared to the frequency and force measurements made using the same tactors when attached to an impedance head, as described in section 3.1.2. Additionally, two tactors were activated at voltage levels ranging from 0.5 to 4.5 V. Again, frequency and acceleration data measured when the tactors were attached to the Skinsim were compared with the frequency and force measurements when the tactors were attached to the impedance head. Also, in order to determine the effect of mass loading on the frequency and acceleration of the tactors, various masses were attached to the top of a tactor, using double-stick foam mounting tape, weighing 0.19 g. Accelerations were recorded from two tactors that were loaded with masses ranging from 2 to 50 g.

In order to formulate an equation to describe the traveling waves created by the tactors in Skinsim, the acceleration and speed of these waves must be determined. Because of the damping in Skinsim, the acceleration of the traveling wave decreases at points farther away from the tactor. Three tactors were activated, with accelerometers placed at 20 mm intervals away from the tactor. Between 9 and 18 trials were recorded for each experimental condition. The speed was recorded by placing accelerometers at varying distances away from a tactor, and measuring the phase shift in the traveling wave at each of the accelerometers. Additionally, an impulse was created in the Skinsim, and the speed of the resulting traveling wave was also measured.

To determine the linearity of the Skinsim, the superposition of two traveling waves was measured. Two tactors, placed 80 mm apart, were activated, and an accelerometer was placed midway between them at 40 mm. The predicted superposition, assuming linearity, was compared with measured acceleration midway between the tactors.

4.1.2. Tactor Measurements on Skinsim

Figure 45 shows that the frequency of vibration of a tactor driven at a given voltage level was lower when the tactor was mounted on Skinsim than when it was on the impedance head. On average, the frequencies of the tactors were reduced by 62% when mounted on Skinsim. One possible explanation for this lower frequency is the additional mass of the accelerometers. As mentioned above, accelerometers were mounted on top of the tactors on the Skinsim, adding the weight of the accelerometer as well as the accelerometer cable to the tactor.

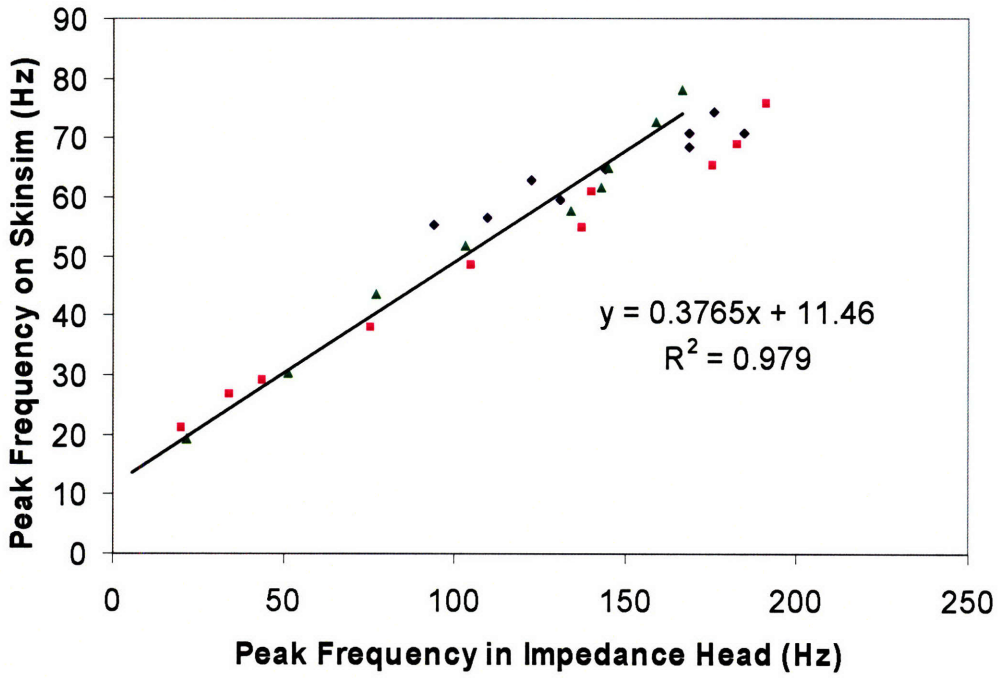

Figure 45: Tactor vibration frequency on Skinsim as a function of the frequency measured when the tactor was on impedance head. The blue data are means for different tactors driven at 3.3 V. The pink and green data were obtained by varying the voltage for two individual tactors. The line shown was fit to the pink and green data using the method of least-squares.

In order to determine how much of this change in frequency can be attributed to mass loading on the tactors, various masses were attached to the top of a tactor, using

double-stick foam mounting tape. In the no-load condition, the tactor still had the accelerometer and the cable on it. Accelerations were recorded with the additional mass. The effect of mass loading on frequency can be seen in Figure 46. As shown in the figure, loading causes a decrease in frequency, although a load of 50 g is needed to reduce the peak frequency by 7.4 Hz. This is much smaller than the change in peak frequency shown in Figure 45, in which frequencies were reduced on average by 62% of those measured with the impedance head. When placed on the Skinsim, the frequency was reduced by as much as 93 Hz. These results indicate that the change in peak frequency when the tactors are placed on Skinsim cannot be attributed to mass loading alone. As expected, additional load also reduced the mean acceleration of the tactors when placed on the Skinsim, as can be seen in Figure 47.

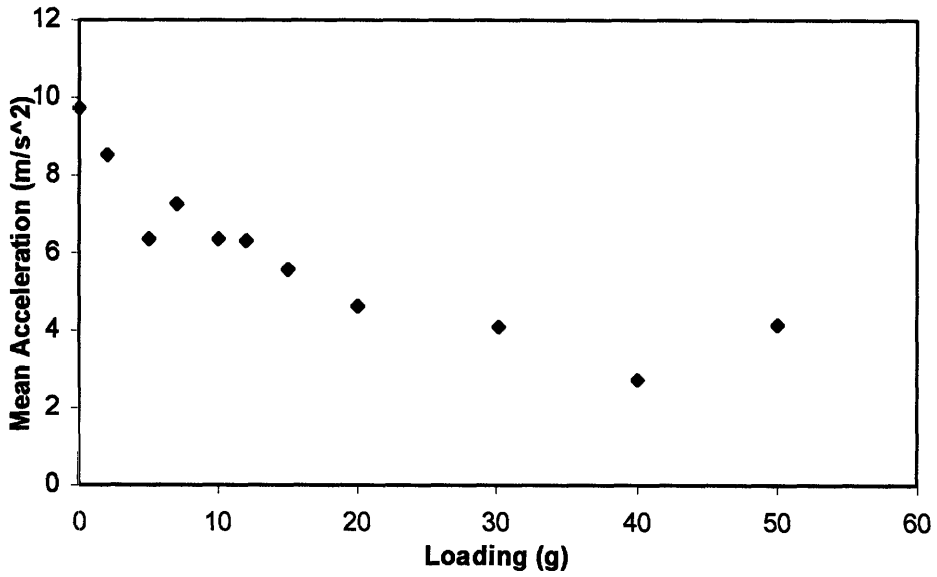

Figure 46: Effect of added mass on the peak frequency of a tactor when placed on Skinsim. The mass values do not include the mass of the accelerometer or double-stick tape.

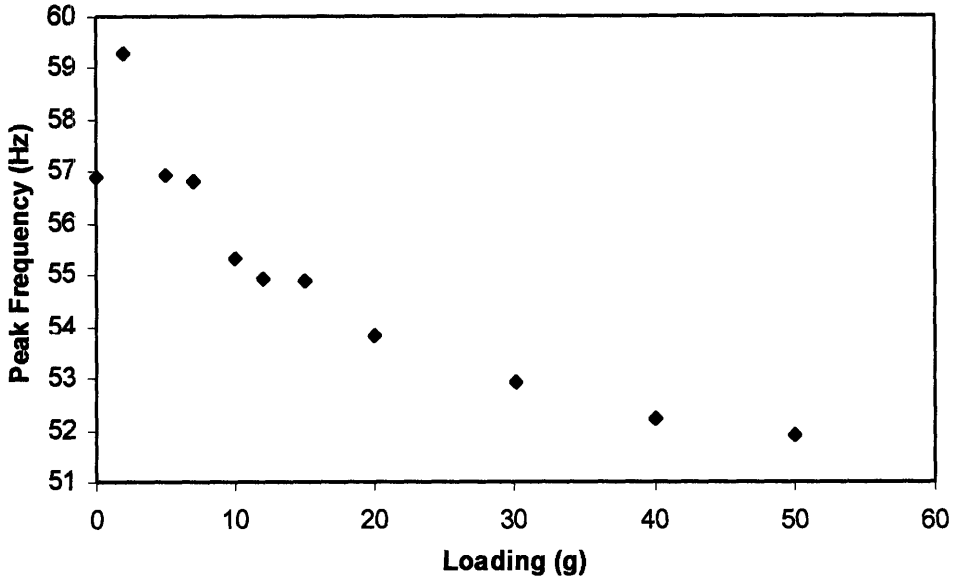

Figure 47: Effect of added mass on the mean acceleration of a tactor when placed on the Skinsim. The mass values do not include the mass of the accelerometer or double-stick tape.

Figure 48 shows a plot of the mean acceleration of eight encased tactors when placed on Skinsim. The relationship between acceleration and force is shown, with the force measured normal to the plane of rotation using the impedance head. All tactors in this figure were driven at 3.3 V. There is no clear relationship between the mean force and the mean acceleration of the tactors. This is similar to the graph in Figure 19, in which no clear trend was found for the forces produced by the tactors in the normal direction as a function of frequency. As described above, the motion of the tactors in the direction normal to the plane of rotation is complex, and may be caused by slight asymmetries in the rotation of the eccentric.

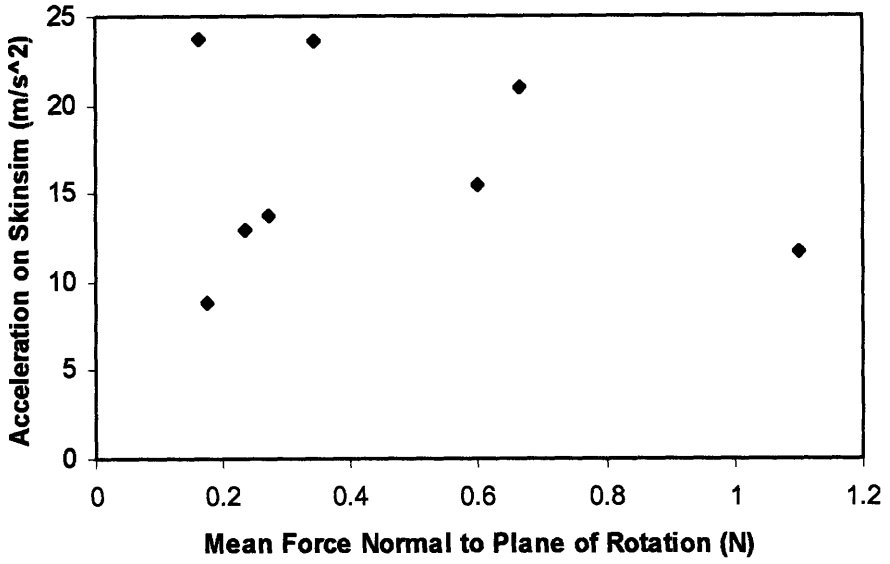

Figure 48: Relationship between the acceleration of the tactors on Skinsim, and the force produced in the impedance head, measured normal to the plane of rotation of the eccentric, for eight encased tactors

As before, a trend becomes apparent only when individual tactors are examined. As mentioned above, two tactors were activated at voltages ranging from 0.5 to 4.5 V. Figure 49 shows that, as expected, the acceleration of the tactors increased when the voltage is increased. Figure 50 illustrates that the frequency of vibration of two encased tactors on Skinsim increased with acceleration. As discussed above, an increased voltage increases the torque on the eccentric, which causes the eccentric to rotate faster, creating a higher peak frequency. At the same time, the entire tactor vibrates faster and with greater force, leading to higher accelerations and larger forces. Figure 51 shows that, for a varying voltage level on an individual tactor, the acceleration of the tactors on Skinsim becomes a monotonically increasing function of the force produced by the tactor in the normal direction as measured when it is attached to the impedance head. This is in

contrast to Figure 48, which shows no relationship between acceleration and force, when considering multiple tactors all driven at 3.3 V.

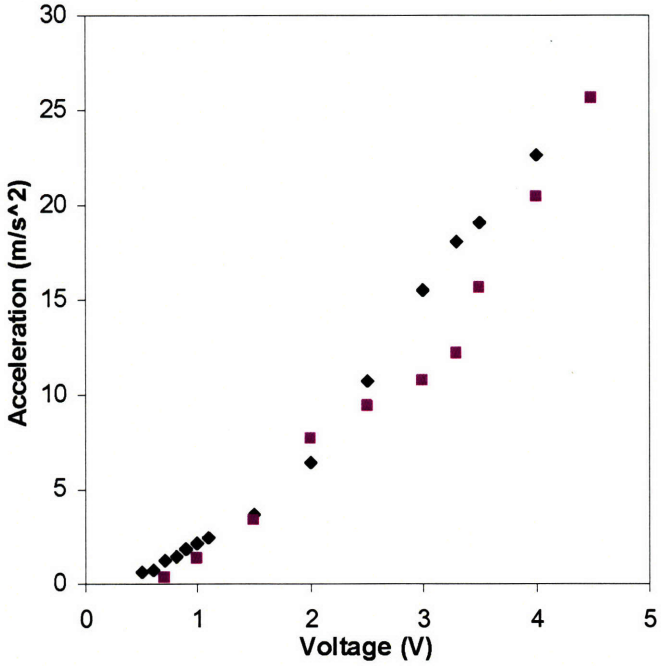

Figure 49: Acceleration of the vibration for two tactors, when attached to Skinsim, for a varying input voltage

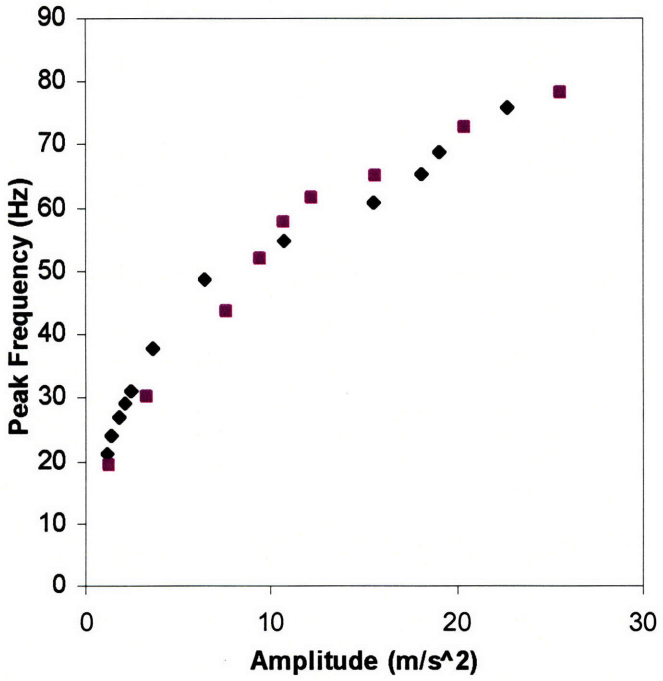

Figure 50: Relationship between peak frequency of vibration and acceleration for two tactors, when placed on Skinsim, for a varying input voltage

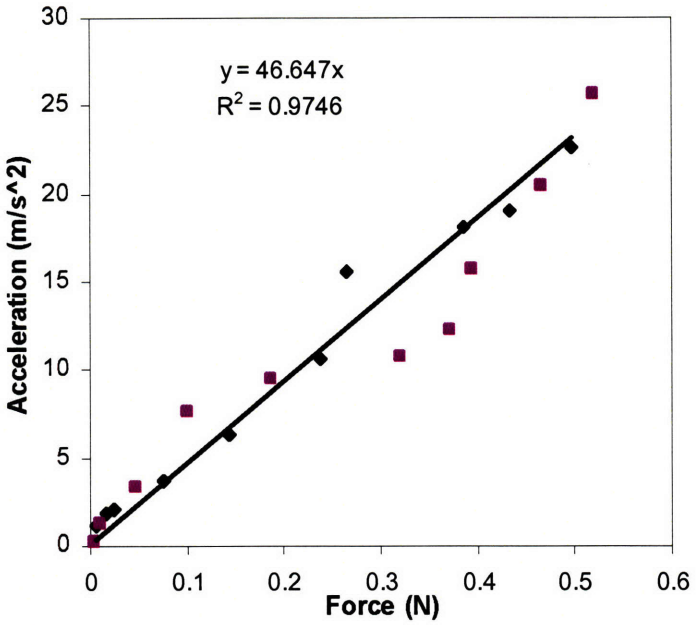

Figure 51: Relationship between acceleration on Skinsim and force in the normal direction, as measured when attached to the impedance head, for two encased tactors, for a varying input voltage

4.1.3. Traveling Waves in Skinsim

The vibration of the tactor creates a traveling wave in the Skinsim, which decreases in acceleration at points farther away from the tactor. Figure 52 shows the amplitude of the oscillating acceleration of the traveling wave at various distances away from the tactor, for three tactors. As discussed above, there is considerable variation in the forces produced by different tactors. Due to differences between the tactors tested, each tactor causes Skinsim to vibrate at a different level of acceleration. This difference is seen in Figure 52, in which the tactor shown in blue causes Skinsim to vibrate at 25.7 m/s^2 at the location of the tactor, whereas the tactors shown in green and red both cause Skinsim to vibrate at 9 m/s^2.

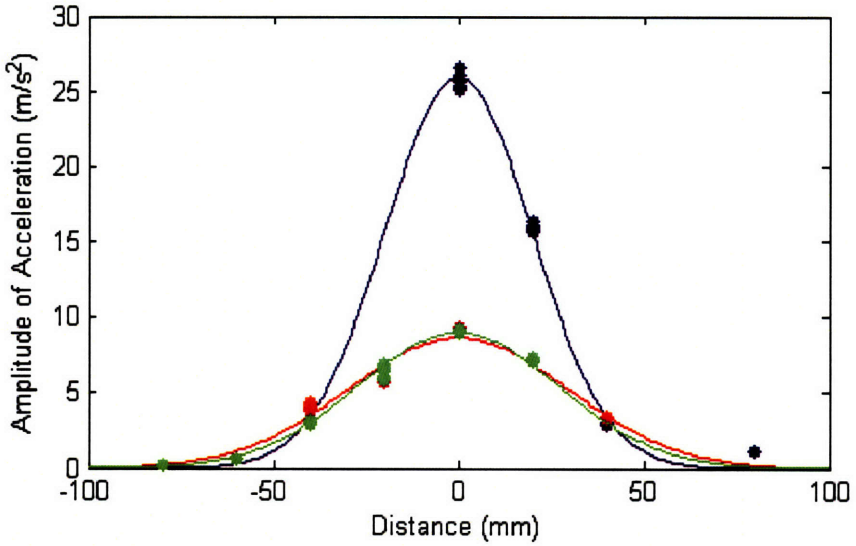

Figure 52: Amplitude of the oscillating acceleration of the traveling wave at various distances from the tactor, for three tactors. For all three tactors, the zero point represents the location of the tactor that is being actuated.

These accelerations can be fit to a Gaussian distribution, which has the equation

$$a = a_0 * \exp(-(d/b)\ ^\wedge 2)$$

where a is the acceleration in m/s^2, d is the distance in mm, a_0 is a constant that represents the acceleration of the tactor, and b is a constant that represents the amount of damping in the Skinsim. For the three tactors tested, b took on values of 28.18 mm, 38.4 mm, and 42.13 mm.

This experiment has implications for the spacing of tactors used in vibrotactile displays. At a distance of 60 mm, the Skinsim vibrations are damped to a level of less than 10% of the acceleration at the tactor. For the accelerations produced by the various tactors tested, at 60 mm away, the acceleration would generally be less than 2 m/s^2. To put this in perspective, the sensor noise in the accelerometers is about 0.2 m/s^2. Thus the tactor spacing should be at least 60 mm if the tactile display is to be used for precise spatial information.

If two tactors were actuated at the same time, they created two traveling waves. The acceleration at any point on Skinsim can be seen as a superposition of these two waves. Two tactors, placed 80 mm apart, were used to measure this superposition effect. An accelerometer was placed midway between them at 40 mm. Figure 53 shows the predicted effect of this superposition on the amplitude:

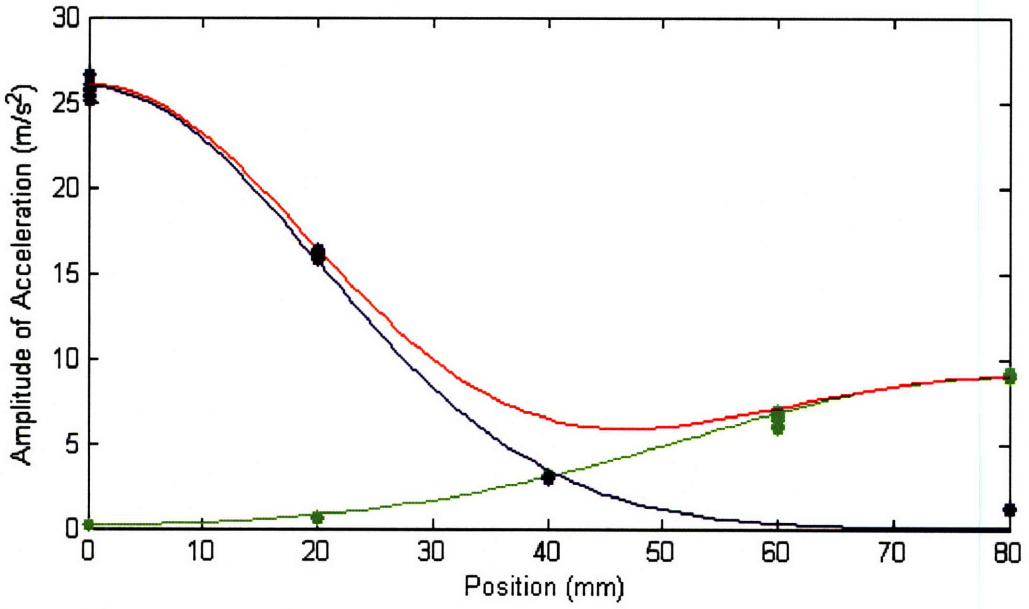

Figure 53: Schematic showing the separate distribution of amplitudes created by two tactors. Red line shows the predicted amplitude of the superposition of the sine waves.

When placed on Skinsim, the left tactor created a vibration with a mean amplitude of 3.45 m/s² at a distance of 40 mm away from the tactor, with a mean peak frequency of 70.8 Hz, or 444.8 rad/sec. The right tactor created a vibration with a mean amplitude of 3.02 m/s² at a distance of 40 mm away from the tactor, with a mean peak frequency of 51.7 Hz or 324.8 rad/sec. Thus, a priori, the predicted acceleration at a position of 40 mm away from both tactors (i.e. midway between both tactors) is

$$a = 3.02 * \sin(324.8 * t + c_1) + 3.45 * \sin(444.8 * t + c_2)$$

where a is the acceleration in m/s^2, and c_1 and c_2 are the phase shifts of the sine waves.

Figure 54 shows the normalized Fourier transform of the measured data midway between the two tactors. There are two clear peaks, one from each of the tactors, that occur at 53.2 Hz (334.3 rad/sec) and 70.8 Hz (444.8 rad/sec). Thus the new predicted acceleration at the midway position is

$$a = 3.02 \sin (334.3\ t + c_1) + 3.45 \sin (444.8\ t + c_2).$$

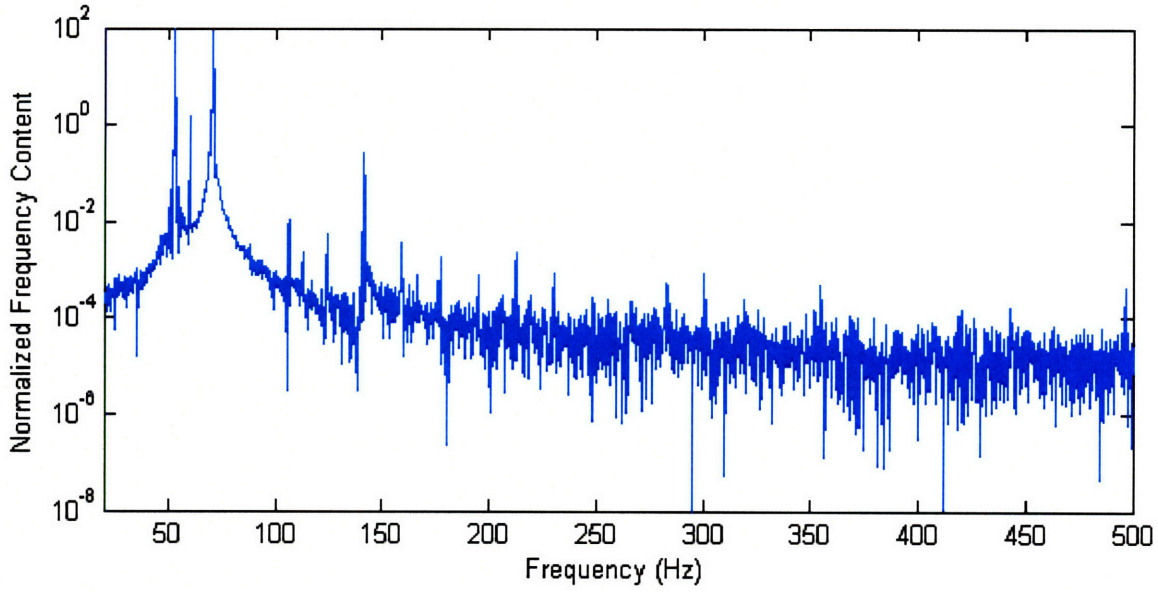

Figure 54: Frequency content of acceleration for a location midway between two tactors, plotted on a semi-log scale

Figure 55 shows the measured acceleration midway between the two tactors, along with the plot of the predicted acceleration, using the frequencies from the Fourier transform. A sum of squares regression algorithm is used to determine the phase shifts. At certain points, the predicted plot overestimates the amplitude of acceleration. The coefficient of determination for this model is 0.42. This indicates that the superposition may not be entirely linear. This suggests that a model for Skinsim might have to take into account nonlinear effects.

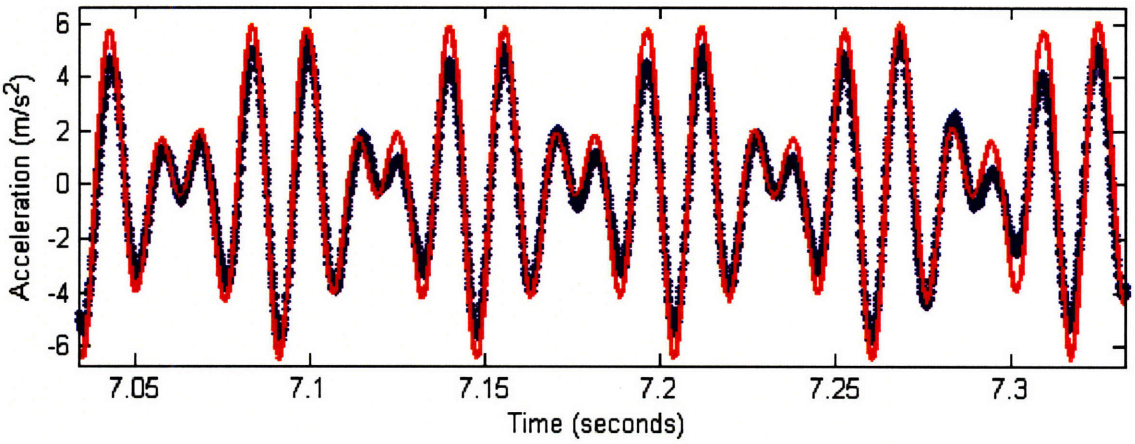

Figure 55: Acceleration at a location midway between two tactors (blue); the acceleration from the model (red) was determined using the Fourier transform of the data.

The general equation which minimizes the sum of the squared errors is given by

$$a = 2.43 \sin (334.6\, t + c1) + 2.76 \sin (445.4 + c2).$$

Figure 56 shows the fit of this equation to the data. The coefficient of determination for this model is 0.91, which indicates that the data are a pure sum of two sinusoids, although as mentioned above, the superposition may not be linear. This is to be expected, because the silicone rubber is a viscoelastic solid, so there are viscous effects that cause the superposition to be nonlinear.

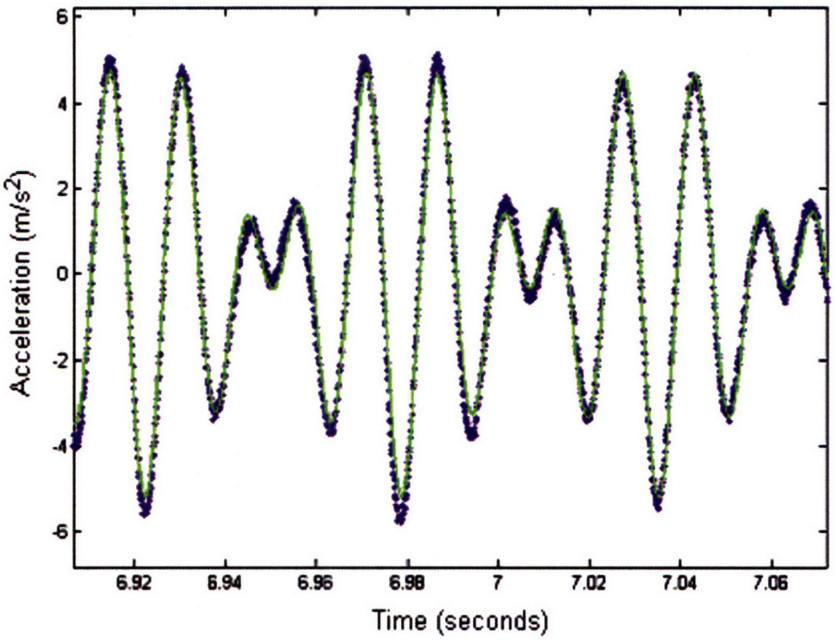

Figure 56: Acceleration at a location midway between two tactors; measured accelerations are shown in blue; the model (green) was calculated to minimize the sum of the squared error of the data

The general equation for a traveling wave with no damping is given by

$$a = a_0 \sin\left(\frac{2\pi}{\lambda}(x - ct)\right)$$

where a_0 is the amplitude of the acceleration, λ is the distance between adjacent points that are in phase, and c is the speed of the waveform (Jog, 2002). The parameter λ is related to the frequency of the waveform by $\lambda = c/f$, where f is the frequency in Hz. The speed was determined by placing accelerometers at various distances from the tactor, and measuring the phase shift in the waves at these locations. In this experiment, five accelerometers were placed at various distances away from the tactor. The phase shift resulting from the speed of the traveling wave can be seen in Figure 57, which shows the acceleration measured by each of the five accelerometers. Because the measured acceleration of the tactor (shown in green) was noisy, a low-pass filtered version of this

data (shown in black) is used to determine the phase of the waveforms. Because the Skinsim itself acted as a natural low-pass filter, the measurements from the other accelerometers did not need to be filtered in post-processing.

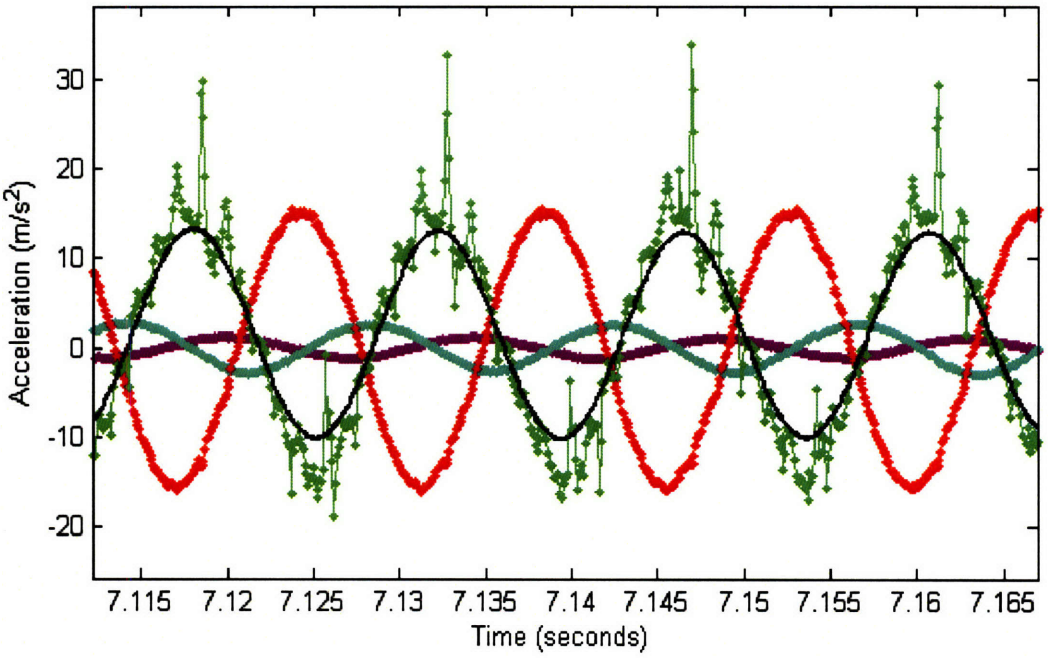

Figure 57: Acceleration at various locations away from the tactor, showing the phase due to the finite speed of the traveling wave. The acceleration of the tactor is shown in green; the red, light blue, and purple data represent points 20 mm, 37 mm, and 52 mm away from the tactor.

The filtering of the tactor data was performed using a fifth order non-causal Butterworth filter, as described earlier, with a cutoff frequency located 20 Hz higher than the peak frequency of the wave. Figure 58 shows the Fourier spectrum of the acceleration data for the tactor, as well as the filtered data.

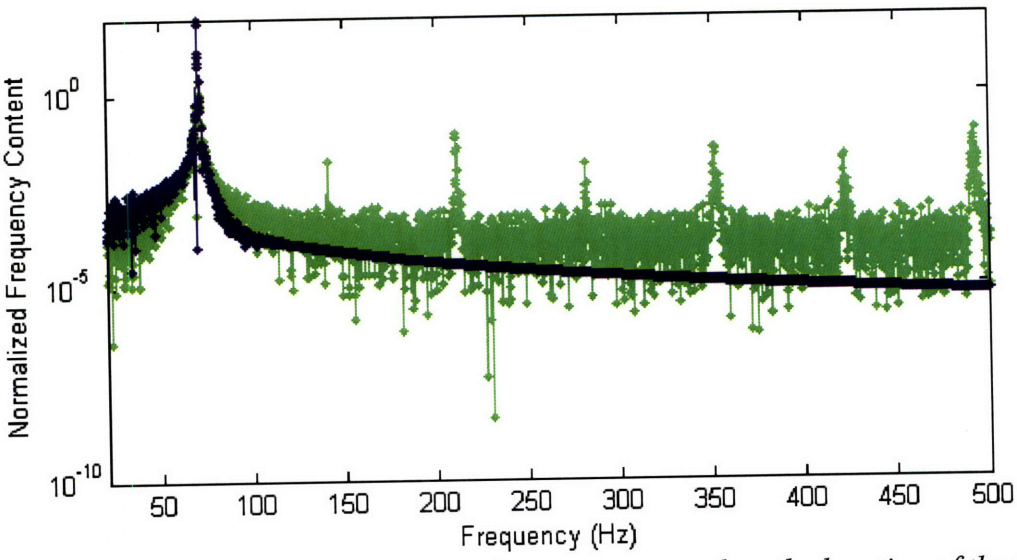

Figure 58: Fourier spectrum of the acceleration measured on the location of the tactor (green), and a filtered version of this data (blue)

The time for the traveling wave to reach each accelerometer is shown in Figure 59. The data can be fit to a least-squares regression line, with a slope of 3023 mm/s. When placed on Skinsim, this tactor oscillates with a frequency of 70.4 Hz. The damping of the amplitude for this traveling wave can be fit to a Gaussian distribution, as above. Thus the equation for the traveling wave produced by this tactor is

$$a = 26.02 \cdot e^{-(x/28.18)^2} \sin\left(\frac{2\pi}{42.94}(x - 3023 \cdot t)\right)$$

where a is the acceleration in m/s^2, at a distance x millimeters away from a tactor, at a time of t seconds.

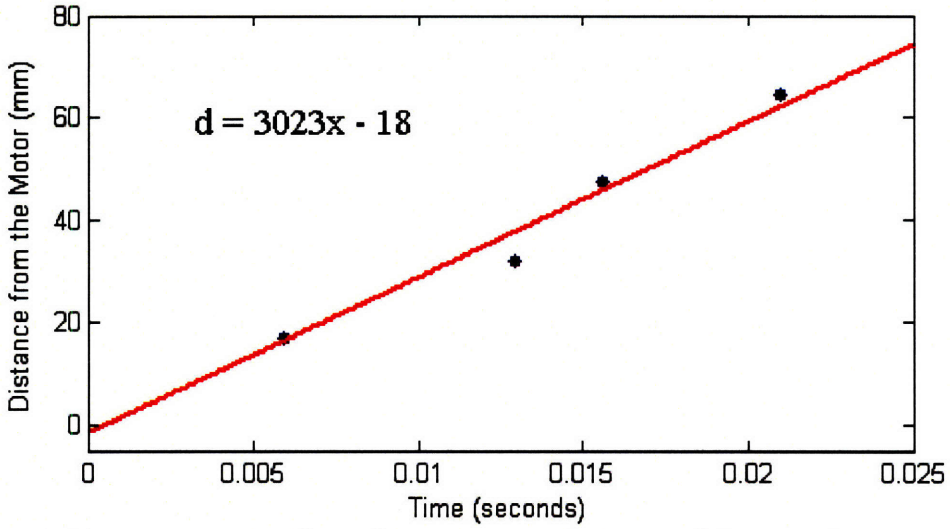

Figure 59: Distance away from the tactor, as a function of the time that it takes a waveform to reach that distance

Measurements were also taken for a traveling wave created by manually pressing a tactor quickly into the Skinsim, thus creating an impulse. The speeds produced by the resulting traveling waves ranged from 1.9 m/s to 2.4 m/s (mean: 2.2 m/s). Franke (1951) measured the group velocity of traveling waves in skin using stroboscopic illumination. The group velocities that he found ranged from 2 to 40 m/s, which is around the same range of speeds measured from traveling waves in the Skinsim. This validates the idea that the Skinsim is a reasonable simulation of human skin for studying the mechanical effects of vibrotactile stimulation.

4.2. Simulating the Two-Point Vibration Test

The dynamic two-point test can be simulated using the model for wave dissipation described in section 4.1.3. In this simulation, two tactors are placed a variable distance apart, and both vibrate at an acceleration of 10 m/s^2. Assuming linear superposition, the combined waveform has an acceleration of

$$a = 10*\exp(-(x/b_1)^2) + 10*\exp(-((x-d)/b_2)^2),$$

where b_1 and b_2 represent the damping of Skinsim, and d represents the distance between the tactors, in millimeters. For this simulation, $b_1 = b_2 = 36.2$, which is the mean value from the three tactors tested in section 4.1.3. A plot of this superposition can be seen in Figure 60, using a distance of d = 11 mm, which is the vibration detection threshold given by Eskildsen et al. (1969).

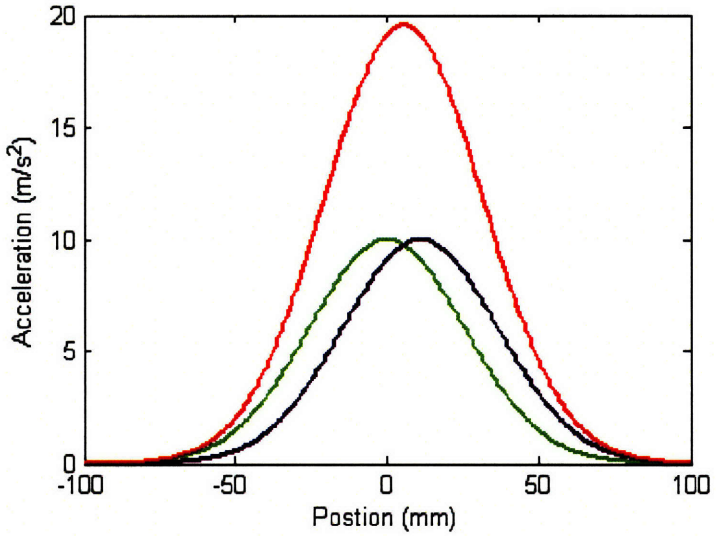

Figure 60: Simulation of a superposition of two tactors placed 11 mm apart, shown in blue and green. The superposition of their accelerations is shown in red.

Because of the proximity of the two tactors, the superimposed acceleration strongly resembles a Gaussian distribution, with a mean at 5.5 mm and a height of 19.55 m/s². Figure 61 shows a plot of this superposition of acceleration, which can be fit to a Gaussian distribution of

$$a = 19.55*\exp(-((x-5.5)/37.05)^2)$$

with a RMSE of 0.001727. Thus, the two tactors vibrating at 10 m/s² placed 11 mm apart simply appear to be one tactor located halfway between them, vibrating at 19.55 m/s².

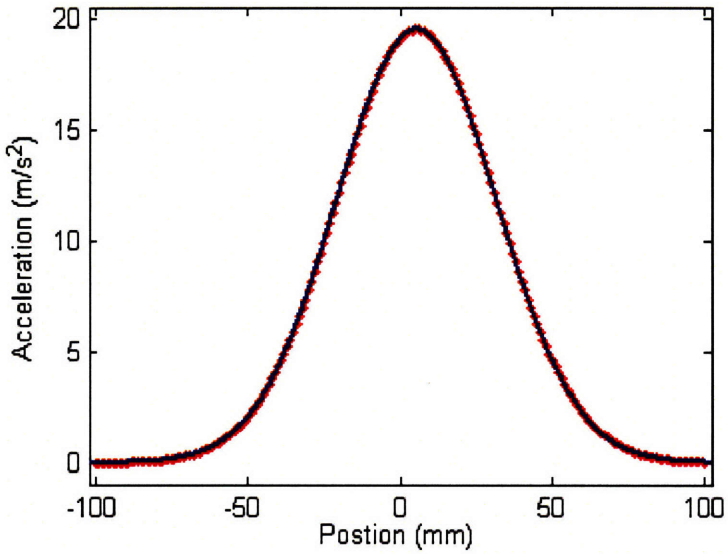

Figure 61: Superposition from two simulated tactors spaced 11 mm apart, fit to a Gaussian.

When the two tactors are spaced 50 mm apart and each vibrates at 10 m/s², the resulting simulation shows that the superposition of their amplitudes no longer has a Gaussian shape as before (see Figure 62).

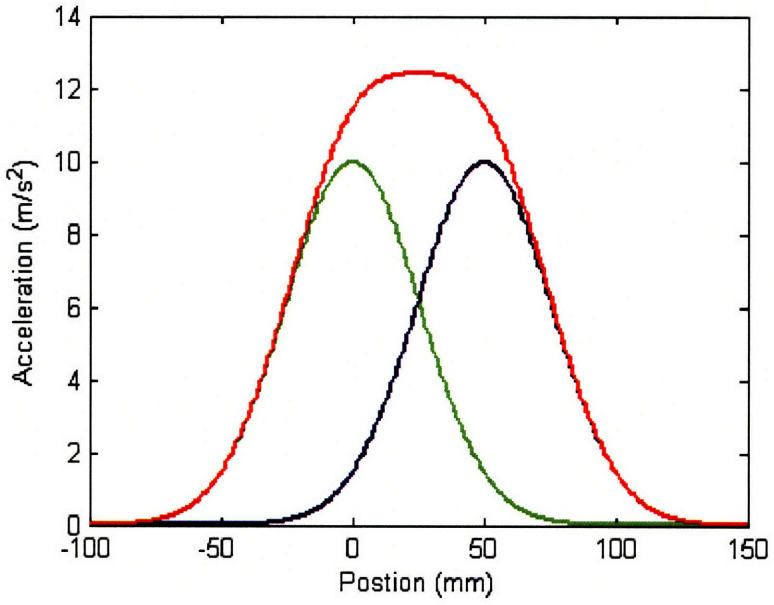

Figure 62: Simulation of a superposition of two tactors placed 50 mm apart, shown in blue and green. The superposition of their accelerations is shown in red.

Figure 63 shows an attempt to fit this superposition to a Gaussian distribution. This fit has a RMSE of 0.5209. At d = 15 mm, the RMSE = 0.005915, and at d = 20 mm, the RMSE = 0.01835. It is proposed that the vibration two-point threshold of 11 mm is based on the RMSE of the superposition of the Gaussian. Perhaps at a distance of 11 mm apart, the superposition of the traveling waves from the two vibrotactile stimuli combine to appear like one wave, whereas at larger distances, two independent waves can be perceived. If this is the case, then the viscoelastic properties of skin might affect the two-point vibrotactile threshold.

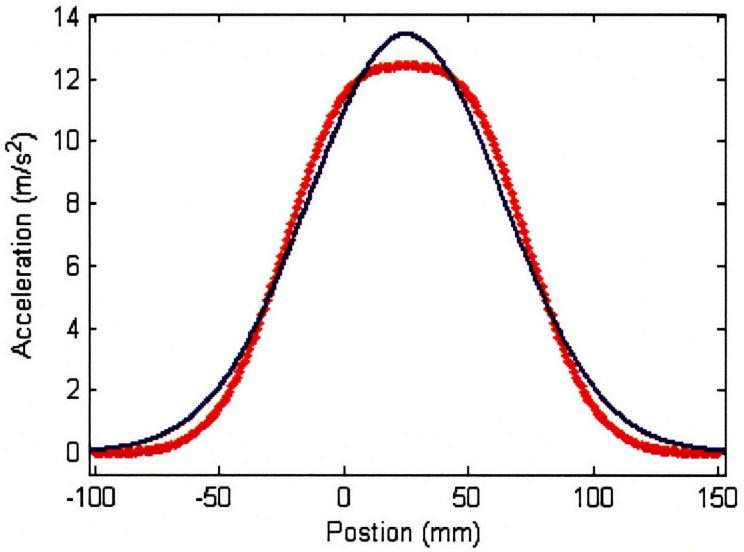

Figure 63: Superposition from two simulated tactors spaced 50 mm apart, fit to a Gaussian.

5. Bluetooth GPS and WTCU

One of the uses for the tactile vest is to display instructions that can be used for navigation. In order to do this, the location of the user must be known. A GPS (Global Positioning System) was therefore integrated into the WTCU. With a GPS, someone can determine the location of the person wearing the vest, and send the appropriate commands to the WTCU to direct the user toward a goal location. Another possible use is to automate the sending of the directional commands; a computer could use a path-planning algorithm, and based on the GPS position of the vest, automatically send the appropriate directional commands to the vest.

As a first step to achieving these aims, a Bluetooth GPS (GlobalSat, BT-359) was integrated into the GUI for the WTCU. This device uses a SiRF Star III GPS microcontroller chip and can access up to 20 satellite channels. The GPS-Bluetooth device is rated to have a horizontal position accuracy of 10 meters RMSE (root-mean squared error) without WAAS, or 1-5 meters RMSE with WAAS enabled. The device receives the GPS data using a built-in ceramic patch antenna, and it is powered by a rechargeable lithium-ion battery. When fully charged, the battery can run for up to 11 hours, although it has an auto shut-off feature that turns the device off if no Bluetooth connection is detected for 10 minutes. The dimensions of the Bluetooth GPS unit are 82.0 x 41.0 x 13.4 mm, enabling it to fit easily inside a small waist pack along with the WTCU. The Bluetooth GPS sends data using the NMEA 0183 protocol, and a new set of coordinates are sent about once a second.

The Bluetooth GPS uses the CSR BC4 chipset to establish the Bluetooth connection to the WTCU. This is a class 2 Bluetooth device, meaning that it has a range

of about 10 meters. The GPS device uses the Bluetooth chipset to wirelessly send signals to a receiver (Belkin, F8T012) that has a USB connection to a laptop. The receiver is a class I device with a range of about 100 m. It uses the Bluetooth 2.0 specification, giving it a data rate of 3.0 Mbit/s. To test the range of the Bluetooth, the Bluetooth GPS was slowly separated from the computer, and the connection was tested at various points. When the Bluetooth GPS was 4 m away from the computer, the connection became intermittent, and at 10 m, the connection was completely lost. This was expected, because the Bluetooth GPS is a class 2 Bluetooth device, and the range for such devices is generally 10 m.

A GUI was designed (Figure 64) to enable a user to simultaneously view the GPS coordinates and send navigational signals of vibration patterns to the WTCU. The left half of the GUI allows the user to connect to the Bluetooth GPS device, and displays information about the user's position in latitude-longitude coordinates. Information is also received about the time, the number of satellites in view, and the accuracy of the position. The right half of the GUI allows the user to connect to the WTCU. Any of a variety of setups can be used to send vibration patterns to the vest. In the setup shown in Figure 64, a grid of 16 buttons maps directly to the 16 tactors on the vest.

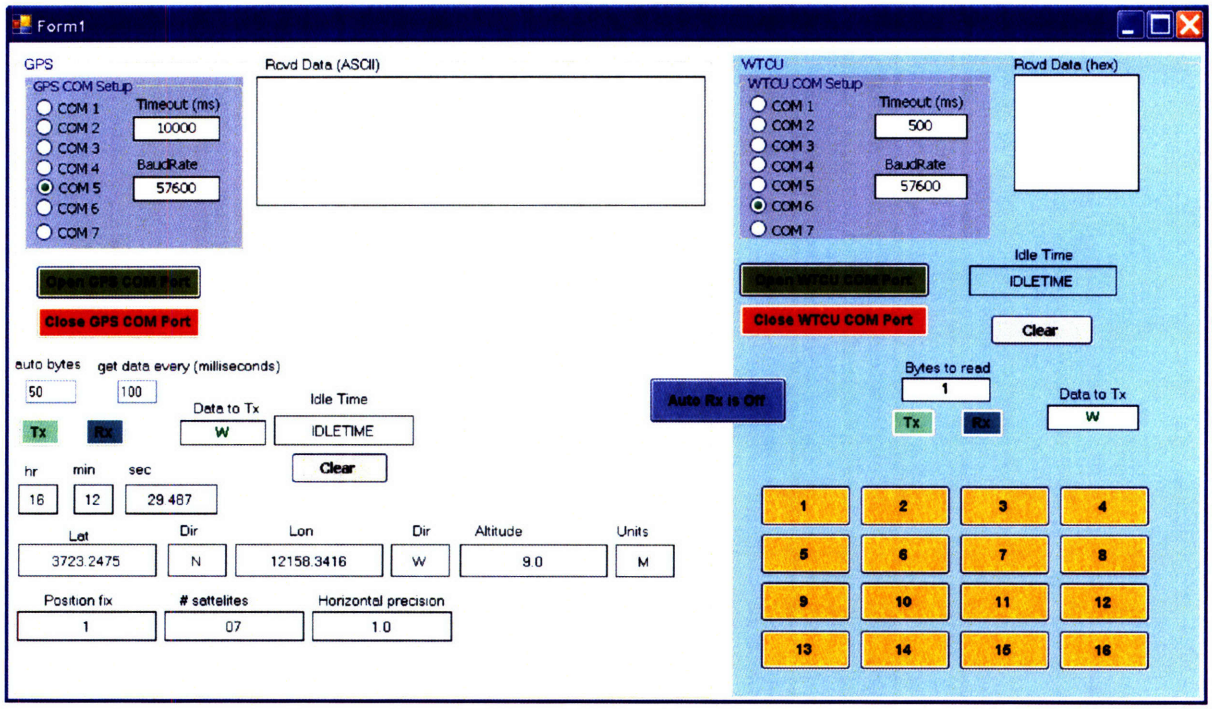

Figure 64: GUI to enable a user to view GPS coordinates and send signals to the WTCU

To test the precision of the GPS, several tests were performed. For all of the tests performed, WAAS was enabled. First, the GPS was turned on and the device was held stationary for 3 minutes. The position of the device was recorded, and the difference between the recorded position and the initial position is shown in Figure 65. This plot represents the sensor drift, which has a maximum value of 1.17 m over 3 minutes. The position is recorded in latitude-longitude coordinates, which were converted into meters using the spheroidal approximation, using a mean radius for the earth of 6372.795 km.

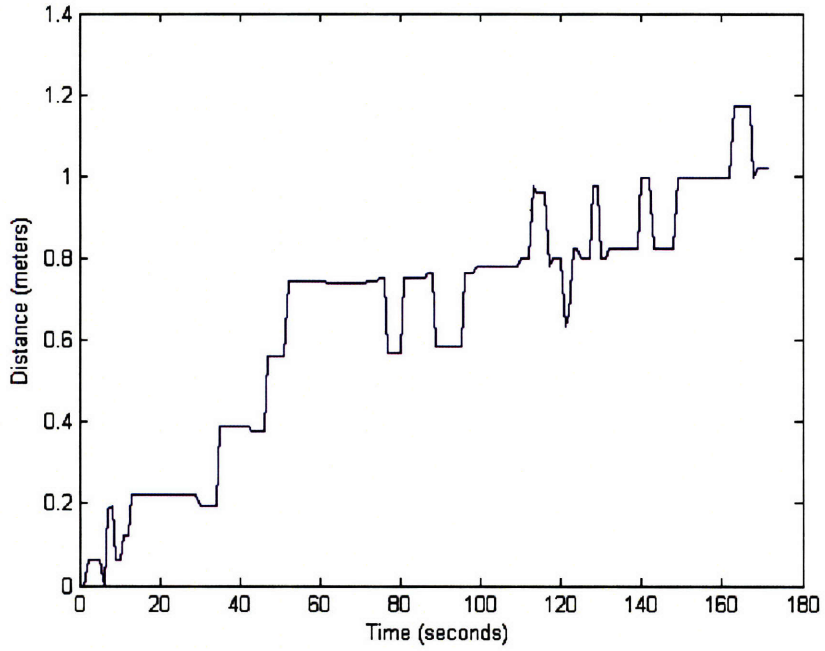

Figure 65: Distance recorded from the starting point, using a stationary GPS

Next, an experiment was performed in which 10 cones were placed 10 meters apart, for a total distance of 90 m, as shown in Figure 66. The Bluetooth GPS was moved from cone to cone, and its location was recorded along the path. This experiment was performed both in the latitudinal and in the longitudinal directions, and because the test was performed in Boston, MA, an offset of 15.4 degrees was used between magnetic north and true north.

Figure 66: Cones spaced 10 meters apart, for testing the precision of the GPS device

Figure 67 shows the test performed in the latitudinal direction. To mark the position of each cone, the GPS device was moved briefly north and then back south, before continuing to the next cone. Because of the sensor drift discussed above, the GPS did not report the same coordinates for the cone before and after this movement. However, the time to walk between cones was only about 9 seconds, so the sensor drift for the measurement between cones was minimal. The same test, performed in the longitudinal direction, can be seen in Figure 68.

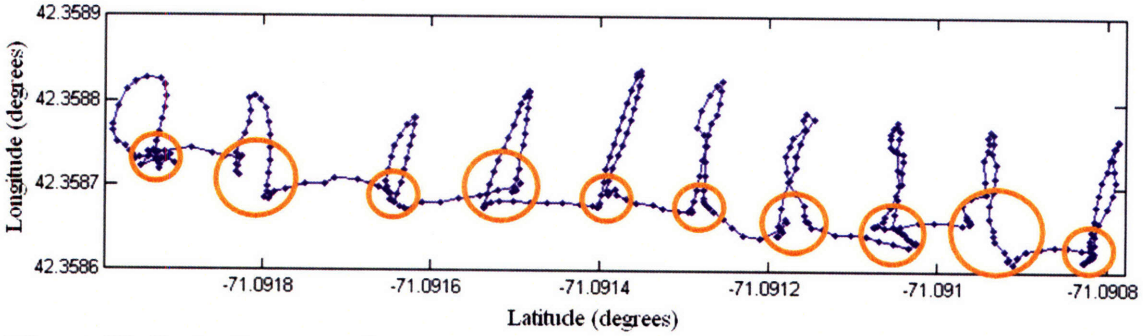

Figure 67: Latitude test, with cones spaced 10 meters apart. Cone locations are circled in orange.

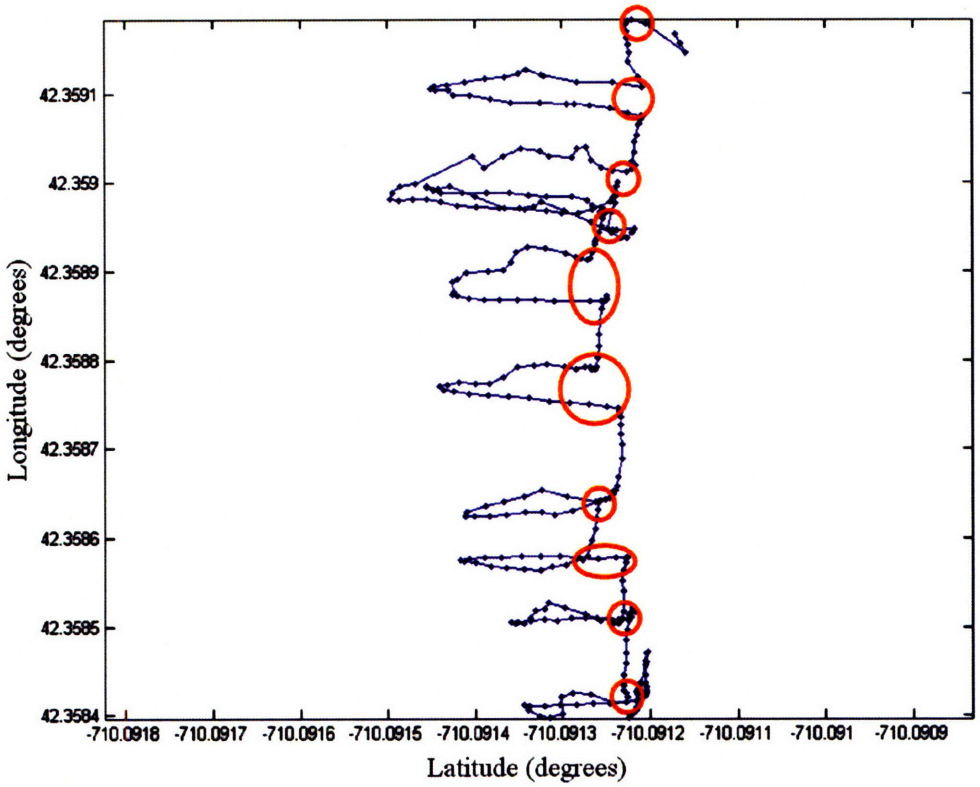

Figure 68: Longitude test, with cones spaced 10 meters apart. Cone locations are circled in orange.

The measured distance between cones can be seen in Figures 69 and 70. Each cone in both of these tests was placed 10 m apart from the next cone. Figure 69 shows the nine measured distances for the test in the latitudinal direction. The measured distance ranged from 9.65 m to 15.76 m, with a mean of 12.25 m, and a RMSE of 3.23 m. Figure 70 shows the measured distances between cones for the longitudinal direction. In this case, the measured distance ranged from 3.33 m to 11.44 m, with a mean of 7.22, and a RMSE of 3.59 m. Because the Bluetooth-GPS device has a reported accuracy of 1-5 RMSE, this test validates the reported accuracy of the device.

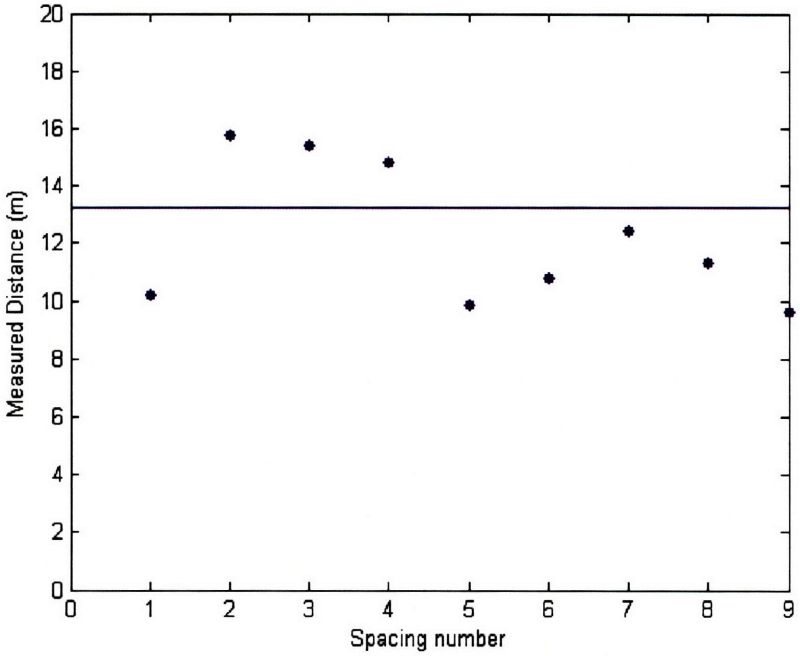

Figure 69: Measured spacing between cones in the latitude test. The RMSE is shown with the straight line

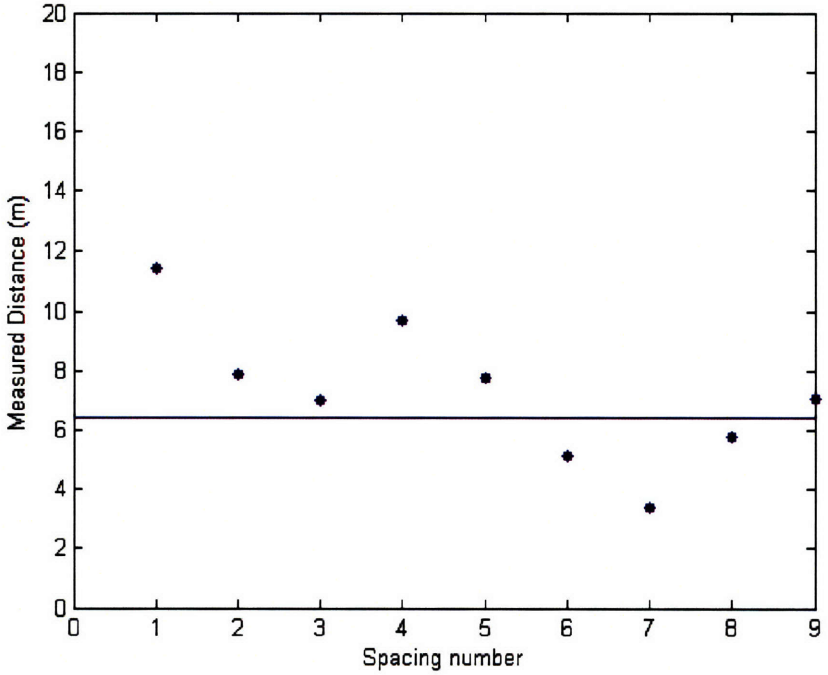

Figure 70: Measured spacing between cones in the longitude test. The RMSE is shown with the straight line

6. Recommendations for a Tactile Vest

By analyzing the characteristics of the tactors used in tactile displays, an increased understanding of the tactors' dynamics was gained. The tactors were evaluated in a rigid mechanical test setup and also when attached to a piece of silicone rubber that was designed to have similar material properties to skin. These measurements revealed that the frequency of vibration of the tactors was reduced by 62% when mounted on Skinsim. This significant performance difference indicates that, when evaluating a tactor for use in a tactile vest, the performance of the tactor must be considered when mounted on a viscoelastic substrate, rather than just considering the manufacturers' specifications for the tactor.

Experiments were performed to determine the damping of the silicone substrate on the tactors. Three tactors were actuated, and the accelerations at various points on the substrate were measured. These measurements indicated that a distance of 60 mm away from the tactor is needed for the acceleration to be damped to less than 10% of the acceleration of the tactor. At a distance of 60 mm, the acceleration for the tactors is less than 2 m/s^2. Thus, in order to be able to distinguish individual tactors on a tactile display using this type of cylindrical pancake tactor, the inter-tactor spacing should be at least 60 mm.

Cholewiak and Collins (2003) studied the effect of introducing an artificial anchor point on localization performance. By actuating one tactor at a different frequency from six other tactors, localization at the unique tactor increased by more than 20%. In this thesis, by analyzing the characteristics of individual tactors, it was found that the tactors vary widely in terms of their peak frequency, force, and acceleration. By placing tactors

with different characteristics next to each other, the subject might learn to localize tactile stimulation more accurately based on differences between the tactors.

The idea that improvements in localization can result from repeated trials with feedback has been demonstrated by Cholewiak et al. (2004). However, in order for this learning to take place, the differences between the tactors need to be large enough to be perceived. The amount that the frequencies of the tactors need to differ by to be distinguishable is indicated by the just-noticeable-difference (jnd). Mahns et al. found that the jnd varied as a function of frequency. At frequencies of 20, 50, 100, and 200 Hz, the jnd was determined to be 7.6, 18.0, 27.2, and 33.9 Hz, respectively. For the 14 encased tactors that were tested in this thesis, frequencies normal to the plane of rotation ranged from 93.7 to 184.7 Hz, thus spanning a range of 91 Hz. This range is much greater than the jnd for this range of 27.2 to 33.9 Hz, and so it would be expected that frequency differences between the tactors could be used to improve localization. Furthermore, the tactors differ in their amplitude and force of vibration, thus providing further characteristics to allow a user to differentiate between tactors. Therefore, it is hypothesized that it if the tactors are placed such that adjacent tactors have different characteristics, it may be possible to improve localization with training.

As discussed in the introduction, vibrotactile sensitivity varies as a function of frequency, with a maximum sensitivity occurring in the range of 200 – 300 Hz in both glabrous and hairy skin (Bolanowski et al., 1994). Additionally, frequency has a small effect on localization, as shown by Cholewiak et al. (2003), in which tactors driven at 250 Hz were slightly easier to localize than tactors driven at 100 Hz. Increasing the frequency of the tactors studied in this thesis to 250 Hz is not possible, as experience

indicates that the tactors used tend to burn out at frequencies higher than 210 Hz. Additionally, about 6 V and 70 mA are needed to cause a tactor to vibrate at 200 Hz. For a tactile vest of 16 tactors, a total of 1.12 A would be needed to drive the tactors alone, and additional current is needed for the microprocessor as well as other chips in the WTCU.

However, this extreme case of driving the tactors at 210 Hz may not be necessary. As shown in Figure 49, any increase in the voltage applied to the tactors will result in an increase in the intensity of vibration. Localization tests performed by Redden et al. (2006) revealed that tactors that vibrate at greater intensities are easier to localize. The graph in Figure 49 can be used to determine the intensity increase resulting from an increase in the applied voltage. The slope at 3.3 V appears to be fairly steep, indicating that even a small increase in voltage would result in a much greater acceleration. For one of the tactors tested, when the applied voltage was increased from 3.3 V to 4 V, the amplitude of acceleration increased from 18.1 m/s^2 to 22.7 m/s^2, a 25% increase. For the other tactor tested, the acceleration increased from 12.2 m/s^2 to 20.5 m/s^2, an increase of 68%. Thus even a small increase in the voltage applied to each tactor could make a large difference in the localization performance. Experiments would need to be performed to determine if this increase in localization performance would justify the increase in the amount of current required to drive the tactors at a higher voltage level.

The tactors used in this experiment were encased before being attached to a tactile vest (Piateski and Jones, 2005). This encasement increased the robustness of the tactors, their consistency, and their contact area with skin. However, the added mass of the encasement resulted in a decrease in the acceleration of the tactor. In the simulated

environment in which the tactors moved on a frictionless surface, the encasing reduced the acceleration of the tactors from 246.4 m/s² to 187.8 m/s², a decrease of 24%. This value seems reasonable considering that the encasing increases the mass of the tactor by 59%. An improved tactor design would use a lighter encasing, although the robustness of the tactors would still need to be considered.

Increasing the frequency of the tactors is even more important when considering the data shown in Figure 45. Although a tactor may vibrate at 150 Hz when rigidly mounted, when placed on Skinsim its vibration may be reduced to 60 Hz. Although this is still within the Pacinian channel's range of 40 to 500 Hz, the maximal sensitivity region is 200 to 300 Hz. Thus increasing the frequency of the tactor could be very important to the tactile perception of the tactor's vibration. At the same time, the tactors on the vest, shown in Figure 1, are not pressed up against human skin as strongly as they were pressed on the Skinsim (see Figure 44). As a result, when the subject is wearing the vest, the vibration frequency may not be reduced as drastically as it was in the Skinsim experiments. Regardless, increasing the frequency of the tactors may make the tactile stimuli easier to perceive.

Alternatively, rather than increasing the voltage applied to all tactors, certain tactors can be selected for use in the vest based on desired characteristics. Because of tactor variability, some tactors vibrate with a greater force and higher frequency than others. Figure 71 shows the force and frequency characteristics of all the tactors, when placed in the impedance head, measured in the direction normal to the plane of rotation of the eccentric. This graph could be used to select only those tactors that vibrate with the highest forces and frequencies.

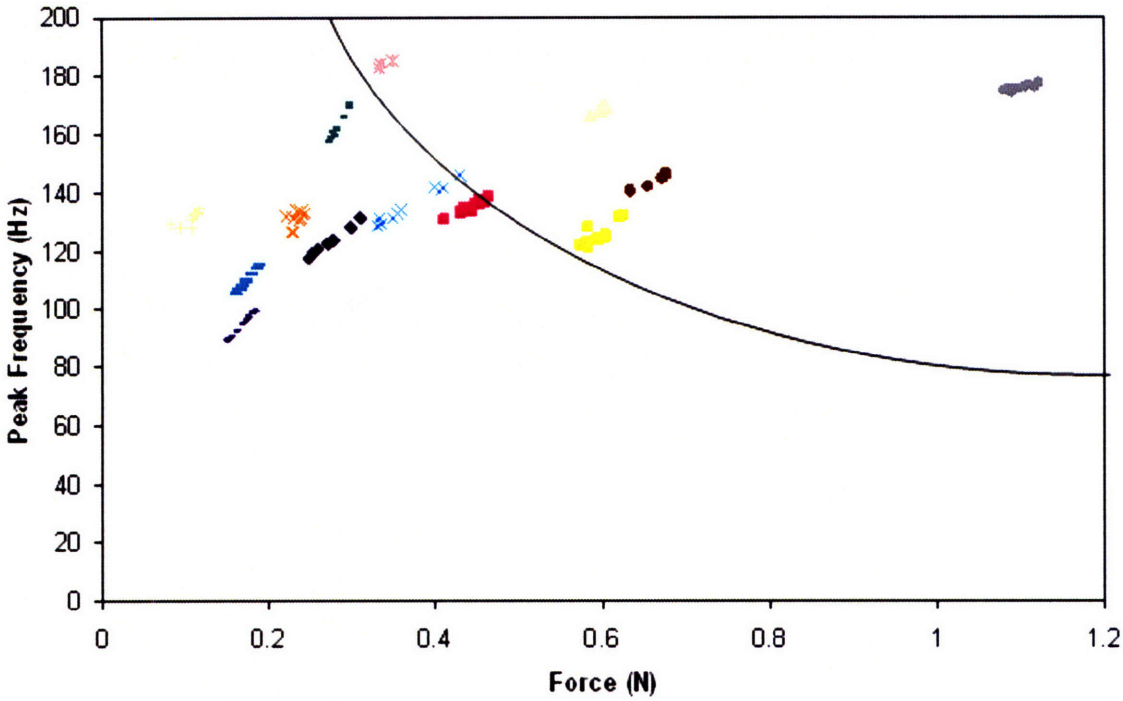

Figure 71: Peak frequency as a function of force, measured in the direction normal to the plane of rotation of the eccentric. Tactors in the top right corner have the highest force and frequency, and thus are ideal for use in a tactile vest.

Another idea would be to position the tactors based on the sensitivity of various tactor locations. For example, in a localization study using the tactile vest shown in Figure 1, tactors in the top corners were localized with the greatest accuracy (Jones and Ray, 2008). Thus tactors that vibrate with lower force and frequency can be placed here, and tactors that vibrate with stronger force can be placed elsewhere, in locations that are more difficult to localize.

Many tactile displays press the tactors against the skin. For example, in tactile vests designed by Rupert (2000) to provide spatial information to pilots, elastic and Velcro straps were used to maintain contact between the tactors and the skin. Lindeman et al. (2004) designed an encasing for pager-motor tactors in a cone-shape so that the point side remains in constant contact with the body. In contrast, the tactile vest shown in

Figure 1 places the tactors on the outside of the vest, not pressed against the body, in order to reduce discomfort to the user.

The effect of the viscoelastic substrate on the frequency of the tactors may provide a further justification for placing the tactors on the outside of the vest. When attached to the impedance head, the tactors ranged in frequency from 93.7 to 184.7 Hz. However, when attached to Skinsim, the frequencies were on average reduced by 62% of their frequency when attached to the impedance head. The reduced frequencies of the tactors are much further from the optimal range of 200 to 300 Hz than the original frequencies, measured in the impedance head. Thus it may be beneficial to place the tactors on the outside of the vest rather than to press them against the skin, which would reduce the frequency of vibration.

7. Conclusions and Future Work

A model was developed to describe the motion of a pancake motor, given an input voltage. The model predicted the relationship between the frequency and force of vibration of the tactors, as well as their current for a varying damping coefficient. This relation was very similar to that measured from the tactors, thus validating the model. Measurements of the forces and frequencies of the tactors, as well as predictions from the model, were used to understand the effect of the tactor encasing on the motion of the tactor. It was proposed that encasing the tactors had no effect on their force or frequency, although the encasing did improve the consistency of the tactors. The model indicated that a varying damping coefficient may be the cause of differences between tactors, as well as the cause of variation within an individual tactor. The model showed that the current through the tactor varies with this damping coefficient, so by measuring the current, the velocity and force of the tactor can be determined.

Additionally, the tactor model, combined with measurements from the tactors, helped to characterize the behavior of the pancake motors. It was seen that there is large variability between the frequencies and forces produced by different tactors. Although this might be a disadvantage to using this type of tactor, suggestions were proposed to turn these variations into an advantage. A tactile display design has been proposed in which tactors that differ in their forces and frequencies are placed next to each other. With training, it is possible that subjects may learn to recognize the differences between adjacent tactors, leading to greater localization performance and improved pattern recognition.

A viscoelastic substrate, named Skinsim, was designed to have similar material properties to skin. It was selected after measuring the Young's moduli of five samples of pig skin, which has similar material properties to human skin (Shergold et al., 2006). These data were compared to the Young's moduli for various silicone rubber compounds, and one compound, Skinsim, was selected as it provided the best match to the material properties of pig skin. Tactors were actuated when attached to the Skinsim, and the properties of the traveling waves formed were measured. Equations to describe the motion of these traveling waves were formulated. The damping of the Skinsim was measured, as well as the speed of the traveling waves. These measurements were used to suggest optimal spacing characteristics in a tactile display. Skinsim also had an effect on the frequency and acceleration of the tactor, and these effects were measured.

Further research should be performed to model the interaction between the tactors and Skinsim, and to determine the causes of the changes in tactor frequency when placed on Skinsim. Because the simulated tactor startup times were much faster than the measured startup times, the tactor model should be refined to better match all of the tactor data. Attempts should also be made to explain the relationship between the force produced by the tactor in the impedance head, and the acceleration of the tactor on Skinsim. Further measurements of Skinsim should be also performed to determine its similarities to human skin. Additionally, a simulation of Skinsim should be developed, and the tactor model should be included in this simulation. By manipulating parameters of this simulation, perhaps an even better understanding of the physics of a tactile display can be gained, leading to further optimizations. This thesis hopefully provided the foundation for such a simulation.

The measurements of damping in Skinsim were used to simulate a two-point vibrotactile test. Gaussian distributions represented the damping of the acceleration at points away from the tactor. The simulation compared the amplitude of the traveling wave produced by one tactor with the amplitude of the traveling waves produced by two tactors. These simulations proposed that the material properties of skin may affect the two-point vibrotactile threshold. If two tactors are spaced 11 mm apart, the superposition of their accelerations, each of which has an amplitude that is shaped like a Gaussian, produces a total acceleration that has a shape very similar to a Gaussian distribution. However, with an increased damping coefficient, a smaller distance would be needed for the combined wave to appear like a Gaussian. Further experiments can be performed that change the damping in human skin, for example by stretching the skin, to determine the effect of the mechanical properties of skin on the two-point vibrotactile threshold.

Last, a GPS device was integrated into the WTCU to determine the location of the wearer of the tactile vest. Currently, the range of the Bluetooth for this GPS is only 10 m, which is not very useful for sending navigation commands. The GPS-Bluetooth is a class 2 Bluetooth device, which limits its range to only 10 m. To expand the range to 100 m, a class 1 Bluetooth device needs to be used. This would probably involve the purchase of a GPS chip, such as the SiRF Star III, which could be directly integrated into the WTCU.

With a GPS connected to the tactile vest, a program can be made to automatically send tactile directional commands based on the position of the vest. Expansions to the WTCU GUI (graphical user interface) would enable a user to view the location of the vest on a map, and to enter, either in real-time or prior to movement, a set of waypoints to

guide the subject. Various control strategies should be used to attempt to keep the subject as close to the intended path as possible. The addition of a digital magnetometer would further improve the ability to send appropriate directional signals to the subject, by providing information about the direction that the subject is facing. Commands could then be sent to direct the subject to turn a certain number of degrees in the appropriate direction. By improving the design of a tactile display, a user that is carrying both a GPS and a digital magnetometer can be directed more precisely to a desired location.

References

P.G. Agache, C. Monneur, J.L. Leveque, and J. De Rigal (1980). "Mechanical properties and Young's modulus of the skin in vivo," Archives of Dermatological Research, vol. 269 pp. 221-232.

H. Asada. "Introduction to Robotics, Chapter 2: Actuators and Drive Systems," MIT OpenCourseWare. Retrieved October 15, 2007, from http://ocw.mit.edu/NR/rdonlyres/E65EDC40-4E8B-4949-8DBD-129783706AC2/0/chapter2.pdf.

S.J. Bolanowski, G.A. Gescheider, R.T. Verrillo, and C.M. Checkosky (1988). "Four channels mediate the mechanical aspects of touch," The Journal of the Acoustical Society of America, vol. 84 pp. 1680-1694.

S.J. Bolanowski, G.A. Gescheider, and R.T. Verrillo (1994). "Hairy skin: psychophysical channels and their physiological substrates," Somatosensory and Motor Research, vol. 11 pp. 279-290.

R.W. Cholewiak and C.E. Sherrick (1986). "Tracking skill of a deaf person with long-term tactile aid experience," Journal of Rehabilitation Research and Development, vol. 23 pp. 20 – 26.

R.W. Cholewiak and A. A. Collins (1991). "Sensory and physiological bases of touch" in The Psychology of Touch, edited by M.A. Heller and W. Schiff. Hillsdale, New Jersey: Lawrence Erlbaum Associates, Publishers pp. 23 – 60.

R.W. Cholewiak, A.A. Collins, and J.C. Brill (2001). "Spatial factors in vibrotactile pattern perception," Proceedings of Eurohaptics, Birmingham: University of Birmingham. pp. 41 – 47.

R.W. Cholewiak and A. A. Collins (2003). "Vibrotactile localization on the arm: Effects of place, space, and age," Perception & Psychophysics, vol. 65 pp. 1058-1077.

R.W. Cholewiak, J.C. Brill, and A. Schwab (2004). "Vibrotactile localization on the abdomen: Effects of place and space," Perception & Psychophysics, vol. 66 pp. 970-987.

J.B.F. van Erp and P.J. Werkhoven (1999). "Spatial characteristics of vibro-tactile perception on the torso," (Report TM-99-B007). Soesterberg, The Netherlands: TNO Human Factors Research Institute.

J.B.F. van Erp (2007). Tactile displays for navigation and orientation: perception and behavior. Leiden, The Netherlands: Mostert & Van Onderen.

P. Eskildsen, A. Morris, C.C. Collins, and P. Bach-Y-Rita (1969). "Simultaneous and successive cutaneous two-point threshold for vibration," Psychonomic Science, vol. 14 pp. 146-147.

E.K. Franke (1951). "Mechanical impedance measurements of the human body surface," (Air Force Technical Report No. 6469). Aero Medical Laboratory, Air Material Command, Wright–Patterson Air Force Base, Dayton, Ohio.

H. Gray (1974). Gray's Anatomy. Philadelphia, PA: Running Press.

C.S. Jog (2002). Foundations and Applications of Mechanics, Volume II: Fluid Mechanics. New Delhi: Narosa Publishing House. pp.195-197.

K.O. Johnson, and J.R. Phillips (1981). "Tactile spatial resolution. I. Two-point discrimination, gap detection, grating resolution, and letter recognition," Journal of Neurophysiology, vol. 46 pp. 1177–1191.

L.A. Jones, J. Kunkel, and E. Torres (2007). "Tactile vocabulary for tactile displays," Proceedings of the Second Joint EuroHaptics Conference and Symposium on Haptic Interfaces for Virtual Environment and Teleoperator Systems, pp. 574-575.

L.A. Jones, B. Lockyer, and E. Piateski (2006). "Tactile display and vibrotactile pattern recognition on the torso," Advanced Robotics, vol. 20 pp. 1359-1374.

L.A. Jones and K. Ray (2008). "Localization and pattern recognition with tactile displays." Symposium on Haptic Interfaces for Virtual Environments and Teleoperator Systems. Submitted for publication.

E.R. Kandel, J.H. Schwartz, and T.M. Jessell (2000). Principles of Neural Science, 4th ed. New York: McGraw-Hill.

P. Leskovsky, M. Harders, and G. Szekely (2006). "Assessing the fidelity of the haptically rendered deformable objects," 14th Symposium on Haptic Interfaces for Virtual Environment and Teleoperator Systems, IEEE Virtual Reality, IEEE Virtual Reality, pp. 19-25.

R.W. Lindeman, R. Page, Y. Yanagida, and J.L. Sibert (2004). "Towards full-body haptic feedback: the design and deployment of a spatialized vibrotactile feedback system," Proc. of ACM Virtual Reality Software and Technology, Hong Kong, China, pp. 146-149.

B.J. Lockyer (2004). "A Wireless Communication System for a Tactile Vest," Master's thesis, Massachusetts Institute of Technology, Cambridge, MA.

D. Mahns, N.M. Perkins, V. Sahai, L. Robinson, and M.J. Rowe (2006). "Vibrotactile frequency discrimination in human hairy skin," Journal of Neurophysiology, vol. 95 pp. 1442–1450.

B.J. Mortimer, G.A. Zets, R.W. Cholewiak (2007). "Vibrotactile transduction and transducers," The Journal of the Acoustical Society of America, vol. 121 pp. 2970-7.

E.M. Piateski (2005). "A tactile communication system for navigation," Master's thesis, Massachusetts Institute of Technology, Cambridge, MA.

E.M. Piateski and L.A. Jones (2005). "Vibrotactile pattern recognition on the arm and torso," Proceedings of the First Joint Eurohaptics Conference and Symposium on Haptic Interfaces for Virtual Environment and Teleoperator Systems, pp. 90-95.

E.S. Redden, C.B. Carstens, D.D. Turner, and L.R. Elliott (2006). "Localization of tactile signals as a function of tactor operating characteristics," (Report ARL-TR-3971). Army Research Laboratory.

M.C. Reed, and N.I. Durlach (1998). "Note on information transfer rates in human communication," Presence, vol. 7 pp. 509-518.

J. Roberts, O. Slattery, and D. Kardos (2000). "Rotating-wheel Braille display for continuous refreshable Braille," Proceedings of Society for Information Display Symposium Digest of Technical Papers, pp. 1130– 1133.

A.H. Rupert (2000). "Tactile situation awareness system: Proprioceptive prostheses for sensory deficiencies," Aviation Space & Environmental Medicine, Section 2 – Supplement, vol. 71 no. 9 pp. A92-A99.

O.A. Shergold, N. A. Fleck and D. Radford (2006). "The uniaxial stress versus strain response of pig skin and silicone rubber at low and high strain rates," International Journal of Impact Engineering, vol. 32 pp. 1384–1402.

C.E. Sherrick (1991). "Vibrotactile pattern perception: Some findings and applications" in The Psychology of Touch, edited by M.A. Heller and W. Schiff. Hillsdale, New Jersey: Lawrence Erlbaum Associates, Publishers pp. 189 - 218.

S. Stageberg (2004). "The device that refreshes: how to buy a Braille display," American Foundation for the Blind. Technology and People Who Are Blind or Visually Impaired. AFB AccessWorld. Retrieved October 15, 2007, from http://www.afb.org/afbpress/pub.asp?DocID=aw050607.

S. Weinstein (1968). "Intensive and extensive aspects of tactile sensitivity as a function of body part, sex and laterality," in The Skin Senses, edited by D.R. Kenshalo. Springfield, IL: Thomas. pp. 195-222.